UNIVERSITY OF CALIFORNIA, SAN DIEGO

Solar fuels: Integration of molecular catalysts with p-type semiconductor photocathode

A dissertation submitted in partial satisfaction of the requirements for the degree of Doctor of Philosophy

in

Materials Science and Engineering

by

Bhupendra Kumar

Committee in charge:

Professor Clifford P. Kubiak, Chair
Professor Sungho Jin, Co-Chair
Professor Prabhakar Bandaru
Professor Yuhwa Lo
Professor Shirley Meng
Professor Joseph Wang

2012

The dissertation of Bhupendra Kumar is approved, and it is acceptable in quality and form for publication on microfilm and electronically:

Co-Chair

Chair

University of California, San Diego

2012

DEDICATION

This dissertation is dedicated to my parents, Mr. Ramesh Sharma and Mrs. Prem Bada Devi, for their limitless love and support and to the rest of my family, blood relations and otherwise.

EPIGRAPH

It’s a wonderful life.

Movie 1946

TABLE OF CONTENTS

LIST OF FIGURES

LIST OF TABLES

ACKNOWLEDGEMENTS

Somebody told me that only thing people read in anyone's thesis is its acknowledgements. It has been a very long journey for me from a small city in India to San Diego, USA with couple of stops at Varanasi and Singapore. Along the way, numerous people have helped me to move forward. Indian culture has high regards for teachers. And I am fortunate enough to have a lot of good teachers along the way. My primary school teacher, Mr. N. C. Mishra, has taught me not to afraid of failures. During my four years of college (IT-BHU), Prof. Devendra Kumar and Prof. Om Parkash helped me build a good foundation of materials science. I got my first exposure to "real research" and hands on experiments at IISc, Bangalore under supervision of Dr. H. N. Vasan during my senior year of college. He was really nice to me and taught me a lot about materials research. Like all undergraduate of my age at that time, I wanted to do MBA and make money. He encouraged me to take research and go for higher study and see if I like it.

It is always easier said than done. Being an intern at IISc, Bangalore was fun. But, when fresh out of college I had to find a thesis project for myself at National University of Singapore. It was not fun at all. I am glad that I had really able advisor in Prof. Gong Hao. Unlike others professors in the department, Prof. Gong Hao never decided projects for me or told me what experiments to do. He taught me to question everything and how to prove my theories with experimental evidences. At that time, it was not pleasant to answer his millions of questions during discussion sessions. I used to get frustrated with it. But, end results usually a conclusion proven beyond the reasonable doubts. This is an invaluable skill. I got my first opportunity to work in a large project with several sub-projects at Nanyang Technological University, Singapore under Prof. Subodh Mhaisalkar. It was interesting experience working with experts in different areas and trying to achieve same goal.

During my first year at UCSD, I got opportunity to work with the two of the very best materials scientist Prof Sungho Jin and Dr. Leon Chan. It opened up my way of think and helped me become more creative. For last few years, I have been working in Prof Clifford P. Kubiak's lab in department of

chemistry and biochemistry. Cliff always says that he do not want to micro-manage his students. He adhered by his version of teaching all throughout my stay in lab. Couple of times when I distinctly benefitted by his enthusiasm for teaching are (a) during my second year literature review examination practice talk (water oxidation) and (b) during a group meeting when he talked about how to estimate the rate of reaction based on collision theory. I am personally jealous with my colleagues working in the self-exchange project because Cliff always shows so much more enthusiasm for the self-exchange project (and not so much for what I did in the lab). But again, I have got away with working with Perchloric acid in lab. I think that I gave him enough reasons to kick me out of the lab several times. However, for some reason (only he knows) he has been really supportive to me throughout my stay in his lab (financially or otherwise). I do not think I could have last so long in this lab without the help and encouragement from Dr. Julia, Dr. John, Dr. Starla, Dr. Sayak, Eric, Jon, Candace, Alissa, Jane, Momo Tomato and Jumbo Sharma (J Sharma). I would like to acknowledge Jon, Mark, Jerry and Gabe for thier help in proof reading the dissertation and Tram and Candace for their help with schematics.

My parents always told me to study when I was school and I never did. Now, they do not really understand why I am still studying. Never the less, they are always supportive to my ambitions. My brothers Pinku, Mukkun, Kundan were great company growing up. They have made my life a lot easier by taking good care of our parents. I made lot of friends along the way till here. I really appreciate all of them. Dr. Srinivas Sista and Dr. Naveen Ramalingam are primary drive force behind my decision to pursue PhD and supported me all through my graduate school. In San Diego, I found three wonderful persons; as my roommates Dr. Bhooshan and Mr. Bishakh and as a colleague Miss Candace. They were there when I tried to quit PhD several times and convinced me against it. My interactions with them have definitely made me a better person. There are a lot of people who made my stay in San Diego a pleasant experience; Neelmani, Neevan, Mohit, Dhritiman, Kowsik, Subra, Abhijit, Nara, Tram, Alex, Justin, Milad, Matt, Jerry, Ricky, Alissa, Mark, Jane, DaThao, Sukhi, Veronica, Maca, David. In case, I missed somebody, I could like to tell them that I really appreciate their friendship.

SPECIFIC CHAPTER ACKNOWLEDGMENTS

Chapter 1: Some of the material in this chapter comes directly from a manuscript entitled, "Photochemical and photoelectrochemical reduction of CO_2" by Bhupendra Kumar, Mark Llorente, Jesse Froehlich, Tram Dang, Aaron Sathrum and Clifford P. Kubiak, which has been published in *Ann. Rev. Phys. Chem.* **2012**, *63,* 24.1-24.29.

Chapter 2: Much of the material in this chapter comes directly from a manuscript entitled "Photoreduction of CO_2 on p-type Silicon using Re(bipy-Bu*t*)$(CO)_3$Cl: Photovoltages exceeding 600 mV for the selective reduction of CO_2 to CO," by Bhupendra Kumar, Jonathan M. Smieja and Clifford P. Kubiak, which has been published in *J. Phys. Chem.*, **2010**, *114*, 14220-14223.

Chapter 3: Much of the material in this chapter comes directly from a manuscript entitled "Artificial photosynthesis of CO: Kinetic and structural studies, origins of selectivity, and importance of interfacial charge transfer," by Jonathan M. Smieja, Eric E. Benson, Bhupendra Kumar, Kyle A. Grice, Candace S. Seu, Alexander J. M. Miller, James M. Mayer and Clifford P. Kubiak, accepted *PNAS* **2012**.

Chapter 5: Much of the material in this chapter comes directly from a manuscript entitled "Tunable, light-assisted co-generation of CO and H_2 from CO_2 and H_2O by Re(bipy-tbu)$(CO)_3$Cl and p-Si in non-aqueous medium" by Bhupendra Kumar, Jonathan M. Smieja, Alissa F. Sasayama and Clifford P. Kubiak, which has been published in *Chem. Commun.*, **2012**, 48*,* 272-274.

Chapter 6: Much of the material in this chapter comes directly from a manuscript entitled "Photoelectrochemical hydrogen generation by a [FeFe] hydrogenase active site mimic at a p-type Silicon/molecular electrocatalyst junction" by Bhupendra Kumar, Maryline Beyler, Clifford P. Kubiak and Sascha Ott, which has been published in *Chem. Eur. J.*, **2012**, 18*,* 1295-1298.

Chapter 8: Some of the material in this chapter comes directly from a manuscript entitled, "Photochemical and photoelectrochemical reduction of CO_2," by Bhupendra Kumar, Mark Llorente, Jesse Froehlich, Tram Dang, Aaron Sathrum and Clifford P. Kubiak, which has been published in *Ann. Rev. Phys. Chem.* **2012**, *63,* 24.1-24.29.

VITA

2002	Bachelor of Technology, Institute of Technology-Banaras Hindu University
2006	Master of Science, National University of Singapore
2012	Doctor of Philosophy, University of California, San Diego

PUBLICATIONS

J. M. Smieja, E. E. Benson, **B. Kumar**, K. A. Grice, C. S. Seu, A. J. M. Miller, J. M. Mayer, C. P. Kubiak, "Artificial photosynthesis of CO: Kinetic and structural studies, origins of selectivity, and importance of interfacial charge transfer" **Proceedings of the National Academy of Sciences**, accepted **2012**.

B. Kumar, M. Llorente, J. Froehlich, T. Dang, A. Sathrum, C. P. Kubiak, ""Photochemical and photoelectrochemical reduction of CO_2", **Annual Review of Physical Chemistry**, *63,* 24.1-24.29 (2012).

B. Kumar, M. Beyler, C. P. Kubiak, S. Ott, "Photoelectrochemical Hydrogen Generation by an [FeFe] Hydrogenase Active Site Mimic at a p-type Silicon/Molecular Electro-Catalyst Junction", ***Chemistry a European Journal*, 18***,* 1295-1298 (2012).

B. Kumar, J. M. Smieja, A. F. Sasayama, C. P. Kubiak, "Tunable, light-assisted co-generation of CO and H_2 from CO_2 and H_2O by Re(bipy-tBu)$(CO)_3$Cl and p-Si", **Chemical Communications, 48***,* 272-274 (2012)**.**

B. Kumar, J. M. Smieja, C. P. Kubiak, "Photo-reduction of CO_2 on p-type silicon using Re(bipy-Bu^t)$(CO)_3$Cl: Photovoltages exceeding 600 mV for the selective reduction of CO_2 to CO", **Journal of Physical Chemistry C, 114(33)**, 114220-14223 (2010).

B. Kumar, H. S. Tan, N. Ramalingam, S. G. Mhaisalkar, "Integration of Ink Jet and Transfer Printing for Device Fabrication using Nanostructured Materials", **Carbon, 47**, 321-324 (2009).

S. Tripathy, S. Vicknesh1, L. S. Wang, V. K. X. Lin, S. A. Oh, R. Grover, K. Y. Zang1, J. Arokiaraj, J. N. Tan, **B. Kumar**, H. Gong, S. R. Shannigrahi, A. Ramam, and S. J. Chua**, "**GaN and ZnO freestanding micromechanical structures on silicon-on-insulator substrates", **Phys. Stat. Sol. (a),** 1– 5 (2008).

S. Vicknesh, S. Tripathy, V. K. X. Lin, **B. Kumar**, H. Gong, and S. J. Chua, " Surface micromachined freestanding ZnO microbridge and cantilever structures on Si(111) substrates ", **Applied Physics Letters, 90**, 091913 (2007).

B. Kumar, H. Gong, V. Shanmugan, S. J. Chua, S. Tripathy, "Luminescence properties of ZnO layers grown on (111)-oriented compliant Si-on-insulator substrate", **Applied Physics Letters, 89**, 141901 (2006).

B. Kumar, H. Gong, S. Y. Chow, S. Tripathy, Y. Hua, "Photoluminescence and multi-phonon resonant Raman scattering in low-temperature grown multilayer ZnO nanostructures", **Applied Physics Letters, 89,** 071922 (2006).

B. Kumar, H. Gong, N. Gosvami, R. Akkipeddi, and S. J. O'Shea, "Nano-scaled electrical homogeneity of indium zinc oxide films", **Applied Physics Letters, 88**, 093111 (2006).

G. Hu, **B. Kumar**, H. Gong, E. F. Chor, and P. Wu, "Transparent Indium Zinc Oxide Ohmic Contact to Phosphorous Doped n–type Zinc Oxide", **Applied Physics Letters, 88**, 101901 (2006).

B. Kumar, H. Gong, R. Akkipeddi, "High mobility undoped amorphous indium zinc oxide thin films with low Indium content" **Journal Applied Physics, 98**, 073703 (2005).

B. Kumar, H. Gong, R. Akkipeddi, "A study of conduction in the transition zone between homologous and ZnO rich regions in the In_2O_3 – ZnO system", **Journal of Applied Physics, 97**, 063706 (2005).

PATENT

B. Kumar, Z. Wang, L.-J. Li, S. G. Mhaisalkar "**Inkjet printing & transfer printing of electronic circuits**" - ETPL Ref: SRC/Z/04875.

ABSTRACT OF THE DISSERTATION

Solar fuels: Integration of molecular catalysts with p-type semiconductor photocathode

by

Bhupendra Kumar

Doctor of Philosophy in Materials Science and Engineering

University of California, San Diego, 2012

Professor Clifford P. Kubiak, Chair

Professor Sungho Jin, Co-chair

Light assisted or driven fuel generation by carbon dioxide and proton reduction can be achieved by a p-type semiconductor/liquid junction. There are four different types of schemes which are typically used for carbon dioxide and proton reduction for fuel generation applications. In these systems, the semiconductor can serve the dual role of a catalyst and a light absorber. Specific electrocatalysts (heterogeneous and homogeneous) can be driven by p-type semiconductor where it works only as light absorber in order to achieve better selectivity and faster rates of catalysis. The p-type semiconductor/molecular catalyst junction is primarily explored in this dissertation for CO_2 and proton photoelectrochemical reduction. A general principle for the operation of p-type semiconductor/molecular junctions is proposed and validated for several molecular catalysts in contact with p-Si photocathode. It is also shown that the light assisted homogeneous and heterogeneous catalysis can coexist. This principle is extended to achieve direct conversion of CO_2 to methanol on Platinum nanoparticles decorated p-Si in aqueous medium through pyridine/pyridinium system for CO_2 reduction.

An open circuit voltage higher than 600 mV is achieved for p-Si/Re(bipy-tBu)$(CO)_3$Cl [where bipy-tBu = 4,4'- tert-butyl-2,2'-bipyridine] (Re-catalyst) junction. The photoelectrochemical conversion of

CO_2 to CO using a p-Si/Re-catalyst junction is obtained at 100 % Faradaic efficiency. The homogeneous catalytic current density for CO_2 by p-Si/Re-catalyst junction under illumination scales linearly with illumination intensity (both polychromatic and monochromatic). This indicates that the homogeneous catalysis is light driven for the p-Si/Re-catalyst junction system up to light intensities approaching one sun. The photoelectrochemical reduction of other active members of Re(bipyridyl)$(CO)_3Cl$ molecular catalyst family is also observed on illuminated p-Si photocathode. Effects of surface modification and nanowire morphology of the p-Si photocathode on the homogeneous catalytic reduction of CO_2 by using p-Si/Re-catalyst junction are also described in this dissertation. For phenyl ethyl modified p-Si photocathode, the rate of homogeneous catalysis for CO_2 reduction by Re-catalyst is three times greater than glassy carbon electrode and six times greater than the hexyl modified and the hydrogen terminated p-Si photocathodes. When hexyl modified p-Si nanowires are used as photocathode, the homogeneous catalytic current density increased by a factor of two compared to planar p-Si (both freshly etched and hexyl modified) photocathode. A successful light assisted generation of syngas (H_2:CO = 2:1) from CO_2 and water is achieved by using p-Si/Re-catalyst. In this system, water is reduced heterogeneously on p-Si surface and CO_2 is reduced homogeneously by Re-catalyst.

The same principle is extended to the homogeneous proton reduction by using p-Si/[FeFe] complex junction where [FeFe] complex [Fe_2(μ-bdt)$(CO)_6$] (bdt = benzene-1,2-dithiolate)] is a proton reduction molecular catalyst. A short circuit quantum efficiency of 79 % with 100 % Faradaic efficiency and 600 mV open circuit are achieved by using p-Si/[FeFe] complex for proton reduction with 300 mM perchloric acid as a proton source. Cobalt difluoroboryl-diglyoximate (Co-catalyst) is a proton reduction catalyst with only 200 mV of overpotential for the hydrogen evolution reaction (HRE). The Co-catalyst is photoelectrochemically reduced with a photovoltage of 470 mV on illuminated p-Si photocathode. For p-Si photocathodes, the overpotential for proton reduction is over 1 V. In principle, p-Si/Co-catalyst junction can reduce proton to hydrogen homogeneously at underpotential.

In a concluding effort, a wireless monolithic dual face single photoelectrode (multi junction photovoltaic cell which can generate a voltage higher 1.7 V) based photochemical cell is proposed for direct conversion of solar energy into liquid fuel. In this device, the two faces of the multijunction

photoelectrode are serve as an anode and a cathode for water oxidation and fuel generation, respectively, and are separated by proton exchange membrane.

1 Chapter 1

Solar fuels: prospective of photoelectrochemical reduction of carbon dioxide to useful products by semiconductor/molecular catalyst junction

1.1 General introduction to semiconductor/liquid junction

Most semiconductors are a class of solid state materials which have moderate gaps between completely filled and unfilled states (for metals, there is no or very small gap and for insulator, there is very large gap). The completely filled state is called valence band, the unfilled stated is called conduction band and the gap between these two states is called forbidden gap or band gap of the semiconductor. Free carriers can be generated in the semiconductor with the help of external energy (light, electrical, thermal energy). Carrier concentration in semiconductors can also be altered by doping the semiconductor with external atoms [for example, Silicon can be doped with group III (acceptor for p-type) and group V elements (donor for n-type)]. Based on the nature of the charge carriers, semiconductors are classified as (1) n-type and (2) p-type. The majority charge carriers are electrons and holes, respectively, for n-type and p-type semiconductors. Figure 1-1 shows a schematic representation of n-type and p-type semiconductors with its dopant level along with conduction band edge, valence band edge and Fermi level. A detail description of semiconductor physics can be found in any semiconductor physics text book.

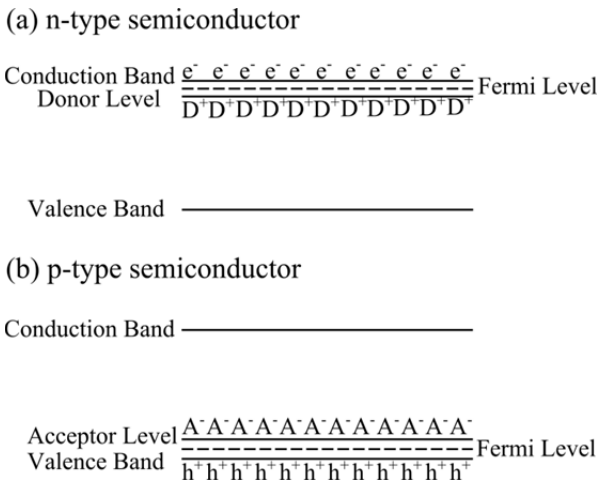

Figure 1-1. (a) Energy bands of an n-type semiconductor, where D^+ represents a fully ionized immobile positively charged donor atom and e^- represents a free negatively charged electron in conduction band of semiconductor. (b) Energy bands of a p-type semiconductor, where A^- represents a fully ionized immobile negatively charged acceptor atom and h^+ represents a free positively charged hole in valence band of semiconductor.

When a semiconductor comes in contact with a solution, electrostatic equilibrium is attained. This means that the Fermi level of both semiconductor and solution phase must at same energy level. The Fermi level of the solution is the electrochemical potential of electrons in the solution. It is usually reported with respect to a reference state (taken as a zero for free electron in a vacuum). The Fermi levels of the solid and solution phases become equal through heterogeneous charge transfer at solid/solution interface. When the Fermi level of the semiconductor is above the Fermi level of solution, electrons are transferred from conduction band of the semiconductor to the solution in order to achieve equilibrium (n-type semiconductor/liquid junction). This leads to an immobile positive charge accumulation inside the semiconductor near the semiconductor/solution interface and it is called space-charge region. This charge distribution is analogous to the charges found in double layer that is formed in the solution side of the semiconductor/solution junction or metal/solution interface. The charge accumulation in the semiconductor results in an electric field in the space charge region and directly affects the local energy (electrochemical potential) of electrons. This leads to upward semiconductor band bending as shown Figure 1-2 (a) with respect to the bulk semiconductor (field free region). When the Fermi level of the solution is above the Fermi level of the semiconductor, the electrons are transferred from the solution to the valence band of the semiconductor to achieve electrostatic equilibrium (p-type semiconductor/liquid junction). The charge re-

distribution (immobile negative charge inside semiconductor) and built-in electric field inside the semiconductor leads to downward band bending at the semiconductor/solution interface as shown Figure 1-2 (b) with respect to the bulk semiconductor (field free region). The above description is for an ideal semiconductor/solution interface where the Fermi level of the solution lies inside the semiconductor band gap. An ideal semiconductor/solution interface is analogous to semiconductor/metal interface (Schottky junction). For a better rectify junction between semiconductor and solution, the Fermi level of the solution (i.e. redox potential of redox species) must be closer to the valence band edge for n-type semiconductor/solution interface and closer to the conduction band edge for p-type semiconductor/solution interface. There are two major differences between a semiconductor/solution junction and a semiconductor/metal junction. First, unlike semiconductor/metal junction, semiconductor/solution junction can be used as a photovoltaic device (solution does not reflect light like a metal surface). Second, differences occur due to distribution of energy states, which is continuous in a metal whereas it is limited to a certain energy range in a redox system. The half-width of the density of occupied and empty states (Gaussian type distribution) of redox species is directly proposition to square root of reorientation energy of redox specie in solution.[1] The reorientation energy varies in the range of 0.5 to 2 eV,[2] the half-width can then be on the order of the semiconductor band gap. The consequence of this is that depending on the overlap of the energy states on the either side of the semiconductor/liquid interface, the charge transfer can either be via the conduction band or the valence band. This also determines whether a cell is a minority or majority carrier device, unlike, Schottky diode (semiconductor/metal junction) which is a majority carrier device (only majority carrier plays a significant role in conduction).

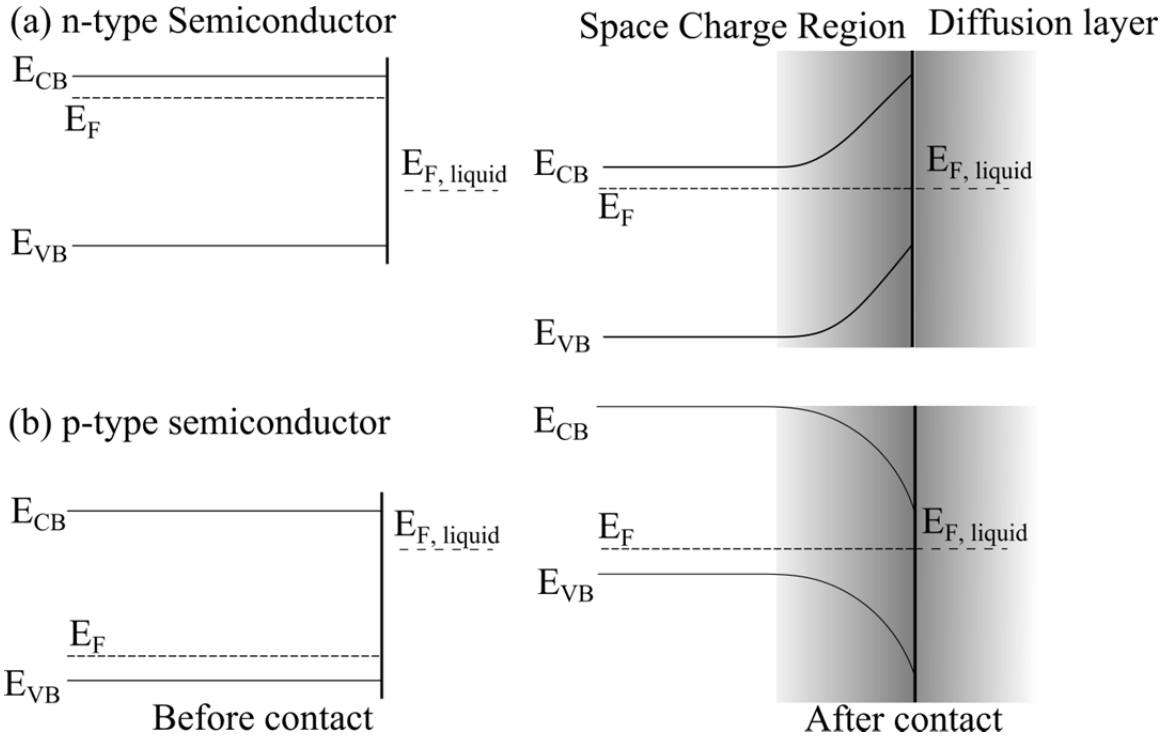

Figure 1-2. Semiconductor/liquid interface before (left hand side) and after (right hand side) contact (electrostatic equilibrium) for (a) n-type semiconductor and (b) p-type semiconductor.

The band bending in the semiconductor is such that the electrons move towards the bulk semiconductor and the holes move towards the interface in case of an n-type semiconductor/solution junction, whereas, in the case of a p-type semiconductor/solution junction, due to the built-in electric field, the holes move towards the bulk semiconductor and the electrons move towards interface. Under dark conditions, the space charge region (depending on doping level and band bending of semiconductor, it could be typically 5 to 200 nm wide) of the semiconductor is completely depleted of any free carrier. Under illumination, when the photon energy is greater than the semiconductor band gap. The absorption of a photon leads to the generation of an electron-hole pair. In the case of an n-type semiconductor/solution junction, the photo-generated holes are available at the interface to oxidize species in solution as shown in Figure 1-3(a). Similarly, in the case of a p-type semiconductor/solution junction, the photo-generated electrons are available at the interface to reduce the species in solution as shown in Figure 1-3(b).

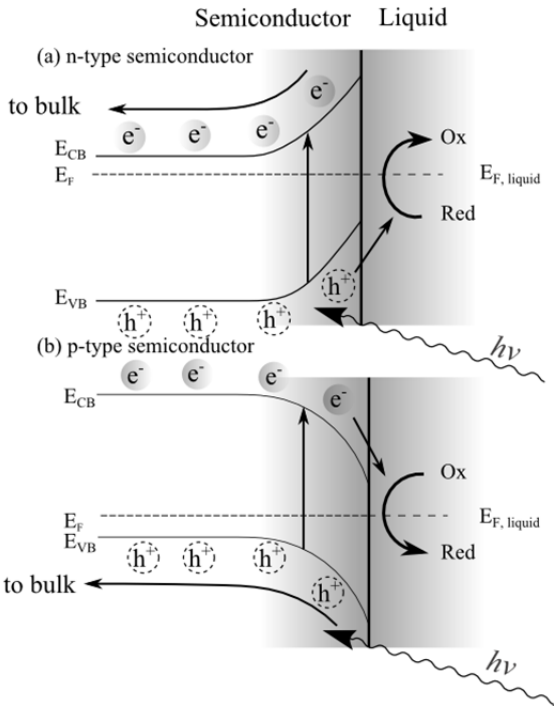

Figure 1-3. Photoelectrochemical oxidation and reduction of redox species in solution through (a) n-type semiconductor/liquid junction and (b) p-type semiconductor/liquid junction, respectively. Here, under illumination the electrons move towards the bulk and the holes towards interface for n-type semiconductor/liquid interface and in opposite direction for p-type semiconductor/liquid interface.

Photocurrent density and photovoltage are two critical parameters for an illuminated semiconductor/liquid interface. Kinetic limited counterpart of the photocurrent density and the photovoltage are the short circuit current density and the open circuit voltage, respectively. The open circuit voltage (V_{oc}) for an ideal semiconductor/solution junction should approach to the band gap of the semiconductor at high illumination intensity ($\leq$ 1 Wcm^{-2}). However, the finite bulk diffusion recombination, the surface states and other trap sites at the interface put an upper limit to the maximum V_{oc} that can be achieved for a semiconductor/solution junction.[3,4] The ideal current-voltage characteristic of a semiconductor/solution junction (similar to a pn junction diode) is given by following express under dark condition

$$J_{dark} = J_0 \left\{1 - \exp\left(\frac{-eV}{nkT}\right)\right\} \quad (1)$$

where J_0= exchange current density, V=applied potential, k=Boltzmann constant, and T= temperature n=ideality factor of a diode. Under illumination with the photon energy higher than that of the

semiconductor band gap, the current density-voltage characteristics of a semiconductor/solution junction is given as

$$J_{total} = J_{photo} + J_{dark} = J_{photo} + J_0 \left\{1 - \exp\left(\frac{-eV}{nkT}\right)\right\} \quad (2)$$

Under open circuit condition, the total current density (J_{total}) is zero. The equation (2) gives an express for open circuit potential (V_{OC}) in terms for photocurrent density,

$$V_{OC} = \frac{nkT}{e} ln\left(\frac{J_{photo}}{J_0}\right) \quad (3)$$

Here it is assumed that the exponential term in equation (2) is quite large compared to unity. The total/maximum photocurrent density at an illuminated p-semiconductor/liquid junction (assuming no recombination of photogenerated carriers within the diffusion layer and fast charge transfer between the semiconductor and redox species) is given as [5].

$$J_{photo} = eQ\left[1 - \frac{e^{(-\alpha W_S)}}{1 + \alpha Z_p}\right] + en_0\left(\frac{D_n}{Z_p}\right) \quad (4)$$

In this equation, Q = photon flux, α = absorption coefficient, W_S = depletion width, D_n = diffusion coefficient of the electron in the semiconductor, n_0 = equilibrium concentration of electrons, and Z_p = electron diffusion length in the semiconductor. From equations (3) and (4), it is obvious that both photocurrent density (linear) and open circuit voltage (logarithmic) depend on the illumination intensity. In solid state physics terminology, the open circuit voltage generated at a semiconductor rectifying junction is a measure of quasi-Fermi level splitting.[6] The quasi-Fermi level splitting is the difference between the holes and electrons quasi-Fermi levels under light illumination. In other words, the quasi-Fermi level splitting is the free energy difference between the majority carriers and the photo-generated minority carriers.[7] It is an individual description of the electrochemical potential of a type of charge carrier under non-equilibrium conditions (like illumination), using Fermi-Dirac statistics to separately describe electrons and holes populations.[8-10] With higher illumination flux, there would be higher number of minority carriers leading to larger quasi Fermi level splitting and consequently higher open circuit voltage at higher illumination intensity.[2] The quasi Fermi level splitting seems consistent with the equation (3). The next question is that whether it is possible to achieve a photovoltage equal to the semiconductor band gap. Ross

et al.[11,12] have derived a thermodynamic limit for highest photovoltage that can be achieved for a given semiconductor/solution junction. This theory is applicable to all types of photochemical solar energy conversion systems. According to this theory, there is a lower limit of a recombination rate which cannot be passed. This condition puts a limit to the maximum quasi Fermi level splitting that can be achieved and consequently maximum photovoltage that can be achieved for a given semiconductor/solution junction. The maximum photovoltage is always considerably smaller than the semiconductor band gap; for example, in case of GaAs (1.4 eV), the maximum photovoltage that can be achieved is only 0.9 eV.

Another critical parameter of a semiconductor/solution interface is the flat band potential (V_{fb}). The flat band potential is a forward biased applied potential at which there is no band bending (space charge region or built-in electric field) within the semiconductor at the semiconductor/solution interface. The flat band potential is also an in situ measure of the Fermi level of a semiconductor at a particular semiconductor/solution interface. With the knowledge of doping density, the band gap and the Fermi level of semiconductor; the positions of the conduction band and the valence band edge of a semiconductor at a particular semiconductor/solution interface can be calculated. A detailed description of the methods to experimentally measure the band edge positions of a semiconductor at a semiconductor/solution interface can be found in the thesis by Joseph Dee Beach Jr.[13]. Among all the methods, the Mott-Schottky plot method and the intensity modulated photo-current vs potential characteristics are the most popular methods. In the Mott-Schottky method, the total capacitance of a semiconductor/solution junction is measured with respect to an applied potential. The space-charge region capacitance is at least two to three times smaller in magnitude compared the capacitance of the Helmholtz and diffusion layer, which are in series. This means that most of the applied potential appears across depletion layer in the semiconductor. The measured capacitance for a semiconductor/solution junction is mainly corresponds to the space charge layer (depletion layer) capacitance (C_{SC}). The Mott-Schottky relationship for an n-type semiconductor/solution junction is given by

$$1/C_{SC}^2 = \frac{2}{N_D e \varepsilon_s}\left[\left(V - V_{fb}\right) - \frac{kT}{e}\right] \quad (5)$$

Where, N_D=donor density, V= applied potential, V_{fb}=flat band potential,ε_s= semiconductor permittivity and C_{SC}= capacitance of space charge region. The slope of the $1/C^2_{SC}$ vs V gives the doping level in the

semiconductor and the intercept with potential axis gives the flat band potential (V_{fb}) with respect to reference electrode used in the measurement. In the intensity modulated photocurrent vs potential method, linear scan voltammetry is used to obtain photocurrent vs voltage characteristics of semiconductor/solution junction under modulated light illumination (light chopping at certain frequency). The onset potential of the photocurrent in this case is taken as the flat band potential.[14-17] However, one must be careful when using this method because the potential measured is actually the potential at which the photocurrent and dark current are equal and opposite. Therefore, this method must be used with careful measurements of the dark current of the semiconductor/solution junction using the same potential range as the modulated photocurrent range.**Why CO_2 reduction is important and difficult?**

CO_2 is an extremely stable molecule generally produced by fossil fuel combustion and respiration. Returning CO_2 to a useful state by activation/reduction is a scientifically challenging problem, requiring appropriate catalysts and energy input. This poses several fundamental challenges in chemical catalysis, electrochemistry, photochemistry, and semiconductor physics and engineering. The thermodynamic potentials for various CO_2 reduction products are shown in equations 6 –10 (pH 7 in aqueous solution vs. Normal Hydrogen Electrode (NHE), 25°C, 1 atm gas pressure, and 1 M for other solutes) [18].

$$CO_2 + 2H^+ + 2e^- \rightarrow CO + H_2O \qquad E° = -0.53\ V \qquad (6)$$

$$CO_2 + 2H^+ + 2e^- \rightarrow HCO_2H \qquad E° = -0.61\ V \qquad (7)$$

$$CO_2 + 6H^+ + 6e^- \rightarrow CH_3OH + H_2O \qquad E° = -0.38\ V \qquad (8)$$

$$CO_2 + 8H^+ + 8e^- \rightarrow CH_4 + 2H_2O \qquad E° = -0.24\ V \qquad (9)$$

$$CO_2 + e^- \rightarrow CO_2^{\bullet -} \qquad E° = -1.90\ V \qquad (10)$$

Although CO_2 has been shown to be reduced directly on metal surfaces, the over potentials are either exceedingly high or the metal surfaces become poisoned and deactivated by the reduction products [19]. In addition to thermodynamic considerations, there are also considerable kinetic challenges to the conversion of CO_2 to more complex products. Typically, multiple proton-coupled electron transfer steps must be orchestrated with their own associated activation energies presenting kinetic barriers to the forward reaction. A great deal of success has been achieved in the reduction of CO_2 to products like CO and formate.[20] However, the multiple electron and proton transfers necessary to produce more useful products

such as methane or methanol have only been demonstrated with low efficiency.[20] To achieve success at efficient production of a CO_2 reduction product that can serve as a liquid fuel directly (i.e. methanol) would be a considerable milestone for renewable energy and energy storage research.

1.3 Molecular catalysis for CO_2 reduction

To overcome the thermodynamic barriers of CO_2 reduction, molecular catalysts can be used to lower the over potential by stabilizing the intermediate transition states between the linear CO_2 molecules and the intended product. CO_2 has multiple known binding modes to transition metal complexes.[21] The metal can then act as an inner sphere electron transfer agent to activate CO_2 for further transformation. With the choice of various metal centers and ligand structures, molecular catalysts are highly tunable to achieve the intended properties such as fast kinetics and long term stability. A recent review has discussed in detail the thermodynamics and kinetics of CO_2 binding to a metal center of a CO_2 reduction molecular catalysts.[22] In addition, molecular catalysts can also be helpful in lowering the kinetic barrier by providing some sort of proton relay mechanism (with the help of ligands) to successfully reduce CO_2 to liquid fuel like methanol. The performance of a molecular catalyst can be judged by the following figures of merit:

Faradaic Efficiency (FE) = (moles product/moles of electrons passed) x (number of electrons needed for conversion)

Overpotential = applied potential/thermodynamic potential for conversion at a given current density

Turn over number (TON) = moles product/moles catalyst

Catalytic Selectivity (CS) = moles product/(moles H_2+ moles other products)

Turn over frequency (TOF) = catalytic turnovers per unit time

Further information regarding molecular catalysts for CO_2 reduction can be found in recently published reviews. [18,23-26]

1.4 Photochemical and photoelectrochemical reduction of CO_2

There are several ways to reduce CO_2 with the assistance of renewable solar energy, and these methods can be divided into three major categories: homogeneous photoreduction by a molecular catalyst,

photoelectrochemical reduction by a semiconducting photocathode, and electrochemical reduction by an electrolyzer powered by commercial photovoltaic (PV) devices.

A homogeneous CO_2 photoreduction system consists of a molecular catalyst, light absorber, sacrificial electron donor, and/or electron relay. When looking at these types of systems, the main figure of merit is the photochemical quantum yield, defined as:

Photochemical quantum yield (Φ) = (moles products/absorbed photons) x (number of electrons needed for conversion)

In a heterogeneous system, p-type semiconductor/liquid junctions are extensively studied as PV devices. The p-type semiconducting electrodes can also act as photocathodes for photo-assisted CO_2 reduction. Figure 1-4 shows four different schemes of photo-assisted reduction of CO_2 using a semiconducting photocathode: (1) direct heterogeneous CO_2 reduction by a biased semiconductor photocathode [27-48], where the semiconductor acts both as light absorber and catalyst; (2) heterogeneous CO_2 reduction by metal particles on a biased semiconductor photocathode [28,35,37,49-57], where the semiconductor acts as a light absorber and the metal particle acts as a catalyst; (3) homogeneous CO_2 reduction by a molecular catalyst through a semiconductor/molecular catalyst junction [58-65], where the semiconductor acts as a light absorber and a molecular catalyst as a catalyst; and (4) heterogeneous CO_2 reduction by a molecular catalyst attached to the semiconductor photocathode surface[14,35,44,66,67], where the semiconductor acts as a light absorber and the surface attached molecular catalyst acts as a catalyst.

There are several examples where PV-powered commercial electrolyzers have been used for hydrogen generation[68-70], but very few of these setups exist for CO_2 reduction to energy dense products[71-74]. The idea to power an electrolyzer by a PV device was first proposed by Bard and Fox for a water splitting electrolyzer[75]. Recently, Delacourt et al. [76] reported a PV-powered electrolyzer that forms syngas (CO and H_2) from CO_2 and water.

For these different systems, the expressions for solar to chemical energy conversion efficiency are complicated because multiple products can form at the cathode and anode. In most cases, CO_2 photoelectrochemical reduction on photocathodes happens at high overpotentials, which further complicates this calculation. A detailed description of the different efficiency expressions for CO_2

photoelectrochemical reduction is provided in the next section. These equations can be used to calculate the efficiency for the following cell configurations: (a) a three-electrode cathodic half-cell reaction (Equation 11-13), (b) a two-electrode photoelectrochemical cell (PEC) (Equation 14), and (c) a two-electrode PV-powered electrolyzer (Equation 15).

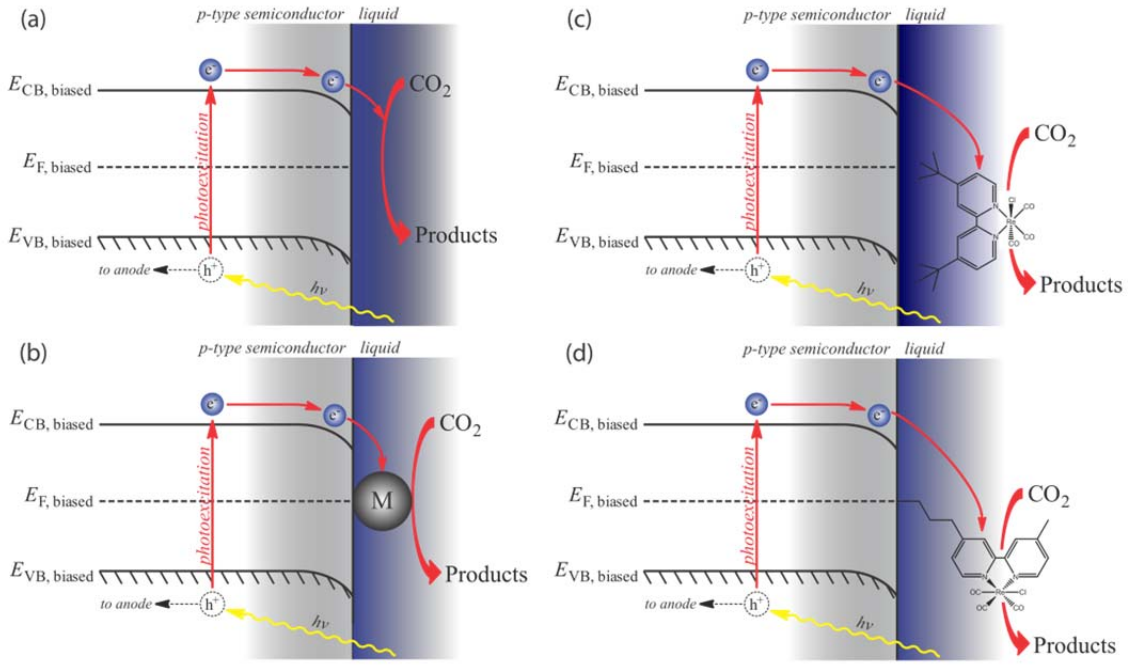

Figure 1-4. Schematic diagrams of four different schemes for light assisted CO_2 reduction of semiconducting photocathode; (a) heterogeneous catalysis on semiconductor electrode, (b) heterogeneous catalysis on metal decorated semiconductor electrode, (c) homogeneous catalysis through semiconductor/molecular catalyst junction, and (d) heterogeneous catalysis through molecular catalyst decorated semiconductor electrode.

1.5 Detailed solar to chemical conversion efficiency definitions for CO_2 reduction

The calculations for the solar to chemical energy conversion efficiency for CO_2 reduction is more complicated than water splitting due to multiple products that can be produced both at cathode and anode. In most of the cases, the CO_2 photoelectrochemical reduction on the semiconductor electrodes happens at a high over potential and this complicates the direct calculation of solar to chemical energy conversion efficiency for CO_2 photoelectrochemical reduction on the semiconductor electrodes. In a three electrode set-up for cathodic half reactions only, the total light to chemical energy conversion efficiency for CO_2 photoreduction is given by[58,64]

$$\eta = \frac{J_m\left[\sum_i \xi_i\left\{\left(\frac{\Delta H_i}{Z_i}\right) - V_{i,op}\right\}\right] - \{\text{IR loss}\}}{I_{h\nu}} \quad (11)$$

Where, J_m = catalytic current density, ξ_i = Faradaic efficiency, ΔH_i = heat of combustion, Z_i = number of electrons involved in the reduction, $V_{i,op}$ = over potential, IR loss= loss associated with non-Faradaic processes, and I_{hv} = incoming light intensity (power density). In the above approach, fuels produced as a result of CO_2 reduction are considered mainly as thermal combustion fuels. At very high over potentials, when $\Delta H_i/Z_i < V_{i,op}$, equation (11) will give a negative value. In that case, the power conversion efficiency is a better expression to evaluate the CO_2 photoreduction process and is given by [64,77,78]

$$\eta = \frac{J_m \sum_i \xi_i \left(\frac{\Delta H_i}{Z_i}\right)}{I_{h\nu} + J_m V_{i,op}} \quad (12)$$

All the symbols in above equations have same meaning as equation (11). Equation (12) represents the ratio of total combustible fuel energy produced as result of CO_2 reduction to the total energy spent (both light and electrical energy). This expression for power conversion efficiency will not give a negative value of efficiency as in the case with equation (11).

There is another approach used to calculate the light conversion efficiency for semiconductor/liquid junction solar cells and/or H_2 evolution semiconductor/liquid junctions.[7,79,80] In this case, the solar conversion efficiency can be calculated from the current-voltage curve when the photocurrent density is diffusion limited and not mass transport limited as shown in Figure 1-5. The conversion efficiency is given [3,4,7] as

$$\eta = \frac{J_m V_m}{I_{h\nu}} \quad (13a)$$

$$\text{Fill Factor (f.f)} = \frac{J_m V_m}{J_{sc} V_{oc}} \quad (13b)$$

where, J_m and V_m are current density and voltage at maximum power output. Another important parameter in this case is the Fill Factor [equation (13b)] which is the ratio of maximum power output to the products of short circuit current density (J_{sc}) and open circuit voltage (V_{oc}). In general, the Fill Factor characteristics of photoelectrochemical (PEC) cell is a measure of several properties of PEC like uncompensated cell

resistance, interface/surface recombination, and bulk recombination in a semiconductor.[4] Equation (13a) represents the part of the solar energy utilized for catalytic reduction of CO_2 on a semiconductor photocathode and the CO_2 reduction potential at a metal electrode (glassy carbon, Hg, In etc.) is taken as the zero potential in this case. A better approach would be to use a degenerated n+-type semiconductor (same kind as the photocathode) instead of a metal electrode for comparison as a dark electrode. Equation (13) is a suitable expression for describing a high over potential CO_2 reduction system half-cell reaction.

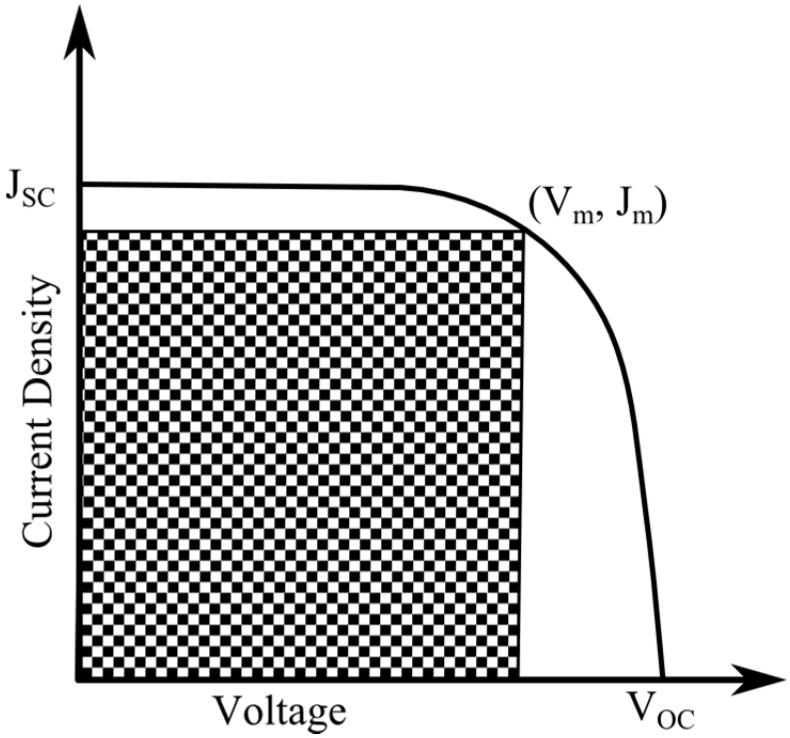

Figure 1-5. Typical current density-voltage characteristics of semiconductor/liquid junction half-cell where V_{OC} = open circuit potential, J_{SC}= short circuit current density, J_m= current density at maximum power point of current density-voltage curve and V_m= potential at maximum power point of current density-voltage curve.

In the two electrode set-up, assuming CO_2 reduction to CO at the cathode and oxygen generation at the anode with 100 % faradaic efficiency, solar conversion efficiency is given as

$$\frac{J_{mp}(1.33 - V_{app})}{P_{in}} \tag{14}$$

Where J_{mp} is the external measured current density, V_{app} is the external potential applied between cathode and anode and P_{in} is the optical power supplied. This is useful when two anode and cathode reactions are light driven and Vapp is smaller than 1.33 V. Similar expressions can be derived for other CO_2 reduction

products too. In case of the two electrodes electrolyzer set-up powered by a photovoltaic device, the total efficiency is a combination of the photovoltaic efficiency, faradaic efficiency of products, and voltage efficiency. The total efficiency is given by

$$\eta_{tot} = \eta_{PV} \sum_i \Phi_i \left(\frac{V_{therm,i}}{V_{op}}\right) \quad (15)$$

Where, η_{PV} is the photovoltaic device efficiency, Φ_i the faradaic efficiency of CO_2 reduction products, and $V_{therm,\ i}$ is the thermonuetral voltage of the product. Another approach is to consider the whole system (photovoltaic device and electrolyzer) as a single entity. The solar to chemical energy conversion efficiency, in this case, is defined as the chemical energy of products produced divided by the total incoming solar energy..

1.6 Photocatalytic semiconductor/molecular electrocatalyst junction

Heterogeneous photoelectrochemical reduction of CO_2 on semiconductor surfaces has been explored extensively in the last three decades.[20] Figure 1-6 shows the band edge positions vs. NHE (Normal of Hydrogen Electrode) for several common p- and n-type semiconductor electrodes with CO_2 reduction potentials for different products at pH=1. The single electron reduction of CO_2 to $CO_2^{\bullet-}$ is above the conduction band of most of the semiconductors shown in the Figure 1-6. Thermodynamically, proton-assisted multi-electron reduction potentials for CO_2 lie within the band gap of several semiconductors. However, kinetic limitations (managing multi-electron multi-proton processes) lead to high over potential for electrochemical reduction of CO_2 on semiconductor photocathodes or dark cathodes. Managing these multi-electron multi-proton processes requires a molecular electro-catalyst. Most molecular electro-catalysts for CO_2 reduction operate at a fixed pH, typically under acidic conditions.[18,23,25,26] For several semiconductors, the flat band potential is also a function of pH. The variation is typically 0.059 V/pH units in accordance with the Nernst equation and reflects a change in the voltage across the Helmholtz layer, which is particularly true for semiconductors like InP, GaAs, GaP, and TiO_2.[79,81] Despite this projected variation, the reduction potential of most molecular electrocatalysts might still be above the conduction band of p-type semiconductors. For ideal semiconductor/liquid junctions, the photo oxidation or photo reduction of a redox species is only possible if the redox potential lies inside the semiconductor band gap as

discussed in section 1.1. It has been shown before, however, that the photoreduction of species with redox potentials more negative than the conduction band edges of p-type semiconductors (Ge, Si, InP, GaAs) is feasible.[82-85] This phenomenon is explained by Fermi-level pinning and/or unpinning of the band edges, which causes the photovoltage observed for a p-type semiconductor/liquid junction to become independent of the redox potentials of the electro active species. This pinning leads to the photoreduction of a molecular electrocatalysts, even if the reduction is above the conduction band edge of the p-type semiconductor, which was shown for the p-Si/Re(bipy-But)$(CO)_3Cl$ molecular electrocatalyst junction.[59] It can be concluded that as long as the reduction potential of the molecular catalyst is above the valence band edge of the p-type semiconductor, the photoreduction of the molecular electrocatalyst is feasible. Fermi-level pinning also places a limitation on the maximum photovoltage/open circuit voltage for a particular semiconductor/molecular catalyst junction to one-half the band gap of the semiconductor.[82-85] The stability of the semiconductor photocathode can be further enhanced by surface modification, either by covalent attachment or coating the surface with polymer films of the molecular electrocatalyst.

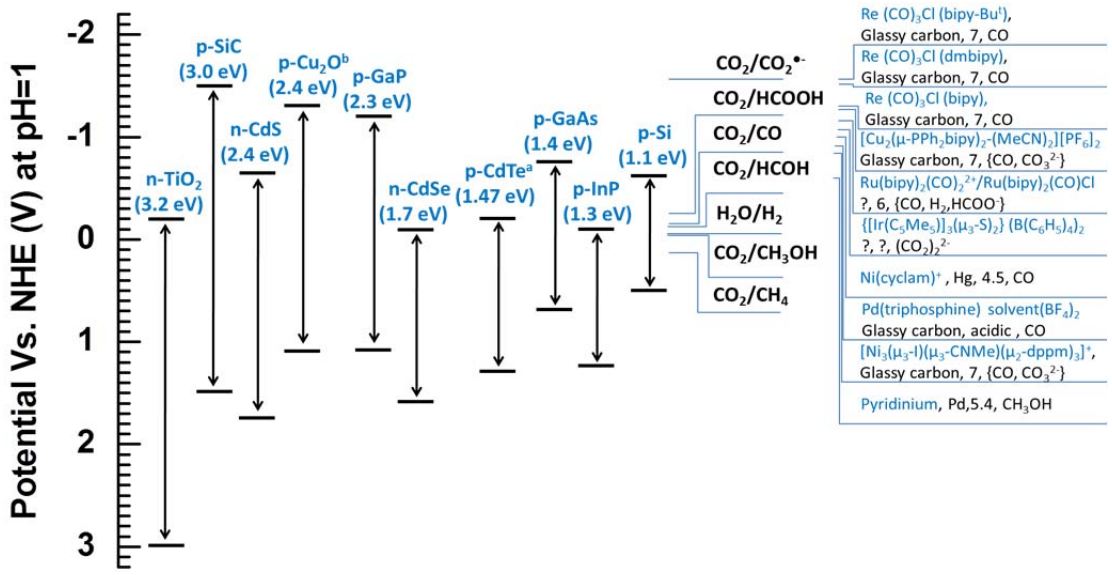

Figure 1-6. Position of conduction and valence band edge of several semiconductors at pH=1 shown vs. normal hydrogen electrode (NHE).[7,79] Thermodynamic potentials for CO_2 reduction to different products at pH=1 vs. NHE is shown beside the band edge positions of semiconductors. CO_2 reduction potentials of the homogeneous catalysts are shown at right hand side. Information presented here in the form of (catalyst, electrode used, pH, product), and detailed information about the homogeneous catalysts can be found in the references[18,23,26,58,86-93]. (*a*) Band edges for p-CdTe are given in reference[94]. (*b*) Band edges for p-Cu_2O are given in references[95,96].

Semiconductor/liquid junction photovoltaic devices and semiconductor/molecular catalyst junction photocatalytic device are two different systems as shown in Figure 1-7. In a photovoltaic semiconductor/liquid junction, there is only an electrochemical step involved and no chemical steps. However, in the photocatalytic semiconductor/molecular catalyst junction, there are chemical steps (like substrate binding and catalytic turn over) in addition to electrochemical steps depending upon the catalytic cycle of the molecular catalysts. For photovoltaic regenerative semiconductor/liquid junction, heterogeneous charge transfer between the semiconductor and the liquid phase as well as redox potential of the redox species are critical parameters. Usually well behaved completely reversible redox species are employed in photovoltaic regenerative semiconductor/liquid junction, so heterogeneous charge transfer is really fast. On the contrary, molecular electrocatalysts may or may not be completely reversible. Therefore, in photocatalytic semiconductor/molecular catalyst junction, either heterogeneous charge transfer or catalytic turn over frequency (catalytic cycle) could be the limiting factor. The photovoltaic regenerative semiconductor/liquid junction is usually analyzed under high concentration of redox specie (may be around 100 to 200 mM) and very fast stirring. The photocatalytic semiconductor/molecular catalyst is usually analyzed under low concentration (1 to 5 mM, depending on rate of catalysis and substrate concentration) and stirring without disturbing the molecular catalyst catalytic cycle. Suppose a system where molecular catalyst concentration is high, high speed stirring is employed, and molecular electrocatalyst has to go through more than one single electron electrochemical steps (heterogeneous charge between semiconductor and molecular catalyst); this system will not work as a photocatalytic system because at sufficiently high catalyst concentrations and stirring rates, the molecular catalyst would not be completely oxidized or reduced (to complete the catalytic cycle) before it moved away from diffusion layer. This type of system will be essential a photovoltaic semiconductor/liquid junction system.

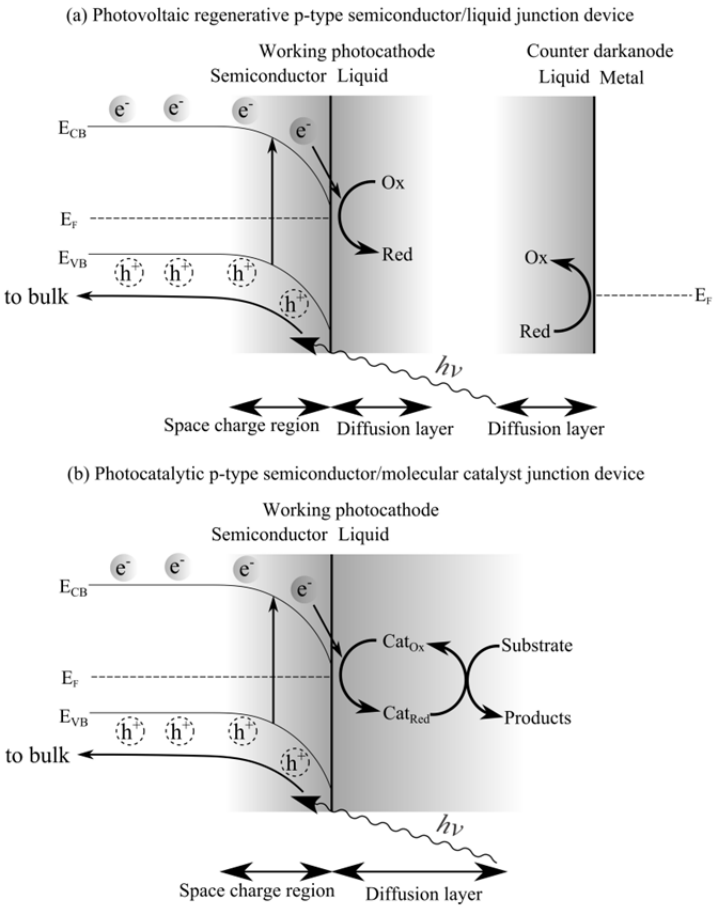

Figure 1-7. (a) Schematic representation of a photovoltaic regenerative p-type semiconductor/liquid junction device, where photo reduced redox specie is re-oxidized at counter metal electrode. (b) Schematic representation of a photocatalytic p-semiconductor/molecular catalyst junction device, where molecular catalyst is regenerated within the diffusion layer of photocathode under catalytic condition (catalyst regenerate itself at the end of catalysis).

Majority of the work reported in this dissertation is related to the semiconductor/molecular catalyst interface for CO_2 photoelectrochemical reduction. A complete literature review of CO_2 photoelectrochemical reduction via p-type semiconductor/molecular electrocatalyst interface is presented in the next section.

1.7 Photoelectrochemical reduction of CO_2 by semiconductor/molecular catalyst junction: a literature review

Bradley et al.[97] showed for the first time a stable photoelectrochemical reduction of tetraazomacrocyclic metal complexes (a CO_2 reduction catalyst) on a p-Si photocathode. For p-

Si/molecular electrocatalyst junctions, photovoltages of 350-400 mV were observed with light to electrical energy conversion efficiency of 0.5 to 1 % under non-catalytic conditions. These reduced tetraazomacrocyclic metal complexes were later shown to catalyze the photoreduction of CO_2 to CO on illuminated p-Si[65]. The highest efficiency achieved in this system (2 CO:1 H_2, FE = 95 ± 5 %) was obtained with 18 mM of $[(Me_6[14]aneN_4)Ni^{II}]^{2+}$ as a molecular catalyst in 1:1 acetonitrile-water solution with 0.1 M $LiClO_4$ as the supporting electrolyte. However, in completely dry acetonitrile with 0.1 M tetrabutyl ammonium perchlorate only an equimolar amount of CO and CO_3^{2-} was observed at -1.3 V vs. SCE. No information regarding illumination intensity or catalytic current density was provided, making it difficult to calculate efficiency.

Zafrir et al.[64] studied the vanadium V(II)/V(III) redox couple in a highly acidic aqueous medium[98,99] for photoreduction of CO_2 on a p-GaAs photocathode. V(II) does not electro-catalytically reduce CO_2, which resulted in poor FEs of less than 2 % [64]. Parkinson et al. [63] overcame this by introducing a formate dehydrogenase enzyme as a catalyst for CO_2 reduction to formate. In this work, the enzyme was used in conjunction with methyl viologen (MV) as an electron relay on a p-InP photoelectrode [63]. The advantages of a p-InP/(MV^{2+}/MV^{1+})/biological catalyst system are low overpotential for CO_2 reduction, selectivity, and excellent FE. The disadvantages of this system include instability of the formate hydrogenase enzyme and low efficiency.

Tinnemans et al.[100] reported CO_2 photoreduction by p-GaP/ and p-GaAs/tetraaza-macrocyclic Co(II) and Ni(II) junctions. However, no stable photoreduction of the catalysts was observed on p-GaP and no photovoltage was observed for the p-GaAs/catalyst junction. Beley et al. [62] and Petit et al. [61] also reported the photoreduction of CO_2 on p-GaAs and p-GaP photocathodes with $Ni(cyclam)^{2+}$ (cyclam=1,4,8,11-tetraazacyclotetradecane) as the molecular catalyst. A comprehensive review and further investigation was reported later by Petit et al. [60] on p-GaAs (111) and p-GaP (111)/$Ni(cyclam)^{2+}$ molecular catalyst junctions in aqueous media. CO_2 photoreduction with $Ni(cyclam)^{2+}$ on p-GaP was achieved as low as 200 mV below the thermodynamic potential for CO_2 to CO reduction, at -0.2 V vs. NHE. Selectivity of CO over H_2 was found to be between 1and 2 for p-GaAs and between 5and 10 for p-GaP with a FE of 80-100 % [60-62]. The difference in selectivity for p-GaAs and p-GaP could be due to their inherent surface

chemistry characteristics. The best performance was observed for 5 mM of catalyst at 20 $mWcm^{-2}$ light intensity, which was explained by the occupation of accessible sites on the semiconductor surface by $Ni(cyclam)^{2+}$ or other intermediate species. No efficiency data were provided for this case. More work is necessary to fully understand the potential of the p-type semiconductor/$Ni(cyclam)^{2+}$ system.

Barton et al.[58] reported another system consisting of a p-GaP (111) photocathode and a soluble pyridinium molecular catalyst for direct selective photoreduction of CO_2 to methanol at 300 mV of underpotential at pH 5.2 with 63-100 % FE. In this system, an overall conversion efficiency of 11 % was achieved using an illumination wavelength of 365 nm at 650 μWcm^{-2}. FE of methanol formation decreased and catalytic current density increased as the applied under potential decreased, which was explained by competing proton/water reduction processes. Apart from p-GaP, pyridinium was only active with platinum group metal electrodes, and inherently has low catalytic current density and FE for methanol formation.

On account of competing advantages of homogeneous catalysts (selectivity, tunability) and heterogeneous catalysts (robustness, easy separation of products from catalysts), there is considerable interest in "heterogenizing" homogeneous catalysts, by covalently linking them to surfaces. There have been several reports regarding surface modification of dark electrodes using the polymeric form of the molecular catalysts and/or enzymes for electrochemical reduction of CO_2 to various products [23,24,66,101-115]. These modified dark electrodes have several advantages: control over the active site environment for better performance [101,116], prevention of aggregation or dimerization of the molecular catalyst which leads to higher TONs [117], efficient charge transfer to the molecular catalyst, usability of water insoluble molecular catalysts in aqueous media once anchored to electrodes [118], and stabilization of the catalyst and electrode [119-122]. The physical nature of these junctions is similar to semiconductor/liquid junction with unbound molecular electrocatalysts [94]. Molecular catalyst surface modified semiconductors can be subdivided into two categories: (1) polymeric backbone attachment, and (2) direct anchoring to the semiconductor surface.

Aurian-Blajeni et al. [67] reported CO_2 photoreduction on polyaniline coated p-Si at -1.0 V vs. SCE in aqueous solution. In this report, formic acid and formaldehyde were formed with a FE of 20-30% after bulk electrolysis performed at -1.9 V vs. SCE, with power conversion efficiency of 3-4 %. Cabrera et al. [66] reported CO_2 photoreduction to CO by an electro-polymerized molecular catalyst ($Re(CO)_3$(4-vinyl,4'-

methyl-2,2'-bipyridine)Cl) on p-Si and p-WSe_2. A lower TON of 450 was reported compared to electro-polymerized molecular catalyst on a metal surface (600 for surface modified Pt) with FE of 100 %. No calculations for conversion efficiency were made, as no information was provided about the illumination intensity for these systems.

Arai et al. [14] reported CO_2 photoreduction to formate in an aqueous medium by a p-InP/ruthenium-complex polymer junction. The ruthenium-complex polymer (RCP) used was $[Ru(L\text{-}L)(CO)_2]_n$ (L-L=diimine ligand), which was previously reported as an electropolymerized catalyst (L-6) on Pt and vitreous carbon electrodes[109]. CO_2 photoreduction was achieved at a potential -800 mV less negative vs. glassy carbon/RCP [14]. The best FE (63 %) for formate production was obtained for p-InP/RCP junction prepared by a two-step polymerization of RCP [109], which stabilized the polymeric film when under a cathodic bias [109] and in aqueous media [14]. Low FE was reported in the above case due to competing H_2 and CO generation processes. No supporting electrolyte was added, which can result in high cell resistance and IR losses. Photoreduction of CO_2 to format is achieved by a two electrode set-up in a two compartment cell separated by a proton exchange membrane with the cathode being p-InP/RCP (CO_2 reduction) and the anode being TiO_2/Pt (water oxidation) in water as the solvent.[123] Later, similar approach is extended to the earth abundant material based semiconductors Cu_2ZnSnS_4 and $Cu_2ZnSn(S, Se)_2$.[17]

Unlike dark electrodes, there are not many reports of semiconductor photocathodes modified with polymeric films. This could be due to the absorption of incoming light as well as a high number of photogenerated-carrier trapping sites in the polymeric films.

To the best of our knowledge, there are no reports of photoelectrochemical CO_2 reduction by molecular catalysts directly attached to semiconductor surfaces. Recently, however, CO_2 reduction by molecular electrocatalysts/enzymes attached to semiconductor surface has been reported.[16,124-126] Two of these report the photocatalytic reduction of CO_2 to formate [16] or CO [125]. Both systems are analogous to homogeneous photocatalytic reduction of CO_2 by photosensitizers and molecular catalysts. In the above cases, the molecular catalyst is either adsorbed or electrostatically attached to the semiconductor surface. A recent theoretical study[126] has shown covalent bond formation between $Re(CO)_3Cl(dcbpy)$ (dcbpy=4,4′-

dicarboxy-2,2′-bipyridine) and the TiO_2 rutile (001) surface, but failed to recognize that $Re(CO)_3Cl(dcbpy)$ has no catalytic activity for CO_2 reduction.[93]

Substantially more effort in molecular catalysts covalently bound to semiconductor surfaces is needed, with special consideration given to the accessibility of the catalystic site and its structural/activity requirements. The large cathodic bias required for photoelectrochemical reduction of CO_2 can cause adsorbed or electrostatically attached molecular catalysts to detach from the semiconductor surface. Therefore, well-designed covalent attachment of the catalyst is imperative for the stability of this method.

Note: Some of the material in this chapter comes directly from a manuscript entitled, "Photochemical and photoelectrochemical reduction of CO_2" by Bhupendra Kumar, Mark Llorente, Jesse Froehlich, Tram Dang, Aaron Sathrum and Clifford P. Kubiak, which has been published in *Ann. Rev. Phys. Chem.* **2012**, *63,* 24.1-24.29.

1.8 References

(1) Memming, R. In *Photochemistry and Photophysics,* Rabek, J. F., Ed.; CRC press Taylor & Francis Group: 1989; Vol. II, chapter V.

(2) Fahrenbruch, A. L.; Bube, R. H. *Fundamentals of solar cells : photovoltaic solar energy conversion*; Academic Press: New York, 1983.

(3) Lewis, N. S. *Annu. Rev. Mater. Sci.* **1984**, *14*, 95.

(4) Lewis, N. S. *Acc. Chem. Res.* **1990**, *23*, 176.

(5) Soedergren, S.; Hagfeldt, A.; Olsson, J.; Lindquist, S.-E. *J. Phys. Chem.* **1994**, *98*, 5552.

(6) Tan, M. X.; Kenyon, C. N.; Lewis, N. S. *J. Phys. Chem.* **1994**, *98*, 4959.

(7) Walter, M. G.; Warren, E. L.; McKone, J. R.; Boettcher, S. W.; Mi, Q.; Santori, E. A.; Lewis, N. S. *Chem. Rev.* **2010**, *110*, 6446.

(8) Kenyon, C. N.; Tan, M. X.; Krüger, O.; Lewis, N. S. *J. Phys. Chem. B* **1997**, *101*, 2850.

(9) Krüger, O.; Kenyon, C. N.; Tan, M. X.; Lewis, N. S. *J. Phys. Chem. B* **1997**, *101*, 2840.

(10) Tan, M. X.; Kenyon, C. N.; Krüger, O.; Lewis, N. S. *J. Phys. Chem. B* **1997**, *101*, 2830.

(11) Ross, R. T.; Hsiao, T.-L. *J. Appl. Phys.* **1977**, *48*, 4783.

(12) Ross, R. T.; Collins, J. M. *J. Appl. Phys.* **1980**, *51*, 4504.

(13) Beach, J. D., Colorado School of Mines, 2001.

(14) Arai, T.; Sato, S.; Uemura, K.; Morikawa, T.; Kajino, T.; Motohiro, T. *Chem. Commun.* **2010**, *46*, 6944.

(15) Morikawa, T.; Saeki, S.; Suzuki, T.; Kajino, T.; Motohiro, T. *Appl. Phys. Lett.* **2010**, *96*, 142111.

(16) Sato, S.; Morikawa, T.; Saeki, S.; Kajino, T.; Motohiro, T. *Angew. Chem. Int. Ed.* **2010**, *49*, 5101.

(17) Arai, T.; Tajima, S.; Sato, S.; Uemura, K.; Morikawa, T.; Kajino, T. *Chem. Commun.* **2011**, *47*, 12664.

(18) Benson, E. E.; Kubiak, C. P.; Sathrum, A. J.; Smieja, J. M. *Chem. Soc. Rev.* **2009**, *38*, 89.

(19) Kedzierzawski, P.; Augustynski, J. *J. Electrochem. Soc.* **1994**, *141*, L58.

(20) Kumar, B.; Llorente, M.; Froehlich, J.; Dang, T.; Sathrum, A.; Kubiak, C. P. *Annu. Rev. Phys. Chem.* **2012**, *63*, 24.1.

(21) Leitner, W. *Coord. Chem. Rev.* **1996**, *153*, 257.

(22) Schneider, J.; Jia, H.; Muckerman, J. T.; Fujita, E. *Chem. Soc. Rev.* **2012**.

(23) Savéant, J.-M. *Chem. Rev.* **2008**, *108*, 2348.

(24) Collin, J. P.; Sauvage, J. P. *Coord. Chem. Rev.* **1989**, *93*, 245.

(25) Morris, A. J.; Meyer, G. J.; Fujita, E. *Acc. Chem. Res.* **2009**, *42*, 1983.

(26) Rakowski Dubois, M.; Dubois, D. L. *Acc. Chem. Res.* **2009**, *42*, 1974.

(27) Halmann, M. *Nature* **1978**, *275*, 115.

(28) Taniguchi, Y.; Yoneyama, H.; Tamura, H. *Bull. Chem. Soc. Jpn.* **1982**, *55*, 2034.

(29) Aurian-Blajeni, B.; Ahsan Habib, M.; Taniguchi, I.; Bockris, J. O. M. *J. Electroanal. Chem.* **1983**, *157*, 399.

(30) Canfield, D.; Frese, J. K. W. *J. Electrochem. Soc.* **1983**, *130*, 1772.

(31) K. W. Frese, J.; Canfield, D. *J. Electrochem. Soc.* **1984**, *131*, 2518.

(32) Taniguchi, I.; Aurian-Blajeni, B.; Bockris, J. O. M. *Electrochim. Acta* **1984**, *29*, 923.

(33) Yoneyama, H.; Sugimura, K.; Kuwabata, S. *J. Electroanal. Chem.* **1988**, *249*, 143.

(34) Bockris, J. O. M.; Wass, J. C. *J. Electrochem. Soc.* **1989**, *136*, 2521.

(35) Bockris, J. O. M.; Wass, J. C. *Mater. Chem. Phys.* **1989**, *22*, 249.

(36) Noda, H.; Yamamoto, A.; Ikeda, S.; Maeda, M.; Ito, K. *Chem. Lett.* **1990**, *19*, 1757.

(37) Junfu, L.; Baozhu, C. *J. Electroanal. Chem.* **1992**, *324*, 191.

(38) Ikeda, S.; Yamamoto, A.; Noda, H.; Maeda, M.; Ito, K. *Bull. Chem. Soc. Jpn.* **1993**, *66*, 2473.

(39) Hirota, K.; Tryk, D. A.; Yamamoto, T.; Hashimoto, K.; Okawa, M.; Fujishima, A. *J. Phys. Chem. B* **1998**, *102*, 9834.

(40) Hirota, K.; Tryk, D. A.; Hashimoto, K.; Okawa, M.; Fujishima, A. *J. Electrochem. Soc.* **1998**, *145*, L82.

(41) Hirota, K.; Tryk, D. A.; Hashimoto, K.; Okawa, M.; Fujishima, A. In *Stud. Surf. Sci. Catal.*; T. Inui, M. A. K. I. S. Y., Yamaguchi, T., Eds.; Elsevier: 1998; Vol. 114, p 589.

(42) Kaneco, S.; Katsumata, H.; Suzuki, T.; Ohta, K. *Chem. Eng. J.* **2006**, *116*, 227.

(43) Le, M.; Ren, M.; Zhang, Z.; Sprunger, P. T.; Kurtz, R. L.; Flake, J. C. *J. Electrochem. Soc.* **2011**, *158*, E45.

(44) Ono, H.; Yokosuka, A.; Tasiro, T.; Morisaki, H.; Yugo, S. *New Diamond Front. Carbon Technol.* **2002**, *12*, 141.

(45) Taniguchi, I.; Aurian-Blajeni, B.; Bockris, J. O. M. *J. Electroanal. Chem.* **1984**, *161*, 385.

(46) Taniguchi, I.; Aurian-Blajeni, B.; Bockris, J. O. M. *J. Electroanal. Chem. Inter. Electrochem.* **1983**, *157*, 179.

(47) Aurian-Blajeni, B.; Halmann, M.; Manassen, J. *Solar Energy Materials* **1983**, *8*, 425.

(48) Halmann, M.; Aurian-Blajeni, B. *J. Electroanal. Chem.* **1994**, *375*, 379.

(49) Hinogami, R.; Nakamura, Y.; Yae, S.; Nakato, Y. *J. Phys. Chem. B* **1998**, *102*, 974.

(50) Flaisher, H.; Tenne, R.; Halmann, M. *J. Electroanal. Chem.* **1996**, *402*, 97.

(51) Ikeda, S.; Saito, Y.; Yoshida, M.; Noda, H.; Maeda, M.; Ito, K. *J. Electroanal. Chem. Inter. Electrochem.* **1989**, *260*, 335.

(52) Noda, H. I., S.; Saito, Y.; Nakamura, T.; Maeda, M.; Ito, K. *Denki Kagaku* **1989**, *57*, 1117.

(53) Kaneco, S.; Katsumata, H.; Suzuki, T.; Ohta, K. *Applied Catalysis, B: Environmental* **2006**, *64*, 139.

(54) Kaneco, S.; Ueno, Y.; Katsumata, H.; Suzuki, T.; Ohta, K. *Chem. Eng. J.* **2009**, *148*, 57.

(55) Nakamura, Y.; Hinogami, R.; Yae, S.; Nakato, Y. In *Stud. Surf. Sci. Catal.*; T. Inui, M. A. K. I. S. Y., Yamaguchi, T., Eds.; Elsevier: 1998; Vol. Volume 114, p 565.

(56) Ikeda, S.; Yoshida, M.; Ito, K. *Bull. Chem. Soc. Jpn.* **1985**, *58*, 1353.

(57) Cottineau, T.; Morin, M.; Belanger, D. *ECS Transactions* **2009**, *19*, 1.

(58) Barton, E. E.; Rampulla, D. M.; Bocarsly, A. B. *J. Am. Chem. Soc.* **2008**, *130*, 6342.

(59) Kumar, B.; Smieja, J. M.; Kubiak, C. P. *J. Phys. Chem. C* **2010**, *114*, 14220.

(60) Petit, J.-P.; Chartier, P.; Beley, M.; Deville, J.-P. *J. Electroanal. Chem.* **1989**, *269*, 267.

(61) J.-P. Petit, P. C., M. Beley, and J.-P. Sauvage, *N. J. Chim.* **1987**, *11*, 751.

(62) Beley, M.; Collin, J.-P.; Sauvage, J.-P.; Petit, J.-P.; Chartier, P. *J. Electroanal. Chem.* **1986**, *206*, 333.

(63) Parkinson, B. A.; Weaver, P. F. *Nature* **1984**, *309*, 148.

(64) Zafrir, M.; Ulman, M.; Zuckerman, Y.; Halmann, M. *J. Electroanal. Chem.* **1983**, *159*, 373.

(65) Bradley, M. G.; Tysak, T.; Graves, D. J.; Viachiopoulos, N. A. *J. Chem. Soc., Chem. Commun.* **1983**, 349.

(66) Cabrera, C. R.; Abruña, H. D. *J. Electroanal. Chem.* **1986**, *209*, 101.

(67) Aurian-Blajeni, B.; Taniguchi, I.; Bockris, J. O. M. *J. Electroanal. Chem. Inter. Electrochem.* **1983**, *149*, 291.

(68) Bilgen, E. *Energy Convers. Manage.* **2001**, *42*, 1047.

(69) Gibson, T. L.; Kelly, N. A. *Int. J. Hydrogen Energy* **2010**, *35*, 900.

(70) Atlam, O.; Barbir, F.; Bezmalinovic, D. *Int. J. Hydrogen Energy* **2011**, *36*, 7012.

(71) Ogura, K.; Yamada, M.; Nakayama, M.; Endo, N. In *Stud. Surf. Sci. Catal.*; T. Inui, M. A. K. I. S. Y., Yamaguchi, T., Eds.; Elsevier: **1998**; Vol. Volume 114, p 207.

(72) Ogura, K.; Yoshida, I. *Electrochim. Acta* **1987**, *32*, 1191.

(73) Ogura, K.; Yoshida, I. *J. Mol. Catal.* **1986**, *34*, 309.

(74) Halmann, M.; Ulman, M.; Aurian-Blajeni, B. *Solar Energy* **1983**, *31*, 429.

(75) Bard, A. J.; Fox, M. A. *Acc. Chem. Res.* **1995**, *28*, 141.

(76) Delacourt, C.; Ridgway, P. L.; Kerr, J. B.; Newman, J. *J. Electrochem. Soc.* **2008**, *155*, B42.

(77) Ohashi, K.; McCann, J.; Bockris, J. O. M. *Nature* **1977**, *266*, 610.

(78) Noda, M. *Int. J. Hydrogen Energy* **1982**, *7*, 311.

(79) Nozik, A. J. *Annu. Rev. Phys. Chem.* **1978**, *29*, 189.

(80) Bookbinder, D. C.; Lewis, N. S.; Bradley, M. G.; Bocarsly, A. B.; Wrighton, M. S. *J. Am. Chem. Soc.* **1979**, *101*, 7721.

(81) Harris, L. A.; Wilson, R. H. *Annu. Rev. Mater. Sci.* **1978**, *8*, 99.

(82) Bard, A. J.; Bocarsly, A. B.; Fan, F. R. F.; Walton, E. G.; Wrighton, M. S. *J. Am. Chem. Soc.* **1980**, *102*, 3671.

(83) Bocarsly, A. B.; Bookbinder, D. C.; Dominey, R. N.; Lewis, N. S.; Wrighton, M. S. *J. Am. Chem. Soc.* **1980**, *102*, 3683.

(84) Fan, F. R. F.; Bard, A. J. *J. Am. Chem. Soc.* **1980**, *102*, 3677.

(85) Nagasubramanian, G.; Wheeler, B. L.; Bard, A. J. *J. Electrochem. Soc.* **1983**, *130*, 1680.

(86) Beley, M.; Collin, J. P.; Ruppert, R.; Sauvage, J. P. *J. Am. Chem. Soc.* **1986**, *108*, 7461.

(87) Ishida, H.; Tanaka, K.; Tanaka, T. *Organometallics* **1987**, *6*, 181.

(88) Haines, R. J.; Wittrig, R. E.; Kubiak, C. P. *Inorg. Chem.* **1994**, *33*, 4723.

(89) Kushi, Y.; Nagao, H.; Nishioka, T.; Isobe, K.; Tanaka, K. *J. Chem. Soc., Chem. Commun.* **1995**, 1223.

(90) Tanaka, K.; Kushi, Y.; Tsuge, K.; Toyohara, K.; Nishioka, T.; Isobe, K. *Inorg. Chem.* **1998**, *37*, 120.

(91) DuBois, D. L.; Miedaner, A.; Haltiwanger, R. C. *J. Am. Chem. Soc.* **1991**, *113*, 8753.

(92) Morgenstern, D. A.; Wittrig, R. E.; Fanwick, P. E.; Kubiak, C. P. *J. Am. Chem. Soc.* **1993**, *115*, 6470.

(93) Smieja, J. M.; Kubiak, C. P. *Inorg. Chem.* **2010**, *49*, 9283.

(94) Kumar, A.; Wilisch, W. C. A.; Lewis, N. S. *Crit. Rev. Solid State Mater. Sci.* **1993**, *18*, 327

(95) Bak, T.; Nowotny, J.; Rekas, M.; Sorrell, C. C. *Int. J. Hydrogen Energy* **2002**, *27*, 991.

(96) Roy, S. C.; Varghese, O. K.; Paulose, M.; Grimes, C. A. *ACS Nano* **2010**, *4*, 1259.

(97) Bradley, M. G.; Tysak, T. *J. Electroanal. Chem.* **1982**, *135*, 153.

(98) Heller, A.; Miller, B.; Lewerenz, H. J.; Bachmann, K. J. *J. Am. Chem. Soc.* **1980**, *102*, 6555.

(99) Heller, A.; Lewerenz, H. J.; Miller, B. *J. Am. Chem. Soc.* **1981**, *103*, 200.

(100) Tinnemans, A. H. A.; Koster, T. P. M.; Thewissen, D. H. M. W.; Mackor, A. *Recl. Trav. Chim. Pays-Bas* **1984**, *103*, 288.

(101) Lieber, C. M.; Lewis, N. S. *J. Am. Chem. Soc.* **1984**, *106*, 5033.

(102) Stalder, C. J.; Chao, S.; Wrighton, M. S. *J. Am. Chem. Soc.* **1984**, *106*, 3673.

(103) O'Toole, T. R. M., L. D.; Westmoreland, T. D.; Vining,W. J.; Murray, R. W.; Meyer,T. J. *J. Chem. Soc., Chem. Commun.* **1985**, 2.

(104) Cosnier, S.; Deronzier, A.; Moutet, J.-C. *J. Mol. Catal.* **1988**, *45*, 381.

(105) O'Toole, T. R.; Sullivan, B. P.; Bruce, M. R. M.; Margerum, L. D.; Murray, R. W.; Meyer, T. J. *J. Electroanal. Chem.* **1989**, *259*, 217.

(106) Chardon-Noblat, S.; Collomb-Dunand-Sauthier, M. N.; Deronzier, A.; Ziessel, R.; Zsoldos, D. *Inorg. Chem.* **1994**, *33*, 4410.

(107) Collomb-Dunand-Sauthier, M.-N.; Deronzier, A.; Ziessel, R. *Inorg. Chem.* **1994**, *33*, 2961.

(108) Ramos Sende, J. A.; Arana, C. R.; Hernandez, L.; Potts, K. T.; Keshevarz-K, M.; Abruna, H. D. *Inorg. Chem.* **1995**, *34*, 3339.

(109) Chardon-Noblat, S.; Deronzier, A.; Ziessel, R.; Zsoldos, D. *J. Electroanal. Chem.* **1998**, *444*, 253.

(110) Ziessel, R. In *Stud. Surf. Sci. Catal.*; T. Inui, M. A. K. I. S. Y., Yamaguchi, T., Eds.; Elsevier: 1998; Vol. Volume 114, p 219.

(111) Cecchet, F.; Alebbi, M.; Bignozzi, C. A.; Paolucci, F. *Inorg. Chim. Acta* **2006**, *359*, 3871.

(112) Parkin, A.; Seravalli, J.; Vincent, K. A.; Ragsdale, S. W.; Armstrong, F. A. *J. Am. Chem. Soc.* **2007**, *129*, 10328.

(113) Cheung, K.-C.; Guo, P.; So, M.-H.; Lee, L. Y. S.; Ho, K.-P.; Wong, W.-L.; Lee, K.-H.; Wong, W.-T.; Zhou, Z.-Y.; Wong, K.-Y. *J. Organomet. Chem.* **2009**, *694*, 2842.

(114) Smith, R. D. L.; Pickup, P. G. *Electrochem. Commun.* **2010**, *12*, 1749.

(115) Abe, T.; Kaneko, M. *Prog. Polym. Sci.* **2003**, *28*, 1441.

(116) Abe, T.; Yoshida, T.; Tokita, S.; Taguchi, F.; Imaya, H.; Kaneko, M. *J. Electroanal. Chem.* **1996**, *412*, 125.

(117) Chen, Z.; Concepcion, J. J.; Jurss, J. W.; Meyer, T. J. *J. Am. Chem. Soc.* **2009**, *131*, 15580.

(118) Yoshida, T.; Tsutsumida, K.; Teratani, S.; Yasufuku, K.; Kaneko, M. *J. Chem. Soc., Chem. Commun.* **1993**, 631.

(119) Dominey, R. N.; Lewis, N. S.; Bruce, J. A.; Bookbinder, D. C.; Wrighton, M. S. *J. Am. Chem. Soc.* **1982**, *104*, 467.

(120) Wrighton, M. S. *J. Chem. Educ.* **1983**, *60*, 335.

(121) Wrighton, M. S. *Science* **1986**, *231*, 32.

(122) Lewis, N. S. *Inorg. Chem.* **2005**, *44*, 6900.

(123) Sato, S.; Arai, T.; Morikawa, T.; Uemura, K.; Suzuki, T. M.; Tanaka, H.; Kajino, T. *J. Am. Chem. Soc.* **2011**, *133*, 15240.

(124) Huang, J.; Stockwell, D.; Huang, Z.; Mohler, D. L.; Lian, T. *J. Am. Chem. Soc.* **2008**, *130*, 5632.

(125) Woolerton, T. W.; Sheard, S.; Reisner, E.; Pierce, E.; Ragsdale, S. W.; Armstrong, F. A. *J. Am. Chem. Soc.* **2010**, *132*, 2132.

(126) Anfuso, C. L.; Snoeberger, R. C.; Ricks, A. M.; Liu, W.; Xiao, D.; Batista, V. S.; Lian, T. *J. Am. Chem. Soc.* **2011**, *133*, 6922.

2 Chapter 2

Selective photoelectrochemical reduction of CO_2 to CO by using p-Si/ Re-(bipy-*t*Bu)$(CO)_3$Cl (bipy-*t*Bu = 4,4'-di-*tert*-butyl-2,2'-bipyridine) molecular electrocatalyst junction

2.1 General Introduction

The quest for a renewable energy source has become increasingly important in recent years due to the increase in CO_2 emissions and the impending peak of worldwide oil production. Recently, CO_2 capture and subsequent reduction to value added products and liquid fuels has gained interest as a potential technology to recycle atmospheric CO_2.[1] CO_2 is a highly stable molecule and its reduction/activation requires both appropriate catalysts and significant energy input. The challenges of CO_2 reduction have been discussed in several recent reviews.[2-6] Among the more feasible approaches, the conversion of CO_2 to CO is a proton-coupled multi-electron reduction, which is thermodynamically more favorable than the single electron reduction to the radical anion.[7,8] CO and water can be used to produce synthesis gas via the water-gas shift reaction, which can then be used to produce liquid transportation fuels (via Fischer-Tropsch synthesis).

p-type Silicon (Si) is a proven photocathode for water reduction to hydrogen where part of the energy required for the reduction comes from light.[9-11] If a reliable method is developed for CO_2 photoreduction on p-type Si, it may be feasible to produce synthesis gas using sun light on p-type Si. There have been a few reports on the reduction of CO_2 on p-type Si surfaces with metal nanoparticles,[12,13] under high pressures of CO_2,[14] on a polymeric surface modified p-type Si,[15,16] and at a p^+/p-Si junction[17]. Each of these approaches has its own advantages and disadvantages.

Rhenium metal catalysts with bipyridine ligands are known for their ability to catalyze the reduction of CO_2 to CO. The first published catalyst of this type was Re(bipy)$(CO)_3$Cl (**1**) (bipy = 2,2'-bipyridine).[18-20] It operated at a moderate overpotential, with a high turnover number and modest turnover frequency. A similar complex, Re(bipy-*t*Bu)$(CO)_3$Cl (**2**) (bipy-*t*Bu = 4,4'-di-*tert*-butyl-2,2'-bipyridine), was studied for its photo physical properties by Cheung and co-workers[21], but not as an electrocatalyst. Our group recently completed a systematic comparative study of **1** and **2** for CO_2 reduction to CO and

found that **2** had better electrocatalytic activity compared to **1** while operating at only 100 mV more overpotential. A detailed study of catalytic properties of **2** including the synthesis and mechanism of CO_2 reduction has been recently published.[22] Based on that study, we chose **2** as the homogenous catalyst for this study.

Hydrogen terminated silicon (H-Si) has excellent physical and electrical properties with low surface recombination velocity, but H-Si surfaces are short lived due to oxidation in air and water.[23,24] p-type H-Si was chosen as the photocathode for this work due to its low surface recombination velocity and its stability under reducing conditions in deoxygenated acetonitrile. In this chapter, homogeneous electrocatalyst mediated selective photoelectrochemical reduction of CO_2 to CO is reported on p-type H-Si/Re(bipy-tBu)$(CO)_3$Cl molecular electrocatalyst rectifying junction as shown in Figure 2-1.

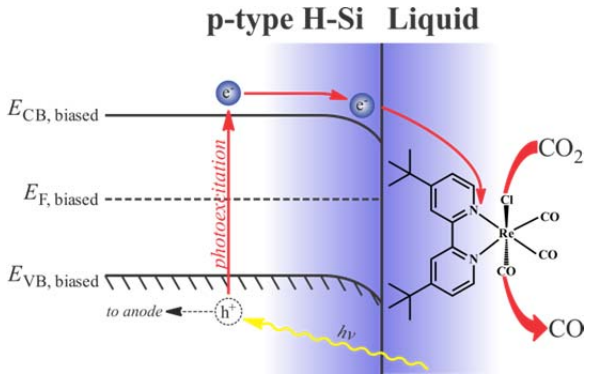

Figure 2-1. Schematic representation of homogeneous catalytic photoelectrochemical reduction of CO_2 to CO by p-type H-Si/Re(bipy-tbu)$(CO)_3$Cl.

2.2 Experimental Section

2.2.1 General Considerations

Prime (111) p-type silicon with a resistivity of 1-100 ohm.cm was purchased from the Ultrasil corporation. Solvents were dried by a custom dry solvent system and were purged with argon before use. Tetrabutylammonium hexafluorophosphate was recrystallized from methanol and dried under vacuum at 80 ºC. Re(bipy-tBu)$(CO)_3$Cl was synthesized by the method described in the literature.[22] The photoelectrochemical (PEC) cell used for electrochemical measurement was designed by the author. A

schematic of PEC cell without cap is shown in Figure 2-2 and micrograph of cell cap is shown in Figure 2-3, which contains a dark electrode, a common reference (Ag/AgCl) and counter electrode (Pt).

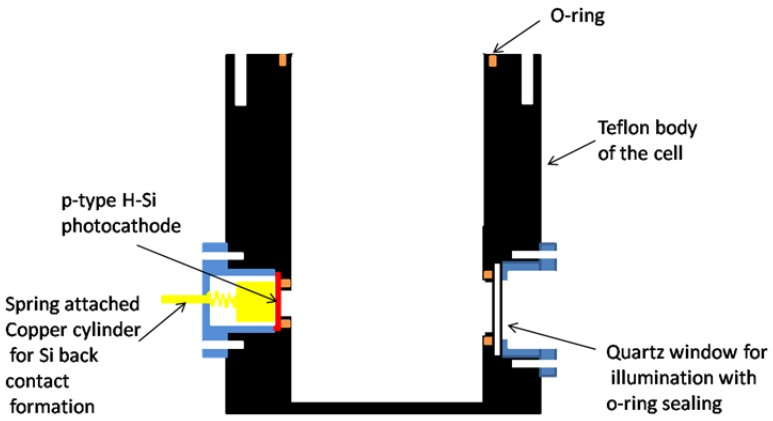

Figure 2-2. Schematic diagram of photoelectrochemical (PEC) cell without the cap.

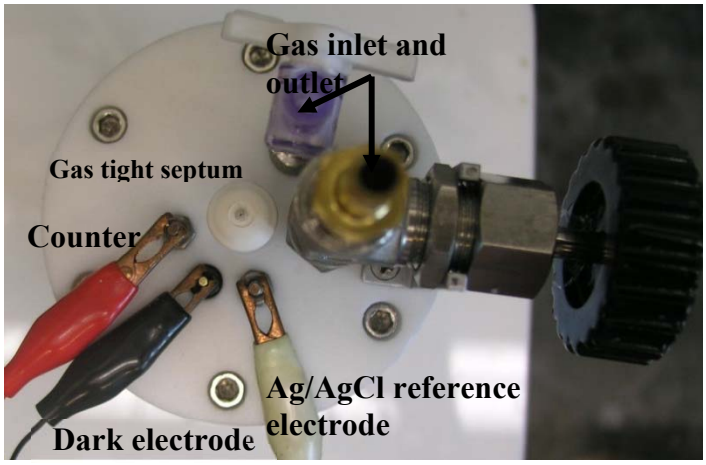

Figure 2-3. Photograph of PEC cell cap with all parts indicated.

Polychromatic illumination was achieved using a Dolan-Jenner MI-150 fiber optic illuminator with quartz halogen lamp and IR filter (cut-off wavelength = 1000 nm). Illumination power measurements were made using an OPHIR 30A-SH-V1 thermopile head and OPHIR NOVA II power monitor/meter. A 661 nm laser diode (ML101J27) was used as a monochromatic light source. The laser diode was controlled by LDC240C laser driver purchased from Thorlabs. The laser power was calibrated using an OPHIR PD300-3W-V1 photodetector and OPHIR NOVA II power monitor/meter. Gaseous products were

identified and quantified by Agilent technologies 7890A gas chromatograph with a mole sieve column and TCD detector**.**

2.2.2 Hydrogen Termination of p-type Si

A 100 mm diameter p-type silicon wafer was first cut into 1 cm^2 pieces and all silicon shreds were cleaned in freshly prepared 3:1 H_2SO_4:H_2O_2 (caution: potentially explosive) for 30 minutes and then rinsed with deionized (DI) water. Hydrogen termination of p-type Si was achieved by submersion of freshly cleaned 1 cm^2 pieces of Si in deoxygenated 40% NH_4F solution under argon for 20 minutes, followed by copious rinsing with deoxygenated DI water.

2.2.3 Electrochemical Studies

Freshly prepared hydrogen terminated Si (H-Si) electrodes made by the above method were immediately fitted into an argon filled Teflon PEC cell. An ohmic contact was made by scratching the back of Si wafer and immediately applying Indium-Gallium (In-Ga) eutectic. The intensity of light from the fiber optic illuminator was measured by the thermopile head by replacing the H-Si sample with a quartz window. All electrochemical measurements were performed with a BASi EC Epsilon instrument using a three electrode configuration containing an Ag/AgCl pseudo reference, a platinum wire as counter electrode, and either a platinum disc working electrode with a diameter of 0.2 cm or a H-Si working electrode with an exposed diameter of 0.59 cm. The electrolyte in all experiments was 0.1 M tetrabutyl ammonium hexafluorophosphate (TBAH) and experiments were carried out in dry acetonitrile. A 6 mM solution of **2** was used in all electrochemical measurements unless stated otherwise. All cyclic voltammograms were taken at a scan rate of 100 mVs^{-1} unless otherwise stated. iR compensation was used for all the CO_2 reduction experiments on p-type H-Si due to large current and high iR losses, similar to the technique reported by Hinogami et al. for CO_2 reduction.[12]

2.3 Results and Discussion

Cyclic voltammetry (CV) measurements of **2** under an atmosphere of argon gives two reduction waves on both illuminated H-Si and Pt electrodes. On a Pt electrode, the cathodic peak potential of the first reduction (a) at -1440 mV (Vs Ag/AgCl) is quasi-reversible and represents a ligand-based reduction, and

the second reduction (b) exhibits a peak current at -1910 mV (Vs Ag/AgCl), is partially reversible, and represents a metal based reduction as shown in Figure 2-4.[22] These two reduction waves appeared at more positive potentials on illuminated H-Si electrode compared to a Pt electrode as shown in Figure 2-4. The photovoltages observed on the illuminated H-Si electrode were 530 ± 10 mV and 580 ± 30 mV for the 1st and 2nd reductions, respectively.

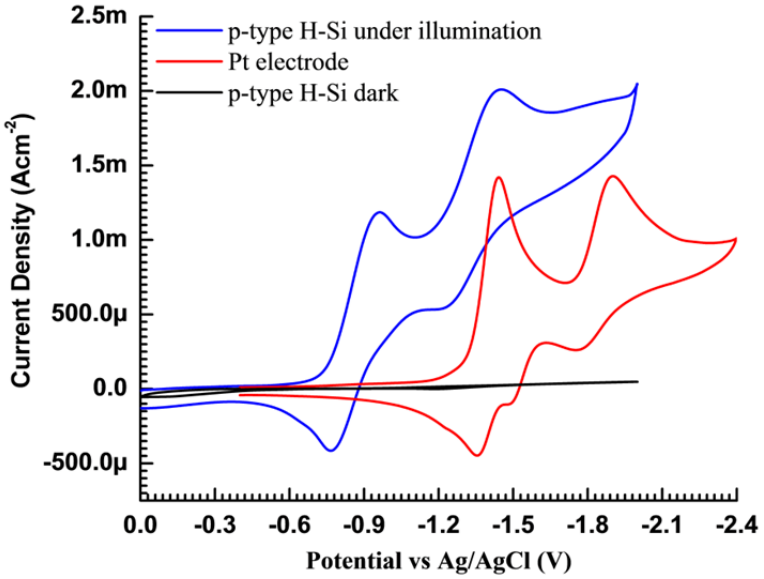

Figure 2-4. Cyclic voltammograms of Re(bipy-tBu)$(CO)_3$Cl (2) under illumination (blue) and dark (black) on p-type H-Si and Pt electrodes (red).

The positions of the conduction band and valence band edge of p-type Si in acetonitrile are -850 mV and +270 mV with respect to the saturated calomel electrode (SCE).[11,25] The positions of the first and second reduction on Pt were found to be ca. -1480 mV and ca. -2000 mV with respect to SCE. A schematic diagram of band edge positions and redox potentials before and after the silicon and **2** come in contact is shown Figure 2-5 (a) and (b).

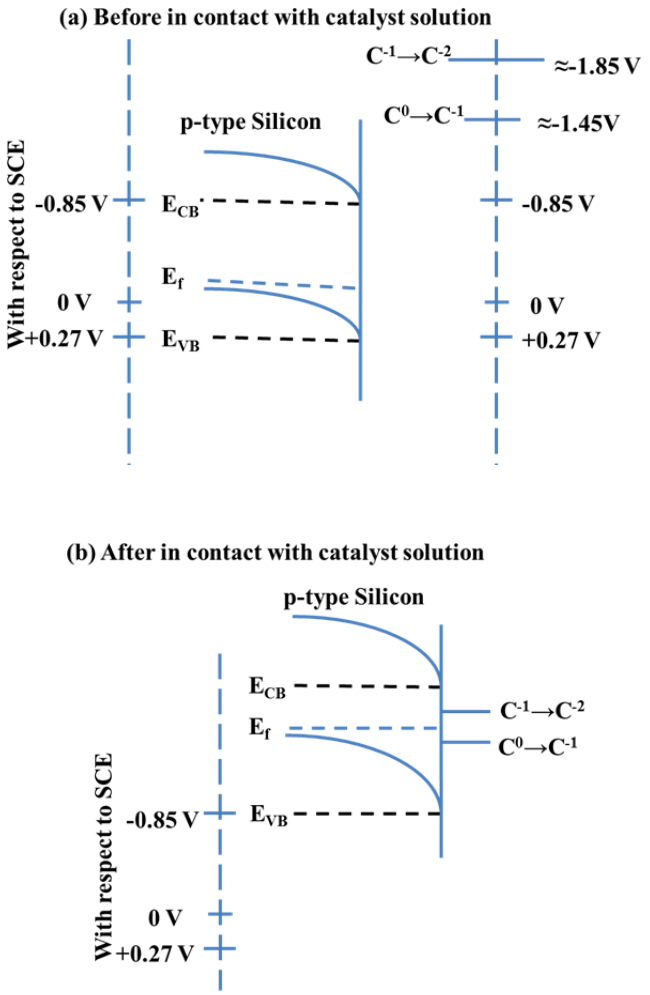

Figure 2-5. A Schematic representation of band edge position of p-type Silicon in acetonitrile with tetraethyl ammonium perchlorate (TEAP) where E_{CB}, E_F, and E_{VB} are conduction band edge, Fermi level and valence band edge of Si (a) before come in contact with catalyst[25] and (b) after come in contact with catalyst. Here, C^0 to C^{-1} is 2's first reduction and C^{-1} to C^{-2} is 2's second reduction.[22]

The positions of the reductions for **2** are above the conduction band edge of silicon, which implies that catalyst reduction should not be feasible on p-type Si. It has been shown that the reduction of species with redox potentials more negative than the conduction band edge of p-type Si can be achieved.[11,25,26] This phenomenon is explained based on Fermi-level pinning/unpinned band edges. In Fermi level pinning, surface states pin the Fermi level at the center or middle of the band gap and charge transfer between the redox species and electrode proceeds through surface states.[11,26] In the unpinned band edge phenomenon, the band edges of a semiconductor move with applied potential, making the semiconductor electrode

behave similarly to a metal electrode.[25] The main consequence of Fermi level pinning/unpinning of band edges is that the photovoltage achieved on p-type Si/semiconductors becomes independent of the redox potentials of the electro-active species. This would explain the photoreduction of the catalyst on p-type H-Si under illumination. The apparent difference in photovoltage for the 2nd reduction compared to the 1st reduction cannot be explained based on the Fermi level pinning or unpinning of band edges. This difference could be explained by the irreversible nature of 2nd reduction or adsorption of the catalyst on the H-Si surface. However, the peak current densities of both reductions of **2** on illuminated p-type H-Si were directly proportional to the square root of the scan rate as shown in Figure 2-6 over the range of 50 to 4000 mVs^{-1}. This implies a mass transport controlled current and no adsorption of **2** on the H-Si surface.

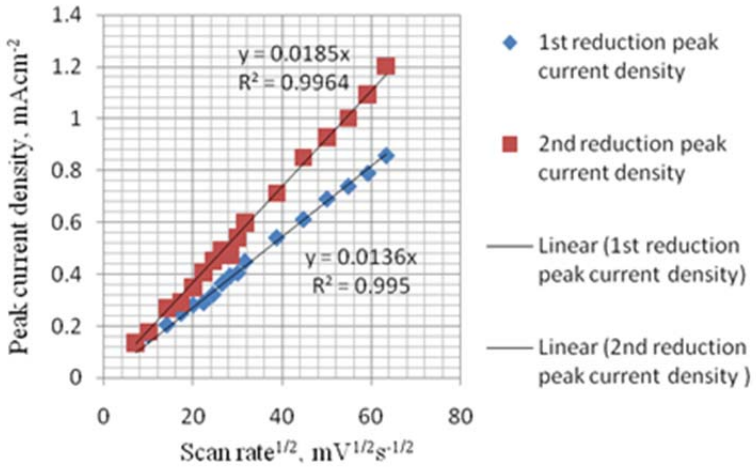

Figure 2-6. Scan rate dependence of peak current densities of 1st and 2nd reductions of 2 on illuminated p-type H-Si.

Cyclic voltammograms of **2** in Ar and CO_2 saturated acetonitrile on a Pt electrode and a p-type H-Si photocathode under illumination are shown in Figure 2-7. A substantial increase in photocurrent for the second reduction on the p-type H-Si photocathode under CO_2 is indicative of catalytic CO_2 reduction and formation of CO was confirmed by gas chromatography (GC). CO_2 reduction to CO is a two electron process, requiring a doubly-reduced catalyst[22] so it is expected at the second reduction wave. Photovoltages for the 1st and 2nd reductions on the illuminated H-Si photocathode under a saturated CO_2 environment were similar to those observed under an argon environment.

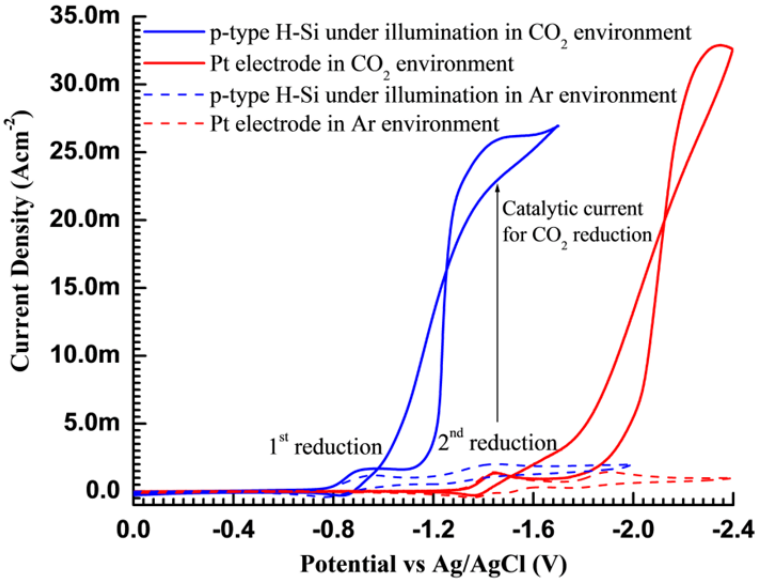

Figure 2-7. Cyclic voltammograms of Re(bipy-tBu)$(CO)_3Cl$ (2) under CO_2 and Ar atmospheres on p-type H-Si photocathode (blue) and Pt electrodes (red).

The Faradaic efficiency for the photoreduction of CO_2 was measured by running a controlled potential electrolysis with stirring at a potential 20-30 mV more negative than the 2nd reduction using a 0.8 mM solution of **2** under CO_2 on p-type H-Si without iR compensation. The number of moles of electrons (N_e) was calculated from the amount of current passed during electrolysis and the number of moles of CO (n) produced was calculated from the integrated area of the CO peak in the gas chromatogram. The number of the moles of electrons had a linear relationship with the amount of CO produced with slope of 2.015 as shown in Figure 2-8 and the Faradaic efficiency in this case was calculated to be 97 ± 3 %. This demonstrates that the electrical to chemical energy conversion efficiency for the photoreduction of CO_2 on the H-Si photocathode is quantitative, within the experimental error. Bipy-supported rhenium catalysts are also known for their photocatalytic activity.[19,27] However, no CO was detected under the conditions above in the absence of an applied potential to the H-Si photocathode. The bulk electrolysis lasted more than 3 hours and at the end of that time both the H-Si and catalyst **2** were fully functional. This shows that the H-Si photocathode is highly durable under the conditions described above for CO_2 to CO reduction. With its

ease of fabrication, the combination of the p-type H-Si and a homogeneous Re catalyst is a viable candidate for photoreduction of CO_2.

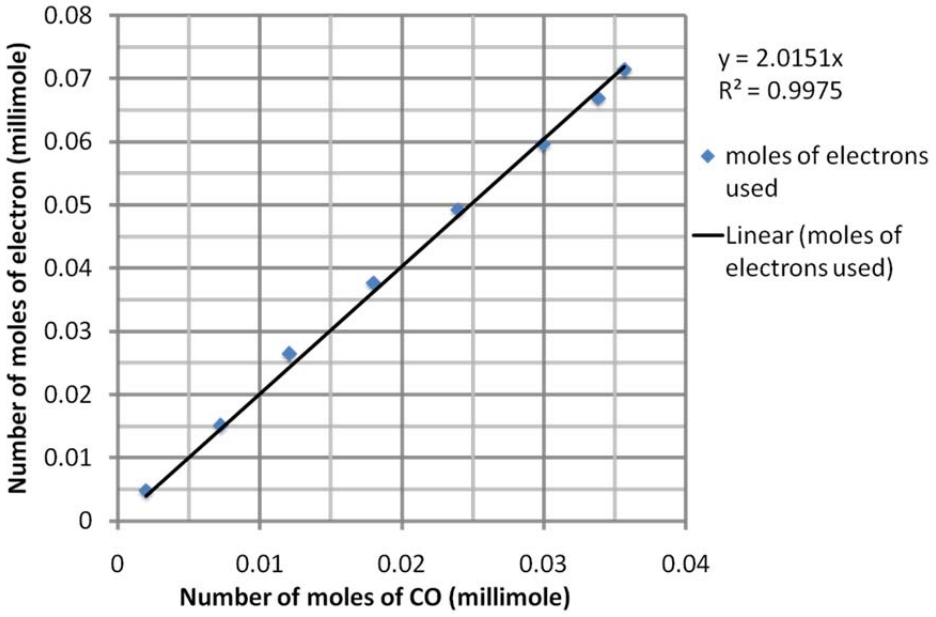

Figure 2-8. Relationship between the numbers of moles of electrons consumed to the moles of CO produced as a result of bulk electrolysis of 2 under a CO_2 environment (Faradaic efficiency curve).

The current-voltage characteristics of the H-Si/**2** junction were measured by linear sweep voltammetry at a 100 mVs^{-1} scan rate in a stirred, CO_2 saturated 6 mM acetonitrile solution of **2** with iR compensation. Higher concentrations of **2** and CO_2 saturated solvent (270 mM of CO_2) were used so that none of the currents were limited by mass transport of CO_2 or catalyst as shown in Figure 2-9 (a) and (b) for monochromatic and polychromatic light illumination, respectively. The current-voltage characteristics of the H-Si/**2** junction were measured under monochromatic light illumination of 661 nm and as well as polychromatic light illumination under CO_2. It is clear from Figure 2-9 that the photocurrent at the 2^{nd} reduction (catalytic current) was not mass transport limited. The zero potential in this case was taken to be the 2^{nd} reduction potential of **2** under the same conditions on a Pt electrode. The shape of the current density-voltage curves for p-type H-Si/**2** junction under CO_2 environment is similar to semiconductor/liquid junction voltaic device current density-voltage characteristics (Figure 1-5).

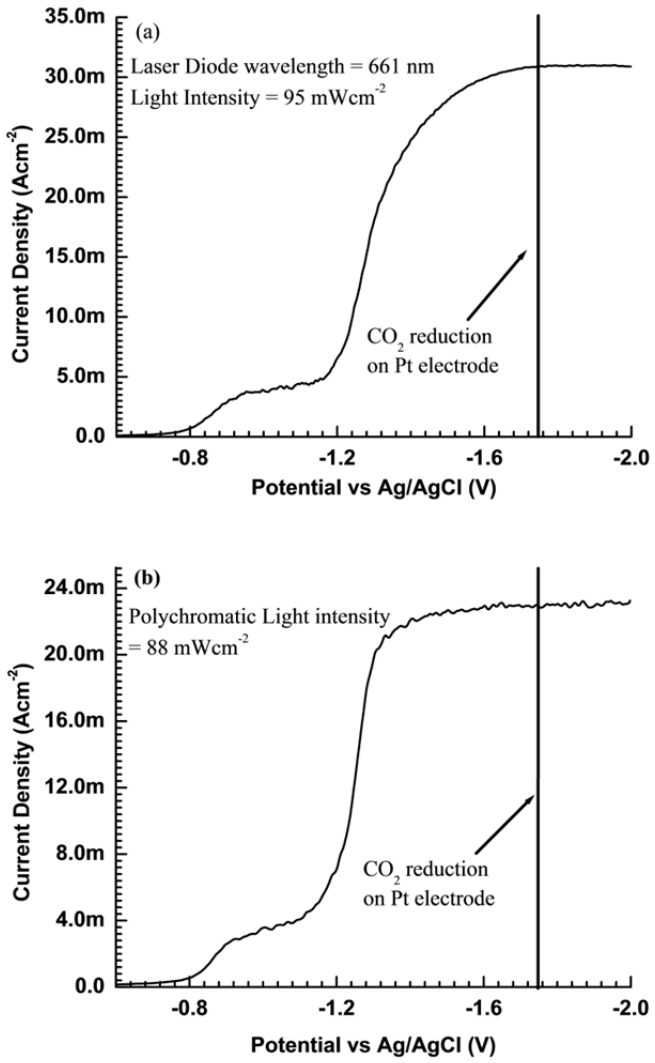

Figure 2-9. Current density-voltage characteristics of p-type H-Si/2 molecular catalyst junction under catalyst condition (under CO_2 saturated solution of acetonitrile and kinetic limited current density) and under (a) monochromatic light (661 nm) illumination of intensity = 96 $mWcm^{-2}$ and (b) polychromatic light illumination of intensity = 88 $mWcm^{-2}$.

This cathodic half-cell catalytic reaction is characterized according to the equation (13) from chapter 1 and properties are summarized in Table 2.1. An open circuit voltage (V_{OC}) of 653 mV and short circuit current density (J_{SC}) of 31 $mAcm^{-2}$ were observed for the CO_2 reduction process at monochromatic light intensity of 95 $mWcm^{-2}$. For polychromatic light illumination, an open circuit voltage (V_{OC}) of 668 mV and short circuit current density (J_{SC}) of 23 $mAcm^{-2}$ were observed for the CO_2 reduction process at a light intensity of 88 $mWcm^{-2}$ with a fill factor of 56 ± 2 %. The maximum current density for CO_2

reduction in aqueous solution is 10 mA cm^{-2} based on CO_2 solubility (ca. 38 mM) and diffusion limitations.[28] A current density of 31 mA cm^{-2} (three times more than an aqueous solution based system[28]) for CO_2 reduction under monochromatic illumination of 95 $mWcm^{-2}$ is noteworthy. However, a relatively low fill factor of ca. 52 ± 6 % was observed. Also, the light to electrical energy conversion efficiency for the CO_2 reduction process was found to be ca. 9.0 to 10.0 % for both monochromatic as well as polychromatic light illumination. The largest short circuit quantum efficiency observed for photon to chemical energy conversion of ca. 60 % (661 nm light illumination with intensity = 95 $mWcm^{-2}$).

Table 2-1. Summary of current density-voltage characteristics of p-type H-Si/2 junction under catalytic condition.

Light source and intensity	Open circuit voltage (mV)	Short circuit current density ($mAcm^{-2}$)	Fill factor (%)	Conversion efficiency (%)	Short circuit quantum efficiency (%)
661 nm/95 $mWcm^{-2}$	650	30	50	9	60
Polychromatic light/88 $mWcm^{-2}$	670	23	60	10	NA

Another interesting aspect of this type of catalytic system is the light intensity dependence of catalytic current density. The Figure 2-10 (a) and (b) show the light intensity dependence of the catalytic current density under monochromatic (661 nm) and polychromatic illumination, respectively. The catalytic current density increases with illumination intensity for both polychromatic and monochromatic light as shown in Figure 2-10. The variation in catalytic current density is linear in nature with respects to illumination intensity as shown in Figure 2-11. It is well known that the maximum photocurrent density for

a semiconductor/liquid junction photovoltaic device is directly propositional to light intensity. This means that the p-type H-Si/**2** molecular catalyst junction forms a good rectifying junction. In addition, this also confirms that the homogeneous photocatalytic reduction of CO_2 in this system is driven by light.

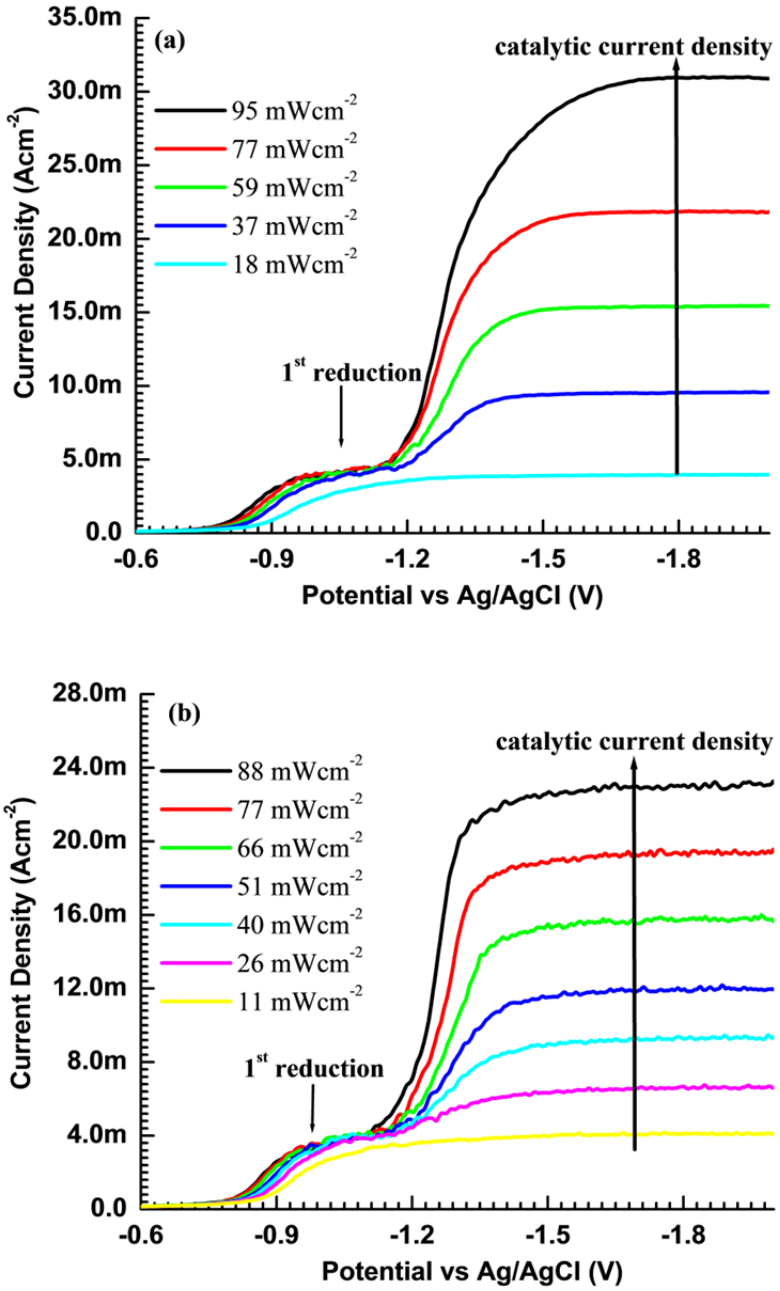

Figure 2-10. Light intensity dependence of homogeneous catalytic current density for CO_2 reduction to CO through p-type H-Si/2 molecular catalyst junction (a) for monochromatic light (661 nm) intensity and (b) polychromatic light intensity.

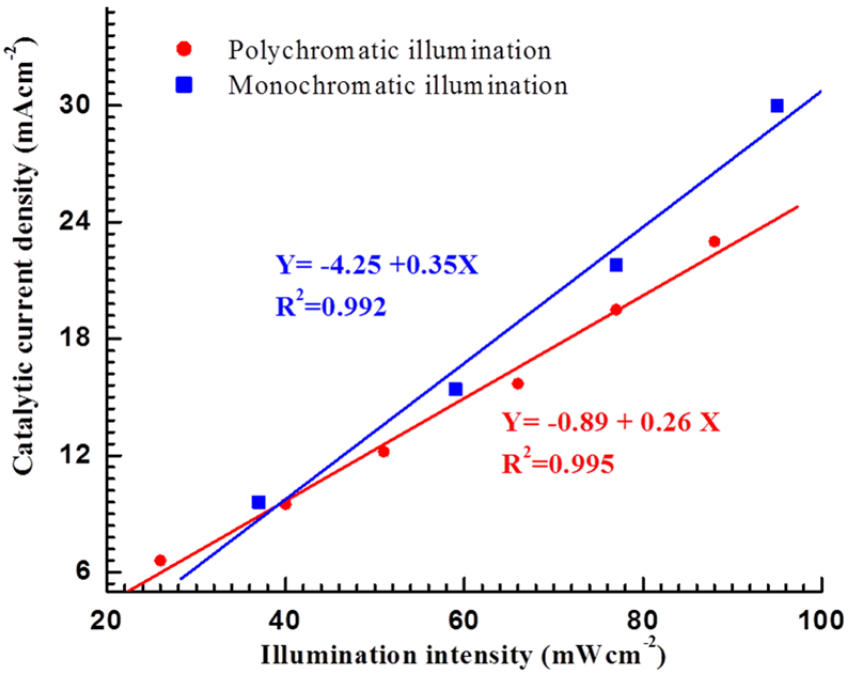

Figure 2-11. Variation of homogeneous catalyst current density of CO_2 reduction through p-type H-Si/2 molecular catalyst junction with illumination intensity. Here, red circular dots represent polychromatic illumination and blue square dots represent monochromatic illumination.

2.4 Conclusion

Photo-assisted electrochemical reduction of **2** was observed on p-type H-Si even though redox potentials for the reductions were above the conduction band edge of the p-type Si. This phenomenon is explained by Fermi level pinning/unpinning of band edges. Selective photoreduction of CO_2 to CO was achieved on planar p-type H-Si photocathode with homogeneous electrocatalyst **2** with a photovoltage of 570 ± 30 mV. For the catalytic reduction of CO_2, a Faradaic efficiency of 97 ± 3 % was observed. An open circuit voltage (V_{OC}) higher than 650 mV, short circuit current density of 31mAcm^{-2} and overall conversion efficiency of 9.0 ± 0.2 % was obtained for the catalytic reduction of CO_2 at the p-type H-Si surface in presence of **2** under monochromatic illumination with an intensity of 95 mWcm^{-2}. The largest short circuit quantum efficiency of ca. 60 % for CO production on p-type H-Si was observed for an illumination intensity of 95 mWcm^{-2}. Similar behavior was observed for polychromatic illumination with an open circuit voltage higher than 650 mV, short circuit current density of 23 mAcm^{-2}, fill factor of 56 ± 2 % and overall

conversion efficiency of ca. 10 %. Both the H-Si and the rhenium catalyst showed excellent stability, lasting for hours without any sign of degradation. The catalytic current density is directly propositional to illumination intensity, which suggests that whole process of homogeneous photoreduction of CO_2 by p-type H-Si/**2** molecular catalyst junction can be subdivided into three different sequential processes: (1) first step; light absorption and charge carrier generation and separation in the semiconductor, (2) second step; heterogeneous charge transfer from illuminated semiconductor to molecular electrocatalyst, and (3) third step; homogeneous catalytic reduction of CO_2 by reduced molecular catalyst as shown in Figure 2-12. Therefore, it is imperative that the homogeneous catalytic current density (on dark electrode) for the molecular catalyst should be match to the maximum photocurrent density of semiconductor/molecular catalyst junction under catalytic condition.

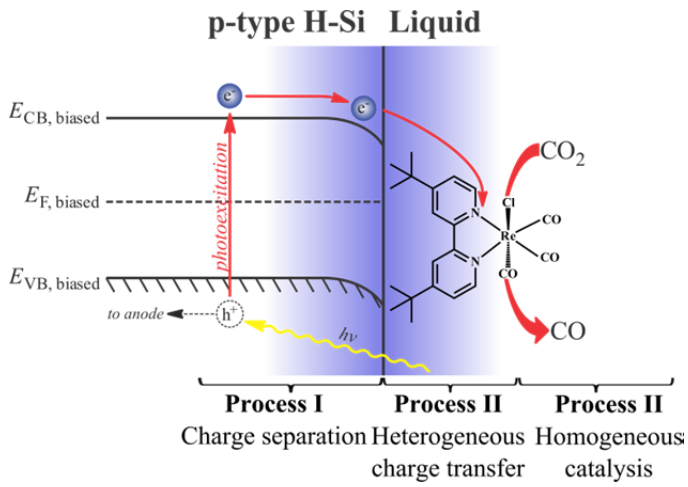

Figure 2-12. Schematic representation of the three processes involved in homogeneous photoreduction of CO_2 driven by p-type H-Si/2 molecular catalyst junction.

Note: Much of the material in this chapter comes directly from a manuscript entitled "Photoreduction of CO_2 on p-type Silicon using Re(bipy-Bu*t*)$(CO)_3$Cl: Photovoltages exceeding 600 mV for the selective reduction of CO_2 to CO," by Bhupendra Kumar, Jonathan M. Smieja and Clifford P. Kubiak, which has been published in *J. Phys. Chem.*, **2010**, *114*, 14220-14223.

2.5 References

(1) Ritter, S. K. C&E News **2007**, 85, 7.

(2) Benson, E. E.; Kubiak, C. P.; Sathrum, A. J.; Smieja, J. M. Chem. Soc. Rev. **2009**, 38, 89.

(3) Collin, J. P.; Sauvage, J. P. Coord. Chem. Rev. **1989**, 93, 245.

(4) Morris, A. J.; Meyer, G. J.; Fujita, E. Acc. Chem. Res. **2009**, 42, 1983.

(5) Rakowski Dubois, M.; Dubois, D. L. Acc. Chem. Res. **2009**, 42, 1974.

(6) Savéant, J.-M. Chem. Rev. **2008**, 108, 2348.

(7) Halmann, M. M. S. M. Greenhouse Gas Carbon Dioxide Mitigation Science and Technology; Lewis Publishers, 1999.

(8) Sutin, N.; Creutz, C.; Fujita, E. Comments on Inorganic Chemistry: A Journal of Critical Discussion of the Current Literature 1997, 19, 67.

(9) Dana C. Bookbinder, N. S. L., Mark G. Bradley, Andrew B. Bocarsly, Mark S. Wrighton J. Am. Chem. Soc. **1979**, 101, 3.

(10) Bookbinder, D. C.; Bruce, J. A.; Dominey, R. N.; Lewis, N. S.; Wrighton, M. S. Proc. Nati. Acad. Sci. USA **1980**, 77, 5.

(11) Bocarsly, A. B.; Bookbinder, D. C.; Dominey, R. N.; Lewis, N. S.; Wrighton, M. S. J. Am. Chem. Soc. **1980**, 102, 3683.

(12) Hinogami, R.; Nakamura, Y.; Yae, S.; Nakato, Y. J. Phys. Chem. B **1998**, 102, 974.

(13) Hinogami, R.; Nakamura, Y.; Yae, S.; Nakato, Y. Appl. Surf. Sci. **1997**, 121-122, 301.

(14) Hirota, K.; Tryk, D. A.; Yamamoto, T.; Hashimoto, K.; Okawa, M.; Fujishima, A. J. Phys. Chem. B **1998**, 102, 9834.

(15) Terrence R. O'Toole, L. D. M., T. David Westmoreland, William J. Vining, Royce W. Murray and Thomas J. Meyer J. Chem. Soc., Chem. Commun. **1985**, 2.

(16) Cabrera, C. R.; Abruña, H. D. J. Electroanal. Chem. **1986**, 209, 101.

(17) Junfu, L.; Baozhu, C. J. Electroanal. Chem. **1992**, 324, 191.

(18) Jeannot Hawecker, J.-M. L. a. R. Z. J. Chem. Soc., Chem. Commun. **1984**, 3.

(19) Hawecker, J.; Lehn, J.-M.; Ziessel, R. Helv. Chim. Acta **1986**, 69, 1990.

(20) B. Patrick Sullivan, C. M. B., David Conrad, William J. Vining and Thomas J. Meyer J. Chem. Soc., Chem. Commun. 1985.

(21) Yam, V. W.-W.; Lau, V. C.-Y.; Cheung, K.-K. Organometallics **2002**, 14, 2749.

(22) Smieja, J. M.; Kubiak, C. P. Inorg. Chem. **2010**, 49, 9283.

(23) Hsu, J. W. P.; Bahr, C. C.; Felde, A. v.; Downey, S. W.; Higashi, G. S.; Cardillo, M. J. J. Appl. Phys. **1992**, 71, 4983.

(24) Bansal, A.; Lewis, N. S. J. Phys. Chem. B **1998**, 102, 4058.

(25) Turner, J. A.; Manassen, J.; Nozik, A. J. Appl. Phys. Lett. **1980**, 37, 488.

(26) Bard, A. J.; Bocarsly, A. B.; Fan, F. R. F.; Walton, E. G.; Wrighton, M. S. J. Am. Chem. Soc. **1980**, 102, 3671.

(27) Hori, H.; Takano, Y.; Koike, K.; Sasaki, Y. Inorganic Chemistry Communications **2003**, 6, 300.

(28) In Mordern Aspects of Electrochemistry; Bockris, J. O. M., White, R. E., Conway, B. E., Ed.; Plenum Publishing: New York, **1989**; Vol. No. 20.

3 Chapter 3

CO_2 photoelectrochemical homogeneous reduction by using p-Si/Re(bipy-*t*Bu)$(CO)_3$Cl (bipy-*t*Bu = 4,4'-di-*tert*-butyl-2,2'-bipyridine) molecular catalyst junction: Effect of p-Si photoelectrode surface modification

3.1 General Introduction

Selective homogeneous photoelectrochemical reduction of CO_2 to CO has been successfully achieved by using p-Si/Re-(bipy-tBu)$(CO)_3$Cl (Re-catalyst).[1] The maximum catalytic photocurrent density observed for this system is 30 $mAcm^{-2}$ at 95 $mWcm^{-2}$ monochromatic (661 nm) illumination intensity with 6 mM Re-catalyst. The simplest form of the maximum photocurrent density for a p-type semiconductor/liquid junction is given by

$$J_{photo} = eQ\left[1 - \frac{e^{(-\alpha W_S)}}{1 + \alpha Z_p}\right] \quad (1)$$

where, Q is the photon flux, α is the absorption coefficient, W_S is the depletion width, and Z_p is the electron diffusion length in the p-type semiconductor.[2,3] The above expression for photocurrent density is based on the assumptions that there is no recombination of photo-generated charge carriers in the depletion region of the semiconductor and that there is very fast heterogeneous charge transfer from the semiconductor to the redox species through the semiconductor/liquid junction. The homogeneous limiting catalytic current density (plateau current density) for an EC' type mechanism is given by

$$J_{cat} = n_{cat} F[catalyst]\left(D_{catalyst} k[sub]^x\right)^{1/2} \quad (2)$$

where n_{cat} = number of electrons involved in the homogeneous catalysis, F = Faraday's constant, [catalyst] = catalyst concentration, $D_{catalyst}$ = the diffusion coefficient of the catalyst, k = pseudo first order rate constant of the catalysis, [sub] = substrate concentration, x = order of the homogeneous catalytic reaction.[4,5] A detailed discussion about the above equation (2) applicability is presented in chapter 7. As discussed in chapter (2), the whole process of homogeneous photoreduction of CO_2 by p-Si/Re-catalyst molecular catalyst junction can be subdivided into three crtical sequential processes: (a) light absorption and charge

carrier generation and separation in the semiconductor, (b) heterogeneous charge transfer from illuminated semiconductor to molecular electrocatalyst, and (c) homogeneous catalytic reduction of CO_2 by reduced molecular catalyst as shown in Figure 3-1.

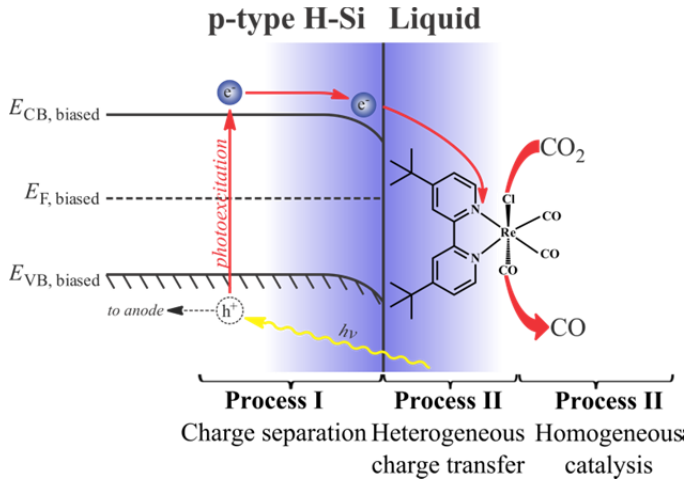

Figure 3-1. Schematic representation of the three processes involved in homogeneous photoreduction of CO_2 driven by p-Si/Re-catalyst molecular catalyst junction.

Experimentally determined rate of homogeneous catalysis on a glassy carbon electrode for Re-catalyst is 650 $M^{-1}s^{-1}$.[6] In Table 3-1, a comparison between the maximum homogeneous catalytic current density by using p-Si/Re-catalyst junction with the maximum theoretical homogeneous catalytic current density for Re-catalyst and the maximum theoretical photocurrent density for p-Si/liquid junction is tabulated. The homogeneous catalytic photocurrent density is significantly smaller than both the theoretical homogeneous catalytic current density and the maximum theoretical photocurrent density. p-Si photoelectrode being single crystalline materials. Loss within the p-Si is minimal and the homogeneous catalysis by Re-catalyst has 100% faradaic efficiency.[6] Even after accounting for 10 to 20 % of reflection loss associated with planar p-Si, there is significant discrepancy between theoretical and experimental results. As discussed earlier, the first and third of the three sequential steps are efficient. So, the reason behind the discrepancy might be the second step of the process i.e. the heterogeneous charge transfer from p-Si to Re-catalyst. In this chapter, p-Si surface is modified with phenyl ethyl functional group and the performance of phenyl ethyl modified p-Si/Re-catalyst junction for CO_2 photoelectrochemical reduction is compared with unmodified/hydorgen terminated p-Si/Re-catalyst junction and hexyl modified p-Si/Re-catalyst junction.

Table 3-1. Summary and comparison of the theoretical homogeneous catalytic current density and the maximum photocurrent density with the experimental homogeneous catalytic photocurrent density for CO_2 reduction

C_O^* (mM)	***Intensity (mWcm^{-2}) At 661 nm***	Theoretical current density		Experimental current density (mAcm^{-2})
		J_∞ (mAcm^{-2})	J_{total} ***(mAcm^{-2})***	
6	96	**52**	***51***	***30***

3.2 Experimental Section

All the experimental conditions and techniques used for this work are described earlier in chapter 2 except for p-Si surface modification.[1] Lewis acid method for Si surface modification has been frequently used. In this method, ethyl aluminum dichloride ($EtAlCl_2$, lewis acid) is mixed with alkene/alkyl and put it with hydrogen terminated Si for some time at room temperature.[7] Styrene and hexene were used for surface modification of hydrogen terminated planar p-Si. Hydrogen termination of planar p-Si was done in 40% deoxidized NH_4F solution under argon for 20 minutes. Then, hydrogen terminated p-Si was transferred to glove box under Ar. The hydrogen terminated p-Si were placed in bottle under Ar and transferred to a glove box. Then, 5 ml of 1.0 M solution of $EtAlCl_2$ (in hexane for hexyl modification and in toluene for ethyl phenyl modification) was added to bottle. For ethyl phenyl modification, 1 mL of styrene is added and for hexyl modification, 5 mL of hexene is added. The reaction is allowed to complete for 12 to 24 hours. Samples are first clean with THF under inert environment for couple of times (inside glove box) followed by rinsing with acetonitrile and water (outside). The formation of good monolayer of organic molecules is confirmed by contact angle measurement and no FTIR signal was observed for either hexyl or phenyl ethyl modified p-Si samples. For electrochemical experiments, surface modified samples are placed in the photoelectrochemical (PEC) cell described in chapter 2. All potentials in this chapter are reported vs Fc/Fc^+ reference electrode and Fc/Fc+ is +0.38 V vs Ag/AgCl reference.

3.3 Results and Discussions

The contact angle measurement image of phenyl ethyl modified p-Si photoelectrode is shown in Figure 3.2(a), a contact angle of 84^o for water is observed for most of ethyl phenyl modified p-Si samples. For the samples with contact angle higher than 90^o, no electrochemical reduction of Re-catalyst was

observed. This might be due to formation of polymer on Si surface during the surface modification. Cyclic voltammogram of Re-catalyst on phenyl ethyl modified p-Si is shown in Figure 3.2 (b). Photovoltage of around 480 mV is consistently observed for ethyl phenyl modified p-Si/Re-catalyst junction under polychromatic illumination. The peak to peak separation for the 1st and 2nd reduction of Re-catalyst in case of phenyl ethyl modified p-Si/Re-catalyst is around 360 mV similar to a glassy carbon electrode. For freshly etched p-Si photocathode, the peak to peak separation for the 1st and 2nd reduction of Re catalyst is usually in the range of 460 to 500 mV. This shows a favorable interaction between Re-catalyst and phenyl ethyl modified p-Si surface. The photovoltage achieved for surface modified p-Si/Re-catalyst is lower than freshly etched or hydrogen terminated p-Si/Re-catalyst might be due to incomplete surface coverage by hexyl and phenyl ethyl group. Only methyl group can achieved complete coverage on Si (111) surface.[8] Under oxidizing condition hexyl modified n-Si is not stable[9,10], however, hexyl and phenyl ethyl modified p-Si photocathodes were quite stable under reducing conditions employed in this study. Cyclic voltammograms of Re-catalyst under Ar environment on phenyl ethyl modified p-Si under polychromatic illumination at different scan rates are shown in Figure 3.3(a). A linear relationship was observed between the peak photocurrent density and the square root of the scan rate. This implies that the Re-catalyst is free diffusing in solution and not adsorbed on phenyl ethyl modified p-Si photocathode. Similar behavior was also observed for hexyl modified p-Si/Re-catalyst junction.

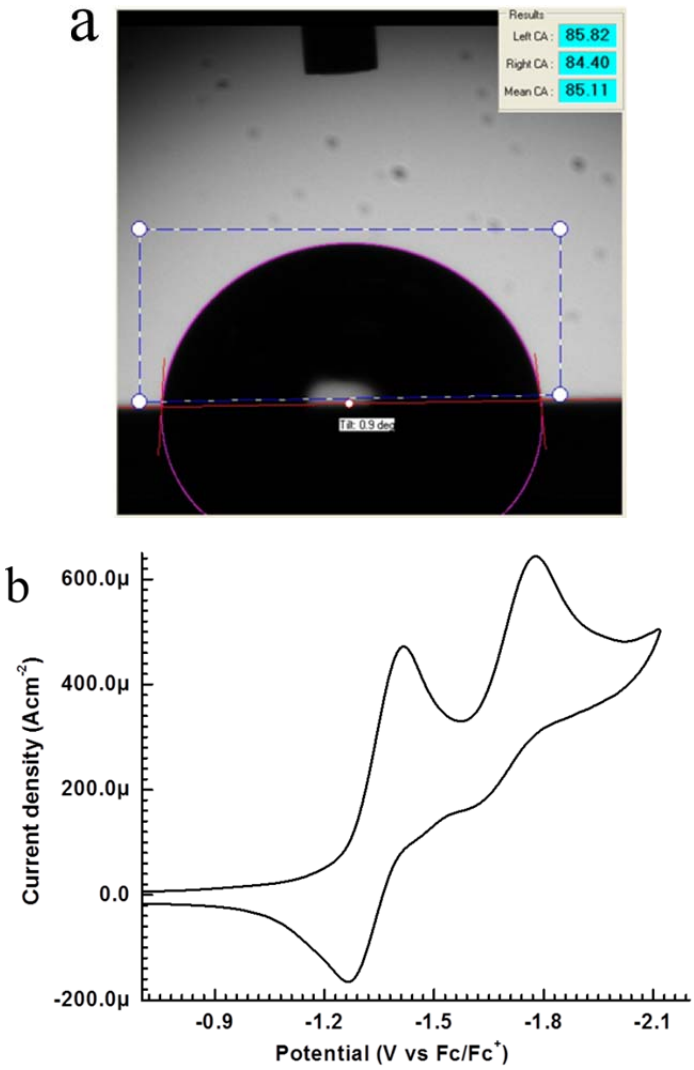

Figure 3-2. (a) Contact angle measurement of water on phenyl ethyl modified p-Si (111) surface. A contact angle of 84 is observed for the modified sample. p-Si (111) with native oxide layer has contact angle of zero. (b) Cyclic voltammogram of 1 mM Re-catalyst in Ar environment on phenyl ethyl modified p-Si under polychromatic light illumination (82 $mWcm^{-2}$). Here 0.1 M of TBAH in acetonitrile is used as electrolyte, Ag/AgCl as a reference electrode, Pt as counter electrode at a scan rate 100 mVs^{-1}.

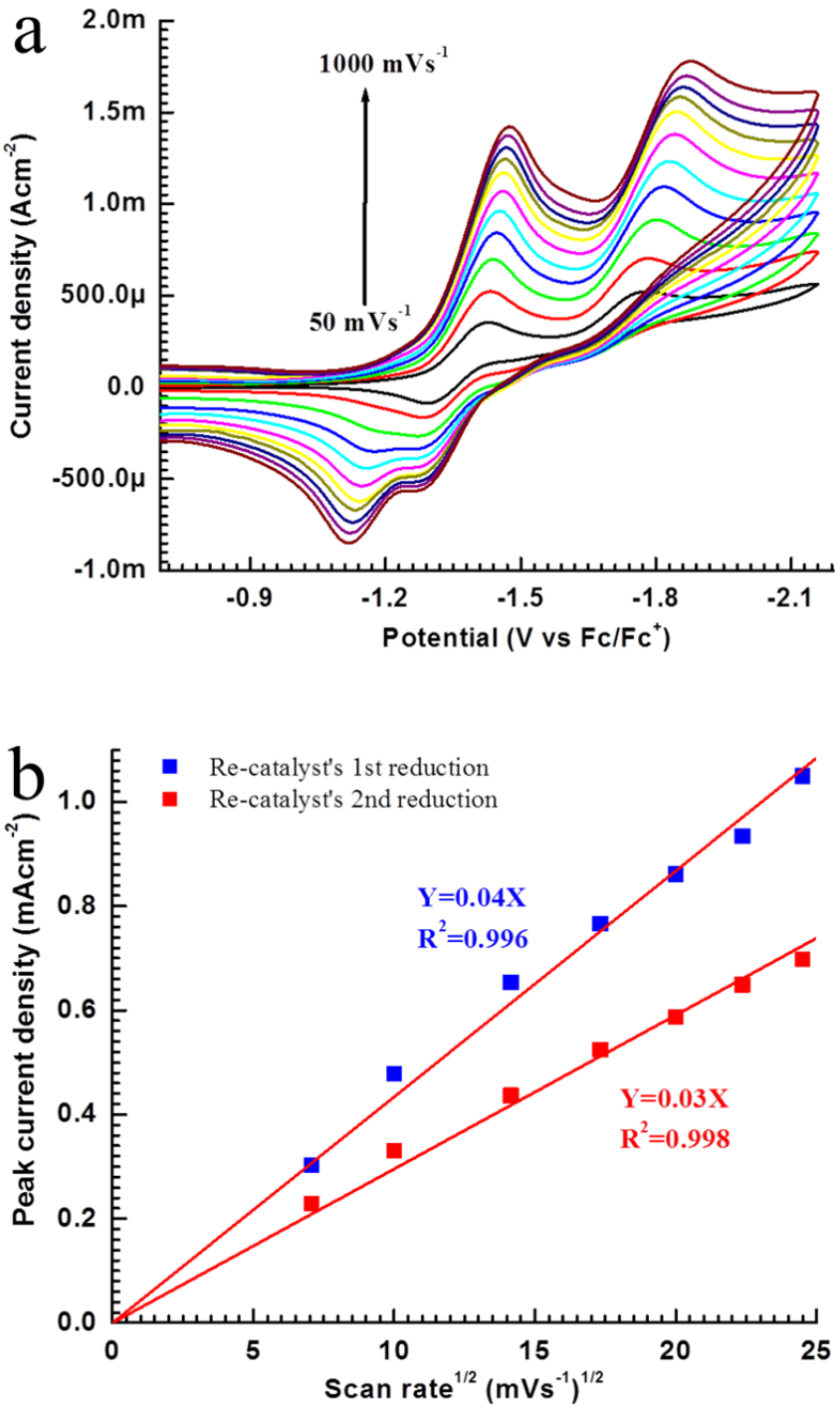

Figure 3-3. (a) Cyclic voltammograms of 1mM Re-catalyst in 0.1 M TBAH in acetonitrile at different scan rates on a phenyl ethyl modified p-Si photocathode under polychromatic illuminated (82 $mWcm^{-2}$). Here Ag/AgCl and Pt are used as reference and counter electrode, respectively. (b) Plot of the peak current density for 1st and 2nd photoelectrochemical reduction of Re-catalyst vs the square root of the scan rate.

Electrochemical homogeneous catalytic reduction of CO_2 by Re-catalyst was achieved in a CO_2 saturated acetonitrile solution. The homogeneous catalytic reduction of CO_2 by using phenyl ethyl modified p-Si/Re-catalyst junction is shown in Figure 3-4 (a). Similar to the unmodified p-Si/Re-catalyst junction, there is significant increase in catalytic current density at the 2^{nd} reduction of Re-catalyst in CO_2 saturated acetonitrile solution. The homogeneous catalytic photocurrent density for CO_2 reduction by using phenyl ethyl modified p-Si/Re-catalyst junction scales up with illumination intensity as shown in Figure 3-4(a). In addition, there is a linear relation between the homogeneous catalytic current density and polychromatic illumination intensity as shown in Figure 3-4(b). It is clear from equation (1) that the photocurrent density is directly proportional to illumination intensity. And since the homogeneous catalytic current density for phenyl ethyl modified p-Si is also directly proportional to the illumination intensity. This implies that the homogeneous catalysis is indeed driven by the light in this system.

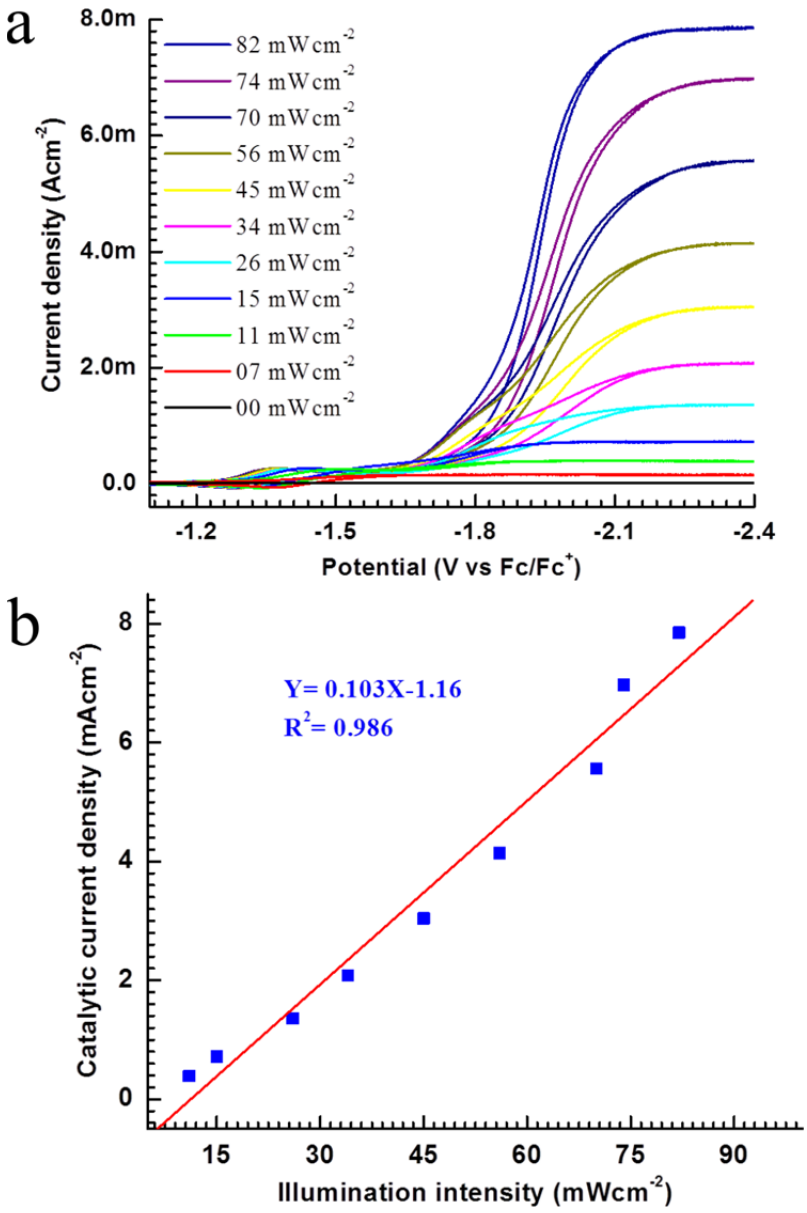

Figure 3-4. (a) Cyclic voltammograms of 0.6 mM Re-catalyst with 0.1 M TBAH as supporting electrolyte in acetonitrile at different polychromatic illumination intensity on a phenyl ethyl modified p-Si photocathode at 100 mVs^{-1} scan rate without any stirring. Here Ag/AgCl and Pt are used as reference and counter electrode, respectively. (b) The relationship between the homogeneous catalytic photocurrent density and polychromatic illumination intensity is shown and a linear fit indicates that the homogeneous catalytic photocurrent density is directly proposition to the illumination intensity.

Table 3-2. Summary of the variation of the apparent rate of homogeneous catalysis by using phenyl ethyl modified p-Si/Re-catalyst with polychromatic illumination intensity.

Polychromatic illumination intensity ($mWcm^{-2}$)	Limiting homogeneous catalytic current density ($mAcm^{-2}$)	Apparent rate of homogeneous catalysis ($M^{-1}s^{-1}$)
82	8.0	1500
74	7.0	1200
70	5.6	800
56	4.1	400
45	3.0	200
34	2.0	100
26	1.4	50
15	0.8	20

The homogeneous rate of catalysis for phenyl ethyl modified p-Si/Re-catalyst junction can be calculated from cyclic voltammograms of Re-catalyst under illumination using equation (2). All the condition proposed by J.-M. Savéant[11] for applicability of this equation is valid here and detailed discussion about this equation is given in chapter 7. The rate of apparent homogeneous catalysis is summarized in Table 3-2 together with illumination intensity and calculated by using equation (2) with limiting catalytic current density, catalyst concentration, catalyst diffusion coefficient ($1.1x10^{-5}$ cm^2s^{-1})[6], CO_2 concentration in acetonitrile (280 mM). The rate of homogeneous catalysis does not change with illumination if the catalyst is photo stable. In the system under consideration, the homogeneous catalysis is limited by illumination intensity and number of sites occupied by the catalyst on semiconducting photoelectrode. The apparent rate of homogeneous catalysis for phenyl ethyl modified p-Si/Re-catalyst is 1500 $M^{-1}s^{-1}$ at 82 $mWcm^{-2}$ polychromatic illumination intensity with 0.6 mM Re-catalyst. For glassy carbon/Re-catalyst, the apparent rate of homogeneous catalysis is only 650 $M^{-1}s^{-1}$ with 1.0 mM Re-catalyst. The superior

performance of phenyl ethyl modified p-Si/Re-catalyst junction is most likely due to the improved charge transport via π-π bond interactions between the aromatic rings on phenyl ethyl modified p-Si surface and the bipyridine ligand of Re-catalyst.

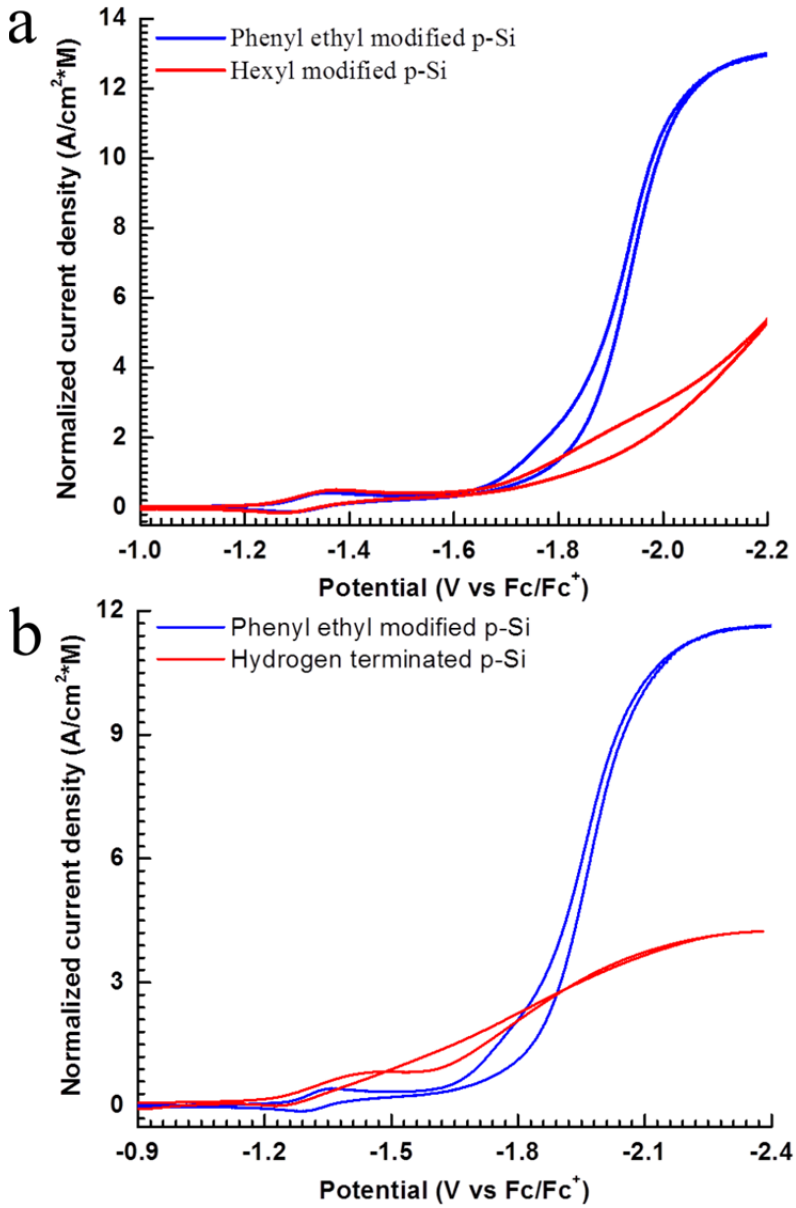

Figure 3-5. (a) Cyclic voltammograms of Re-catalyst at phenyl ethyl modified p-Si and hexyl modified p-Si photocathode with 82 $mWcm^{-2}$ polychromatic illumination under an atmosphere of CO_2. (b) Cyclic voltammograms of Re-catalyst at phenyl ethyl modified p-Si and hydrogen terminated p-Si photocathode with 74 $mWcm^{-2}$ polychromatic illumination under an atmosphere of CO_2. Here Pt is counter electrode and Ag/AgCl is reference electrode with 0.1 M TBAH supporting electrolyte in acetonitrile at 100 mVs^{-1} scan rate. The catalytic photocurrent density is normalized with respect to catalyst concentration, enabling direct comparison.

A direct comparison of phenyl ethyl modified p-Si/Re-catalyst system with hydrogen terminated or freshly etched p-Si/Re-catalyst system and hexyl modified p-Si/Re-catalyst system is shown in Figure 3-5(a) and (b) respectively. The homogeneous catalytic current density is also depended on the catalyst concentration and illumination intensity, so the homogeneous catalytic photocurrent density is normalized and same illumination intensity is used for the comparison. The normalized current density is almost three times higher for the phenyl ethyl modified p-Si compared to the hexyl modified p-Si (Figure 3-5(a)) and the hydrogen terminated p-Si (Figure 3-5(b)). This confirms the superior performance of the phenyl ethyl modified p-Si/Re-catalyst system compared to the hydrogen terminated or freshly etched p-Si/Re-catalyst system and the hexyl modified p-Si/Re-catalyst system.

3.4 Conclusions

The phenyl ethyl modified p-Si photocathode has shown superior performance compared to the hydrogen terminated p-Si, the hexyl modified p-Si and glassy carbon electrode for the homogeneous catalytic reduction of CO_2 by Re-catalyst. This might be due to the favorable π-π bond interaction between immobilized aromatic ring on p-Si surface and bipyridine ligand of Re-catalyst in solution. This result also encouraging for surface immobilization of molecular catalysts for better performance and detailed discussion is provided in chapter 8.

Note: Much of the material in this chapter comes directly from a manuscript entitled "Artificial photosynthesis of CO: Kinetic and structural studies, origins of selectivity, and importance of interfacial charge transfer," by Jonathan M. Smieja, Eric E. Benson, Bhupendra Kumar, Kyle A. Grice, Candace S. Seu, Alexander J. M. Miller, James M. Mayer and Clifford P. Kubiak, accepted *PNAS* **2012**.

3.5 References

(1) Kumar, B.; Smieja, J. M.; Kubiak, C. P. *J. Phys. Chem. C* **2010**, *114*, 14220.

(2) Butler, M. A. *J. Appl. Phys.* **1977**, *48*, 1914.

(3) Soedergren, S.; Hagfeldt, A.; Olsson, J.; Lindquist, S.-E. *J. Phys. Chem.* **1994**, *98*, 5552.

(4) DuBois, D. L.; Miedaner, A.; Haltiwanger, R. C. *J. Am. Chem. Soc.* **1991**, *113*, 8753.

(5) Savéant, J. M.; Vianello, E. *Electrochim. Acta* **1962**, *8*, 905.

(6) Smieja, J. M.; Kubiak, C. P. *Inorg. Chem.* **2010**, *49*, 9283.

(7) Buriak, J. M.; Stewart, M. P.; Geders, T. W.; Allen, M. J.; Choi, H. C.; Smith, J.; Raftery, D.; Canham, L. T. *J. Am. Chem. Soc.* **1999**, *121*, 11491.

(8) Bansal, A.; Li, X.; Lauermann, I.; Lewis, N. S.; Yi, S. I.; Weinberg, W. H. *J. Am. Chem. Soc.* **1996**, *118*, 7225.

(9) Bansal, A.; Lewis, N. S. *J. Phys. Chem. B* **1998**, *102*, 1067.

(10) Bansal, A.; Lewis, N. S. *J. Phys. Chem. B* **1998**, *102*, 4058.

(11) Savéant, J.-M. *Chem. Rev.* **2008**, *108*, 2348.

4 Chapter 4

CO_2 photoelectrochemical homogeneous reduction by using p-Si/Re(bipy-*t*Bu)$(CO)_3$Cl (bipy-*t*Bu = 4,4'-di-*tert*-butyl-2,2'-bipyridine) molecular catalyst junction: Effect of surface modification p-Si nanowire photoelectrode on the homogeneous catalysis

4.1 General Introduction

The indirect band gap nature of Silicon (Si) leads to very low absorption coefficient. This makes it imperative to have large thickness (100 μm) for effective absorption of light in Si. This imposes severe limitations on purity of materials that can be used for the light harvesting using indirect band gap semiconductors. Kayes et al.[1] proposed that a "bed of nails" geometry vertical nanowires with a circumferential junction would be better for light harvesting with indirect band gap semiconductors. The bed of nails geometry of Si wires (nano/micro) is not only provides a larger surface area, but, also enhanced light absorption properties.[2,3] The p-i-n coaxial single Si nanowire diode photovoltaic characterization yielded an open-circuit voltage of 260 mV with a fill factor of 55 %.[4] Si nanowire solar cells with circumferential junction (single crystalline p-type core with conformal coating of n-type amorphous silicon) only yielded an open-circuit voltage of 130 mV with fill factor of 28 %[2] and slightly better performance with an open-circuit voltage of 290 mV and fill factor of 33 % is reported by Erik et al.[5] for a single crystalline n-Si nanowire with polycrystalline p-Si as circumferential coating. There are other reports in the literature about Si nanowire p-n junction diodes[6,7] and solar cells[8,9], but in all these cases the rectifying junction was not along the circumference of the nanowire.

One of the other ways to use nanowire for photovoltaic application is to use a solid-liquid rectifying interface. Recently, Yuan et al.[10] reported an open circuit voltage of 324 ± 50 mV and short circuit current density of 4.85 ± 0.72 $mAcm^{-2}$ for 150 nm diameter and 18 μm long hot-wall CVD system grown Silicon nanowires photovoltaic cell with solid/liquid rectifying junction. Goodey et al.[11] had shown that the vapor-liquid-solid (VLS) method grown p-Si nanowires formed a rectifying SiNW/solution interface with tris(2,2'-bipyridyl)ruthenium(II) hexafluorophosphate (redox species) in acetonitrile with tetra(n-butyl)ammonium tetrafluoborate as supporting electrolyte They observed a photovoltage of only

220-230 mV by cyclic voltammetry method (CV). On the other hand, Maiolo et al. observed a photovoltage of 389 mV by linear sweep voltammetry (LSV) method for n-Si micro-pillars grown by VLS method with solution stirring and high concentration of redox species (1,1'-dimethylferrocene) in CH_3OH.[12] Dalchiele et al. had reported a photovoltage of 323 mV and fill factor of 41 % for wet etched n-Si. [13] Kamat et al. have reviewed the recent developments in the semiconductor/liquid junction for photovoltaic devices using nanostructured semiconductors.[14]

Nanostructured materials have been extensively explored for catalytic conversion of hydrocarbons to chemical.[15] Semiconducting nanotubes and micro wires have been extensively studied for solar water splitting with and without catalysts.[16,17] Semiconductor nanostructured materials have been also used as a support for electrocatalysts in electrochemical conversion of syngas to higher order hydrocarbons.[18] There are very few examples available in literature for the solar splitting of CO_2 by using nanostructured semiconductor materials.[19-23] In this chapter, photoelectrochemical reduction of CO_2 to CO by using surface modified p-Si nanowire/ $Re(bipy\text{-}tBu)(CO)_3Cl$ (bipy-*t*Bu = 4,4'-tetra-butyl-2,2'-bipyridine) (Re-catalyst) catalyst junction is reported.

4.2 Experimental section

All the experimental conditions and techniques used for this work are similar to the methods and techniques described in chapter 2 except p-Si nanowire fabrication and it's surface modification (described in detail in chapter 3). Si nanowire arrays were fabricated by galvanic displacement reaction (electroless etching method)[5,7-9] of (111) primed p type silicon wafer with resistivity of 1-30 ohm-cm purchased from Ultrasil corporation. 100 mm primed p type silicon wafer was first diced into 1 cm^2 pieces. Silicon shreds were cleaned in freshly prepared 3:1 H_2SO_4:H_2O_2 for 30 minutes and then rinsed with deionized (ID) water. Cleaned pieces were immediately placed into a freshly prepared solution of 0.02 M $AgNO_3$ and 4.8 M HF in 1:1 ratio for 60 minutes for nanowire formation. After the nanowire formation, the samples were cleaned capaciously with deionized water and residual silver particles were removed by 1:1 mixture of NH_4OH:H_2O_2. High surface rough was previous observed in similarly etched Si nanowiress[5,24] would lead to high surface state at the interface. If surface states increase beyond certain limit, it will make semiconductor/liquid junction a non-rectifying junction. Surface passivation is one of the ways to improve

the surface quality of Si nanowires fabricated by electroless etching. Formation of organic monolayer through Si-H bond leads to a relatively stable surface with low surface states/traps. Lewis acid method have worked well with porous silicon, where ethyl aluminum dichloride ($EtAlCl_2$, lewis acid) is mixed with alkene/alkyl and put it with hydrogen terminated porous silicon for some time at room temperature.[25] We choice Lewis acid method due to similarity between porous Si and electroless etch Si nanowire. The area used for calculation of the current density in case of nanowire electrodes is the projected surface and not total surface area of nanowires.

4.3 Results and discussion

The formation of nanowires in the "bed of nails" geometry on planar p-Si surface after electroless etching can be seen in Figure 4. The nanowires are 20 to 50 nm diameters and around 5 to 8 μm long. The contact angle measurement showed a contact angle of 161^o for water as shown in the Figure 4.2, whereas, contact angle for water on unmodified p-Si nanowires was zero. High hydrophobicity of the hexyl modified p-Si nanowires is due to the presence of hydrophobic group (hexyl group) on p-Si surface and nanostructured morphology (a contact angle of 94^o for water is observed on hexyl modified planar p-Si surface).

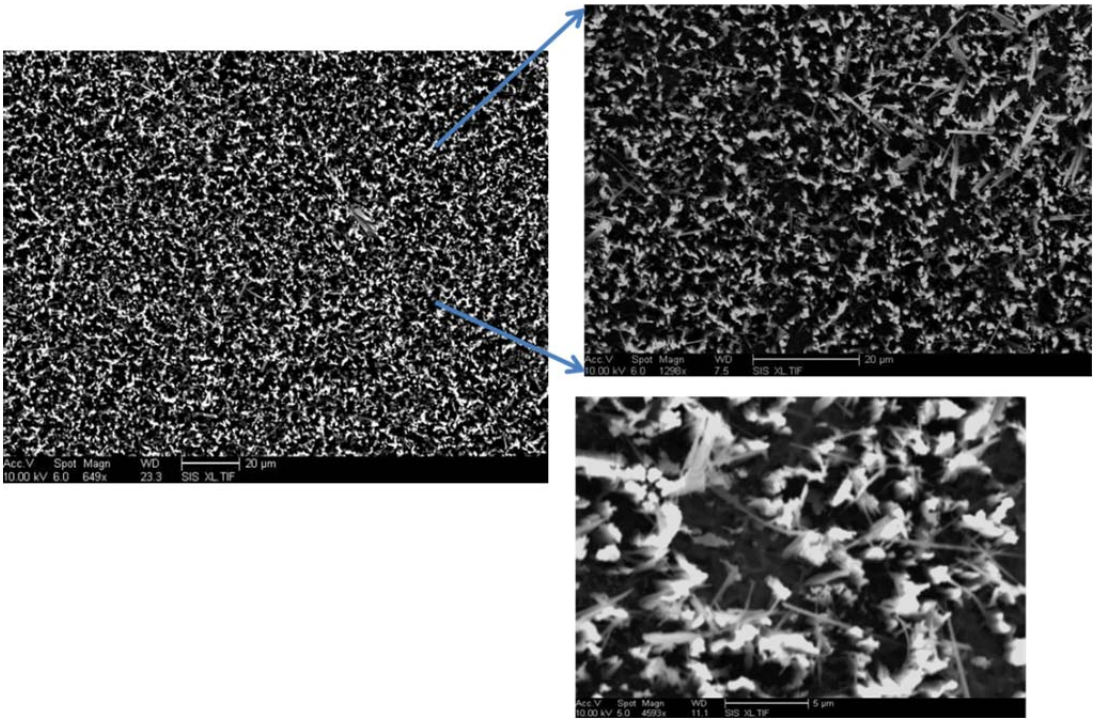

Figure 4-1. Scanning electron microscope (SEM) micrographs of hexyl modified p-Si nanowires.

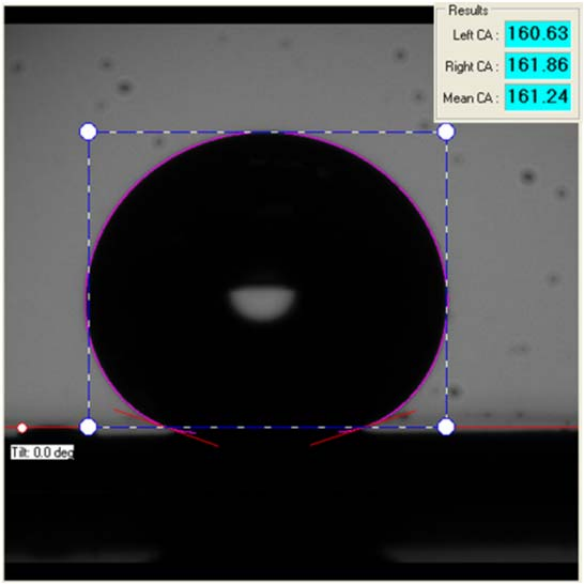

Figure 4-2. Contact angle measurement of hexyl modified p-Si nanowire. A contact angle of ≈ 161^{o} was observed for the modified samples. Unmodified p-Si nanowires have a contact angle of 0^{o} for water.

The cyclic voltammogram of Re-catalyst under an Ar environment on p-Si nanowires photocathodes is shown in Figure 4.3. No photoreduction of Re-catalyst was observed under dark condition on p-Si nanowires photocathode. Under 89 mWcm^{-2} polychromatic illumination, both 1st and 2nd reductions

of Re-catalyst were observed on p-Si nanowires photoelectrode at a potential around 470 mV more positive compared to glassy carbon electrode[26]. The peak current densities for both the 1st and 2nd reductions of Re-catalyst on illuminated p-Si nanowires photoelectrode are directly proportional to the square root of the scan rate as shown in Figure 4.4. Similar to planar unmodified and modified (phenyl ethyl and hexyl group) p-Si photoelectrode, there is no adsorption of Re-catalyst on hexyl modified p-Si photoelectrode.

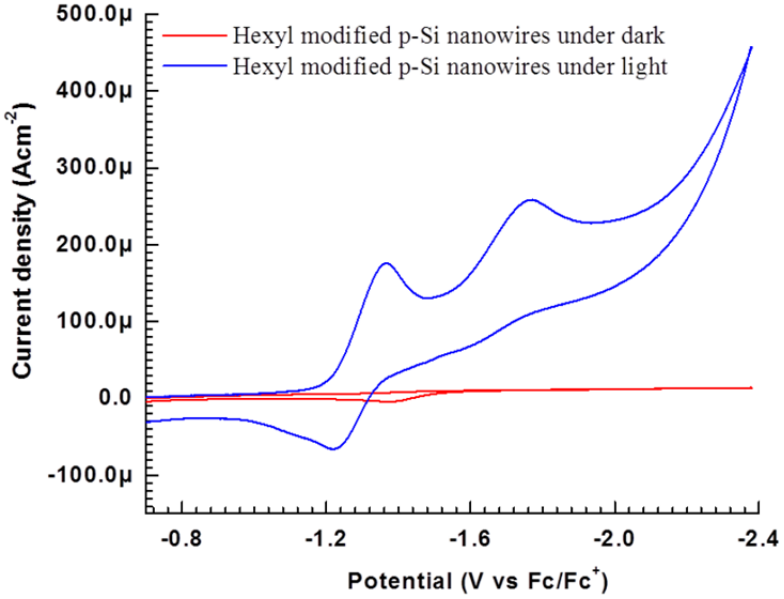

Figure 4-3. Cyclic voltammograms of 1mM Re-catalyst on hexyl modified p-Si nanowires photoelectrode under dark (red) and under 89 mWcm-2 polychromatic illumination intensity (blue) at 100 mVs^{-1} with 0.1 M TBAH as supporting electrolyte in acetonitrile. Here, Ag/AgCl is used as reference electrode and Pt is used as counter electrode.

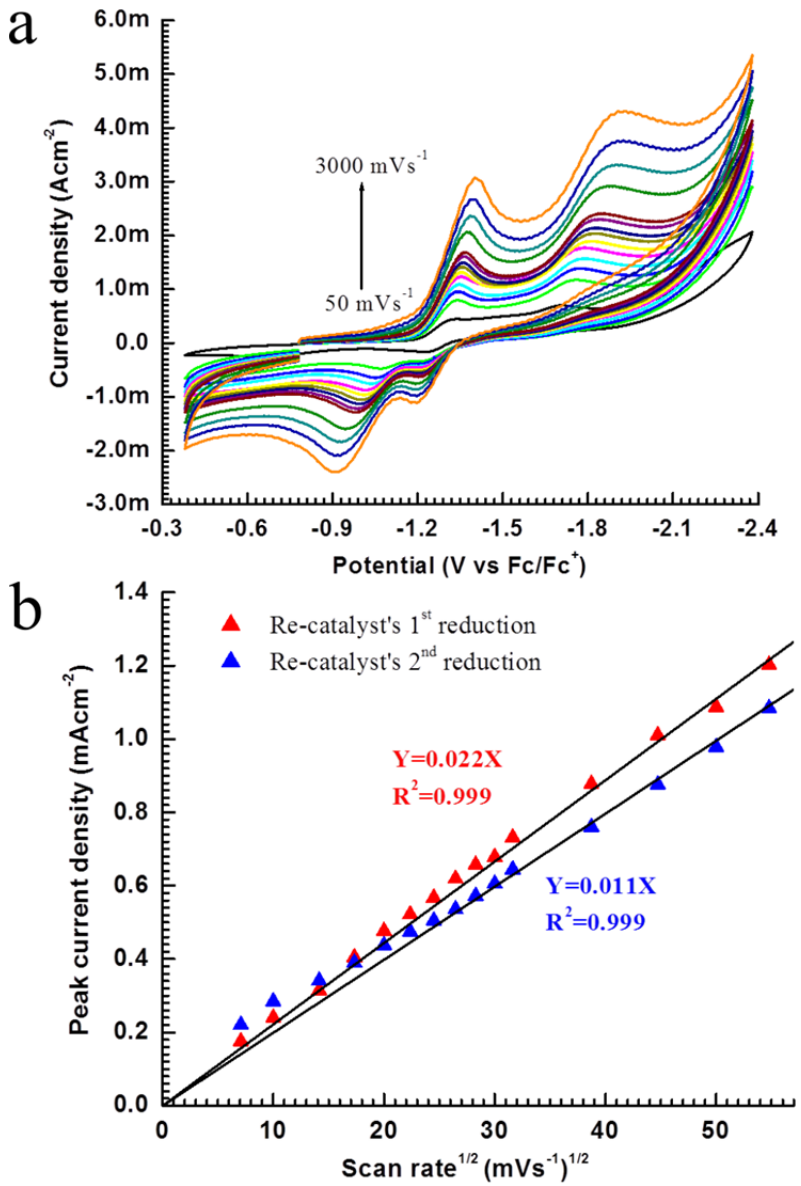

Figure 4-4. (a) Cyclic voltammograms of 1mM Re-catalyst in 0.1 M TBAH in acetonitrile at different scan rates on a hexyl modified p-Si nanowires photocathode under polychromatic illuminated (89 $mWcm^{-2}$). Here Ag/AgCl and Pt are used as reference and counter electrode, respectively. (b) Plot of the peak current density for 1st and 2nd photoelectrochemical reduction of Re-catalyst vs the square root of the scan rate.

The cyclic voltammograms of Re-catalyst under CO_2 environment on hexyl modified p-Si nanowires photocathode are shown in Figure 4.5(a). There is an enhancement of current density under CO_2 at second reduction on illuminated hexyl modified p-Si nanowires photocathode due to homogeneous electro-catalytic reduction of CO_2 to CO the by Re-catalyst. The formation of CO is confirmed by gas chromatography and the electrocatalytic process is 100 % Faradaic efficient on a glassy carbon electrode[26]

as well as on p-Si photoelectrode[27]. A direct comparison of cyclic voltammograms of 1 mM Re-catalyst at 100 mVs^{-1} scan rate under CO_2 environment on the planar and nanowire hexyl modified p-Si photoelectrode showed larger catalytic current density for planar hexyl modified electrode (not shown here). This is counter intuitive. At 100 mVs^{-1} scan rate, the current is limited by mass transport in nanowires electrodes and only tip areas of the nanowires are being used. A kinetic limited catalytic current density was achieved at 10 mVs^{-1} scan rate for homogeneous reduction of CO_2 by using hexyl modified p-Si nanowire/Re-catalyst junction as shown in Figure 4.5(b). From current density-voltage characteristic of the hexyl modified p-Si nanowire/Re-catalyst junction in CO_2 environment and under polychromatic illumination, the calculated open circuit voltage, the short circuit current density, the fill factor and the conversion efficiency are 650 mV, 7.0 mA, 58% and 3.2% per 1mM Re-catalyst, respectively. It is imperative that the properties of a semiconductor/molecular catalyst junction must be reported with respect to the molecular catalyst concentration because the homogeneous catalytic current density is also a function of the catalyst concentration (Chapter 3).

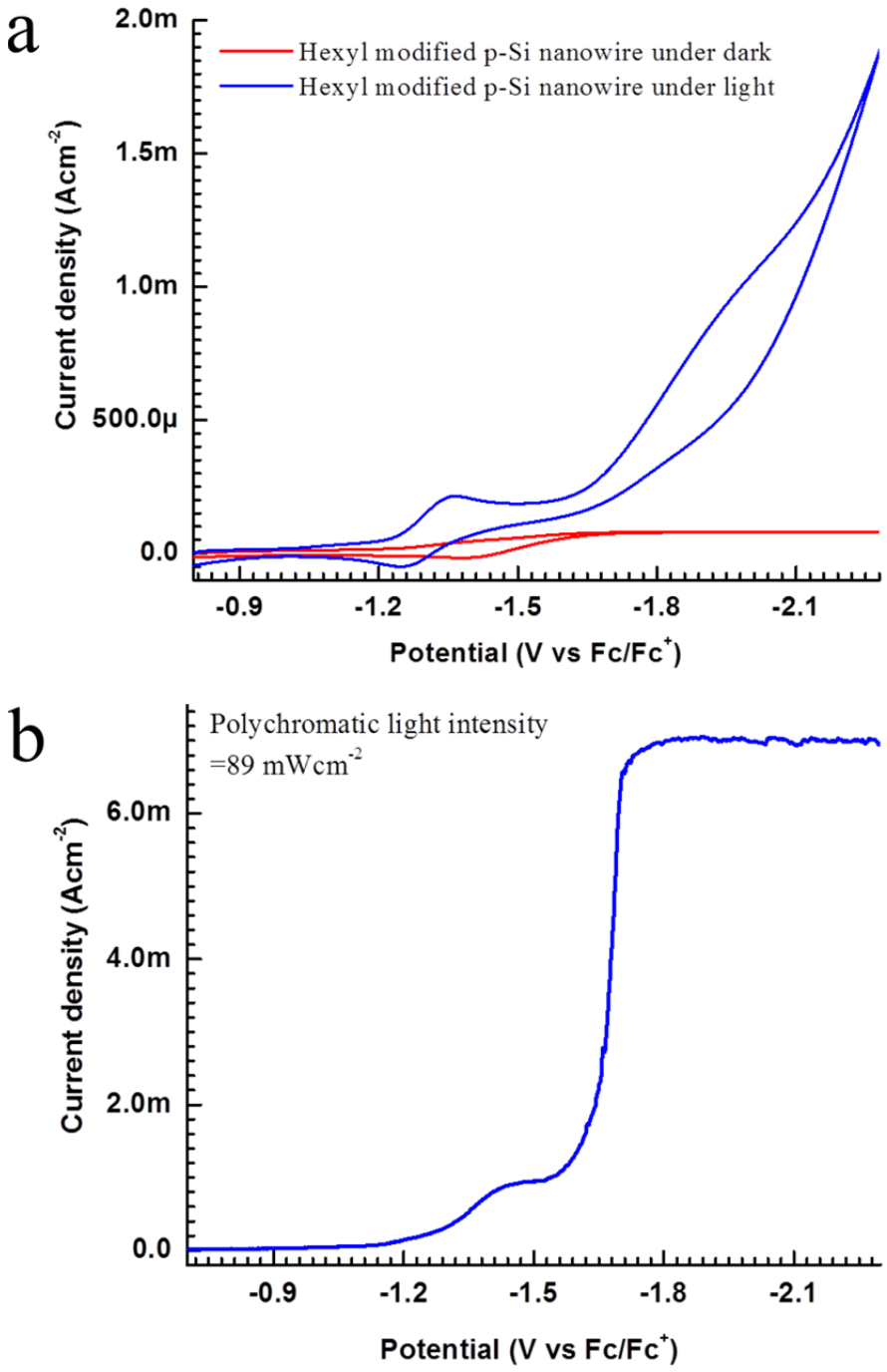

Figure 4-5. (a) Cyclic voltammograms of 1 mM Re-catalyst in CO_2 environment on hexyl modified p-Si nanowires photocathode under dark (red) and polychromatic illumination (blue) (89 $mWcm^{-2}$) at 100 mVs^{-1} scan rate with 0.1 M TBAH as supporting electrolyte in acetonitrile. (b) Current density-voltage characteristic of the hexyl modified p-Si nanowires/Re-catalyst junction with 1 mM Re-catalyst in CO_2 environment under 89 $mWcm^{-2}$ polychromatic illumination intensity at 10 mVs^{-1} scan rate. Here Ag/AgCl and Pt are used as reference and counter electrode, respectively.

The variation in the linear scan voltammograms of Re-catalyst on the hexyl modified p-Si nanowires photocathode with polychromatic illumination intensity is shown in Figure 4-6(a). The limiting homogeneous catalytic current density increases with the illumination intensity and is directly proportion to the illumination intensity as shown in Figure 4-6(b). The photocurrent density for a semiconductor/ liquid junction is directly proportion to the illumination intensity (Chapter 1 equation (4) and Chapter 3 equation (1)). Therefore, from Figure 4-6 it can be concluded that the homogeneous catalytic reduction of CO_2 by the hexyl modified p-Si nanowires/Re-catalytic junction is driven by the light. The homogeneous limiting catalytic current density is directly proportion to the catalyst concentration (Chapter 3 equation (2)). So, the catalytic current density is normalized with respect to the catalyst concentration for the direct comparison of the hexyl modified p-Si planar photoelectrode and the hydrogen terminated p-Si planar photoelectrode with hexyl modified p-Si nanowires photoelectrode for p-type semiconductor/Re-catalyst junction system at a similar illumination intensity. In both the cases, the normalized catalytic current density for the hexyl modified p-Si nanowires is more than twice that of the normalized catalytic current density for planar hexyl modified p-Si photoelectrode and hydrogen terminated p-Si planar electrode as shown in Figure 6.7. This is an indicative that the circumferential surface of the nanowires is also active. Another reason for better performance of nanowires electrode is the better light absorption in nanowire samples.

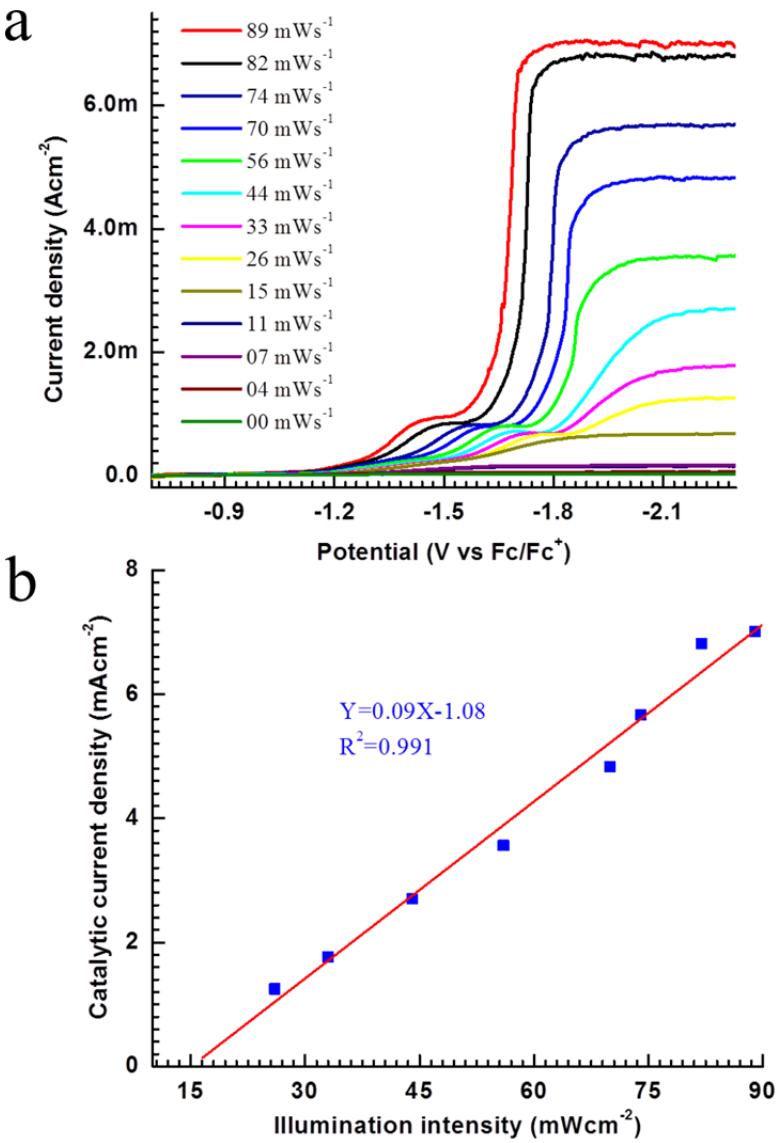

Figure 4-6. (a) Linear voltammograms for 1 mM Re-catalyst on hexyl modified p-Si nanowires photoelectrode at 10 mVs^{-1} scan rate with 0.1 M TBAH as supporting electrolyte in acetonitrile solution with varying polychromatic illumination intensity. Here Ag/AgCl and Pt are used as reference and counter electrode, respectively. (b) The relationship between the homogeneous catalytic photocurrent density and polychromatic illumination intensity is shown and a linear fit indicates that the homogeneous catalytic photocurrent density is directly proposition to the illumination intensity.

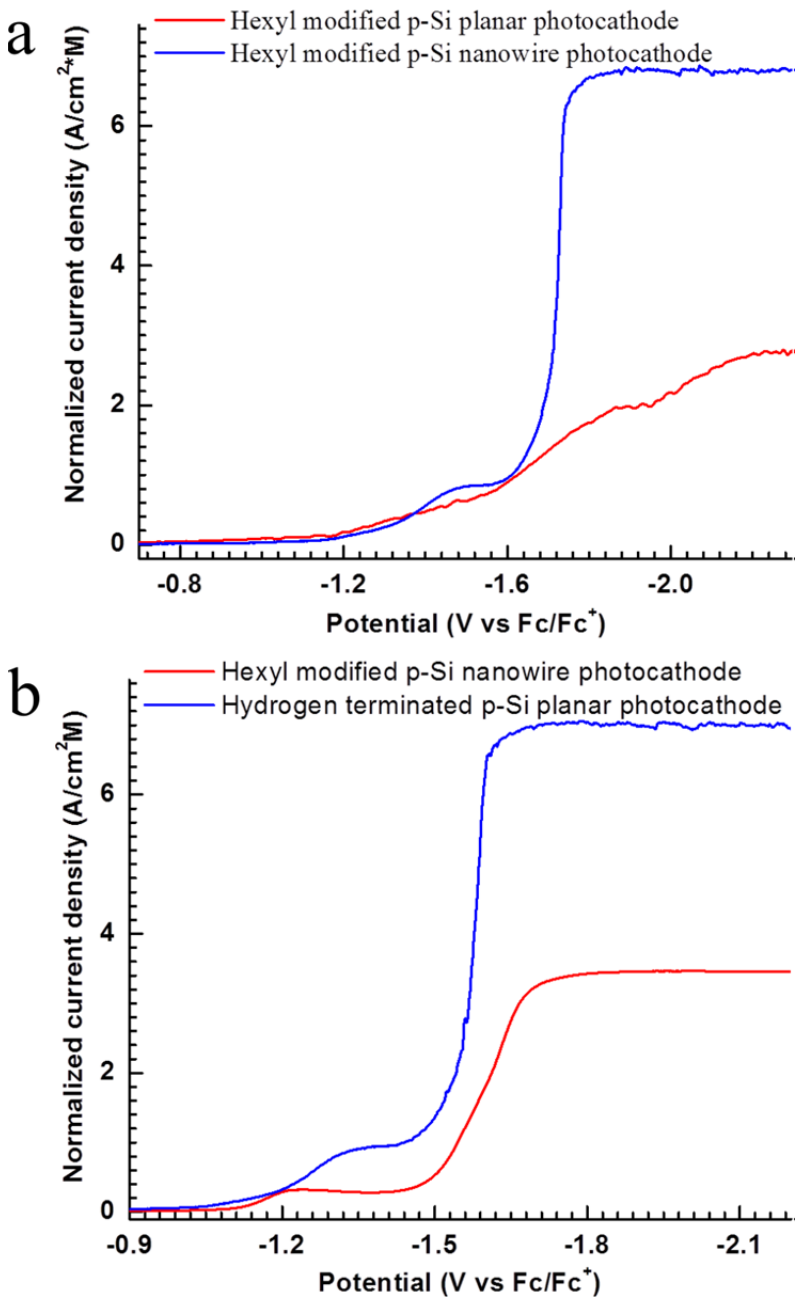

Figure 4-7. (a) Normalized current density-voltage characteristics of the hexyl modified p-Si nanowires and planar photoelectrodes in the p-type semiconductor/Re-catalyst junction system under 82 $mWcm^{-2}$ polychromatic illumination intensity. (b) Normalized current density-voltage characteristics of the hexyl modified p-Si nanowires and the hydrogen terminated p-Si photoelectrodes in the p-type semiconductor/Re-catalyst junction system under 89 $mWcm^{-2}$ polychromatic illumination intensity.

4.4 Conclusions

The applicability of the nanowire photocathode for the homogeneous catalytic reduction of CO_2 to CO by using p-Si/Re-catalytic junction was tested. The behavior of nanowire photoelectrodes is similar to the planar hexyl modified and hydrogen terminated p-Si photoelectrode. The photovoltages observed for the hexyl modified nanowires samples are slightly lower than planar hydrogen terminated p-Si photoelectrodes. The normalized catalyst current density for the hexyl modified p-Si nanowires/Re-catalyst junction is more than twice that of the planar hydrogen terminated p-Si/Re-catalyst junction. This lead to a conversion efficiency of 3.2 % per 1mM Re-catalyst is achieved for hexyl modified p-Si nanowires/Re-catalyst junction, whereas, for planar hydrogen terminated p-Si/Re-catalyst junction the conversion efficiency is only 1.6 % per 1 mM Re-catalyst. The superior performance of nanowire electrodes is due to the higher surface area and the better light absorption compared to planar electrodes.

4.5 References

(1) Kayes, B. M.; Atwater, H. A.; Lewis, N. S. *J. Appl. Phys.* **2005**, *97*, 114302.

(2) Tsakalakos, L.; Balch, J.; Fronheiser, J.; Korevaar, B. A.; Sulima, O.; Rand, J. *Appl. Phys. Lett.* **2007**, *91*, 233117.

(3) Kelzenberg, M. D.; Boettcher, S. W.; Petykiewicz, J. A.; Turner-Evans, D. B.; Putnam, M. C.; Warren, E. L.; Spurgeon, J. M.; Briggs, R. M.; Lewis, N. S.; Atwater, H. A. *Nat Mater* **2010**, *9*, 239.

(4) Tian, B.; Zheng, X.; Kempa, T. J.; Fang, Y.; Yu, N.; Yu, G.; Huang, J.; Lieber, C. M. *Nature* **2007**, *449*, 885.

(5) Garnett, E. C.; Yang, P. *J. Am. Chem. Soc.* **2008**, *130*, 9224.

(6) Hoffmann, S.; Bauer, J.; Ronning, C.; Stelzner, T.; Michler, J.; Ballif, C.; Sivakov, V.; Christiansen, S. H. *Nano Lett.* **2009**, *9*, 1341.

(7) Q. Peng, K.; P. Huang, Z.; Zhu, J. *Adv. Mater.* **2004**, *16*, 73.

(8) Sivakov, V.; Andrä, G.; Gawlik, A.; Berger, A.; Plentz, J.; Falk, F.; Christiansen, S. H. *Nano Lett.* **2009**, *9*, 1549.

(9) Peng, K.; Xu, Y.; Wu, Y.; Yan, Y.; Lee, S.-T.; Zhu, J. *Small* **2005**, *1*, 1062.

(10) Yuan, G.; Zhao, H.; Liu, X.; Hasanali, Z. S.; Zou, Y.; Levine, A.; Wang, D. *Angew. Chem. Int. Ed.* **2009**, *48*, 9680.

(11) Goodey, A. P.; Eichfeld, S. M.; Lew, K.-K.; Redwing, J. M.; Mallouk, T. E. *J. Am. Chem. Soc.* **2007**, *129*, 12344.

(12) Maiolo, J. R.; Kayes, B. M.; Filler, M. A.; Putnam, M. C.; Kelzenberg, M. D.; Atwater, H. A.; Lewis, N. S. *J. Am. Chem. Soc.* **2007**, *129*, 12346.

(13) Dalchiele, E. A.; Martin, F.; Leinen, D.; Marotti, R. E.; Ramos-Barrado, J. R. *J. Electrochem. Soc.* **2009**, *156*, K77.

(14) Kamat, P. V.; Tvrdy, K.; Baker, D. R.; Radich, J. G. *Chem. Rev.* **2010**, *110*, 6664.

(15) Shiju, N. R.; Guliants, V. V. *Applied Catalysis A: General* **2009**, *356*, 1.

(16) Shankar, K.; Basham, J. I.; Allam, N. K.; Varghese, O. K.; Mor, G. K.; Feng, X.; Paulose, M.; Seabold, J. A.; Choi, K.-S.; Grimes, C. A. *J. Phys. Chem. C* **2009**, *113*, 6327.

(17) Boettcher, S. W.; Warren, E. L.; Putnam, M. C.; Santori, E. A.; Turner-Evans, D.; Kelzenberg, M. D.; Walter, M. G.; McKone, J. R.; Brunschwig, B. S.; Atwater, H. A.; Lewis, N. S. *J. Am. Chem. Soc.* **2011**, *133*, 1216.

(18) Gupta, M.; Spivey, J. J. *Catal. Today* **2009**, *147*, 126.

(19) Varghese, O. K.; Paulose, M.; LaTempa, T. J.; Grimes, C. A. *Nano Lett.* **2009**, *9*, 731.

(20) Centi, G.; Perathoner, S. *ChemSusChem* **2010**, *3*, 195.

(21) Roy, S. C.; Varghese, O. K.; Paulose, M.; Grimes, C. A. *ACS Nano* **2010**, *4*, 1259.

(22) Centi, G.; Perathoner, S.; Zang, L., Ed.; Springer London: 2011, p 561.

(23) Sato, S.; Arai, T.; Morikawa, T.; Uemura, K.; Suzuki, T. M.; Tanaka, H.; Kajino, T. *J. Am. Chem. Soc.* **2011**, *133*, 15240.

(24) Hochbaum, A. I.; Chen, R.; Delgado, R. D.; Liang, W.; Garnett, E. C.; Najarian, M.; Majumdar, A.; Yang, P. *Nature* **2008**, *451*, 163.

(25) Buriak, J. M.; Stewart, M. P.; Geders, T. W.; Allen, M. J.; Choi, H. C.; Smith, J.; Raftery, D.; Canham, L. T. *J. Am. Chem. Soc.* **1999**, *121*, 11491.

(26) Smieja, J. M.; Kubiak, C. P. *Inorg. Chem.* **2010**, *49*, 9283.

(27) Kumar, B.; Smieja, J. M.; Kubiak, C. P. *J. Phys. Chem. C* **2010**, *114*, 14220.

5 Chapter 5

Tunable, light-driven co-generation of CO and H_2 from CO_2 and H_2O by Re(bipy-*t*Bu)$(CO)_3$Cl and p-Si in non-aqueous medium

5.1 General Introduction

The co-generation of carbon monoxide (CO) and hydrogen (H_2) is an important step in the synthesis of renewable fuels.[1,2] This mixture, commonly referred to as synthesis gas (or syngas) can be fed into the Fischer-Tropsch process to make synthetic liquid fuels.[3] These fuels can be used in the transportation sector or for the storage of renewable sources such as solar and wind in the intermittent energy form. Over the past three decades considerable research has been performed on both carbon dioxide (CO_2) to CO reduction electrocatalysts[4-6] and proton to hydrogen reduction electrocatalysts.[7-9] This research, however, has been devoid of significant findings on the co-generation of CO and H_2. It is often the case, in fact, that a catalyst for the reduction of protons to H_2 will have no activity towards CO_2, and a catalyst for the reduction of CO_2 to CO will either have no activity towards the reduction of protons or that CO_2 reduction by that catalyst will not be able to compete with hydrogen production in the presence of proton sources. Although syngas can be produced from CO via the water-gas-shift (WGS) reaction or from H_2 via the reverse water-gas-shift (rWGS) reaction, it is desirable to employ a system to make the intended ratio of gasses in one step and thus eliminate the inefficiencies of multiple process integration.

There are very few reports of simultaneous CO_2 and H_2O reduction to syngas. Recently, electrochemical[10] and thermochemical[11,12] methods have been reported to reduce CO_2 and H_2O simultaneously. In the electrochemical method, water and CO_2 were electrochemically reduced at a silver cathode at a potential of approximately -2.00 V vs. SCE.[10] The thermochemical method consists of two steps; (1) thermal dissociation of ZnO to Zn (or Fe_30_4 to FeO) using concentrated solar radiation (endothermic process) and (2) the reduced Zn (or FeO) reacts with H_2O and CO_2 to generate ZnO (or Fe_3O_4) together with syngas (exothermic process).[11,12]

p-Si/Re(bipy-tBu)$(CO)_3$Cl molecular catalyst junction is investigated for light driven co-generation of H_2 and CO from H_2O (proton source) and CO_2. The findings of effect of addition of water in p-Si/Re(bipy-tBu)$(CO)_3$Cl molecular catalyst junction system is reported in this chapter.

5.2 Results and Discussions

The two-electron electrocatalytic reduction of CO_2 to CO by Re(bipy-*t*Bu)$(CO)_3$Cl (where bipy-*t*Bu = 4,4'-di-*tert*-butyl-2,2'-bipyridine) in acetonitrile with high turnover frequency, high turnover number, and a Faradaic efficiency of 99 ± 2% is previously reported on glassy carbon electrode.[13] A photo assisted electrochemical reduction of CO_2 to CO is reported with the same catalyst on p-Si photocathode. In that study we showed the photoelectrochemical reduction of CO_2 to CO with a photovoltage of more than 500 mV and a Faradaic efficiency 97 ± 3% (as discussed in Chapter 1).[14] In both these previous studies there was no intentional proton source added in solution and thus only CO was produced during bulk electrolysis. All the experimental techniques have been used for work in this chapter are same as described in chapter 2.

The characteristic behavior of the p-Si/Re(bipy-*t*Bu)$(CO)_3$Cl molecular catalyst junction, where both the first and second reductions of the Re complex on illuminated p-Si are 530 mV more positive than at metal electrodes (Pt or glassy carbon) under an argon atmosphere, is shown in Figure 2-4 (chapter 2).[14] In the presence of CO_2, there is a large increase in current at the second reduction of the complex, which is assigned to the homogeneous reduction of CO_2 to CO at both the p-Si photocathode and glassy carbon cathode as shown in Figure 5-1a. The kinetically limited photocurrent current density for homogeneous CO_2 reduction at p-Si is modulated by incoming light intensity (Figure 2-10).[14] Upon addition of deoxygenated water under an argon atmosphere, the cyclic voltammogram of the p-Si/Re(bipy-*t*Bu)$(CO)_3$Cl molecular catalyst junction (under illumination) loses its characteristic reduction peaks (Figure 5-1b). Under these conditions the Re(bipy-*t*Bu)$(CO)_3$Cl reduction peaks are obscured by a broad reduction feature in the range of -1.38 to -1.78 V vs. Fc/Fc^+. It was also observed, as expected, that the addition of water narrowed the electrochemical window due to the reduction of protons from water to H_2. A similar feature was observed on p-Si under illumination in acetonitrile upon addition of water with no

Re(bipy-*t*Bu)$(CO)_3$Cl. Gas chromatography of the head space after a bulk electrolysis experiment run at -1.65 V vs. Fc/Fc^+ with and without Re(bipy-*t*Bu)$(CO)_3$Cl under an argon atmosphere showed only hydrogen production. This confirms that this system is in fact heterogeneous reduction of water in a non-aqueous medium at illuminated p-Si.

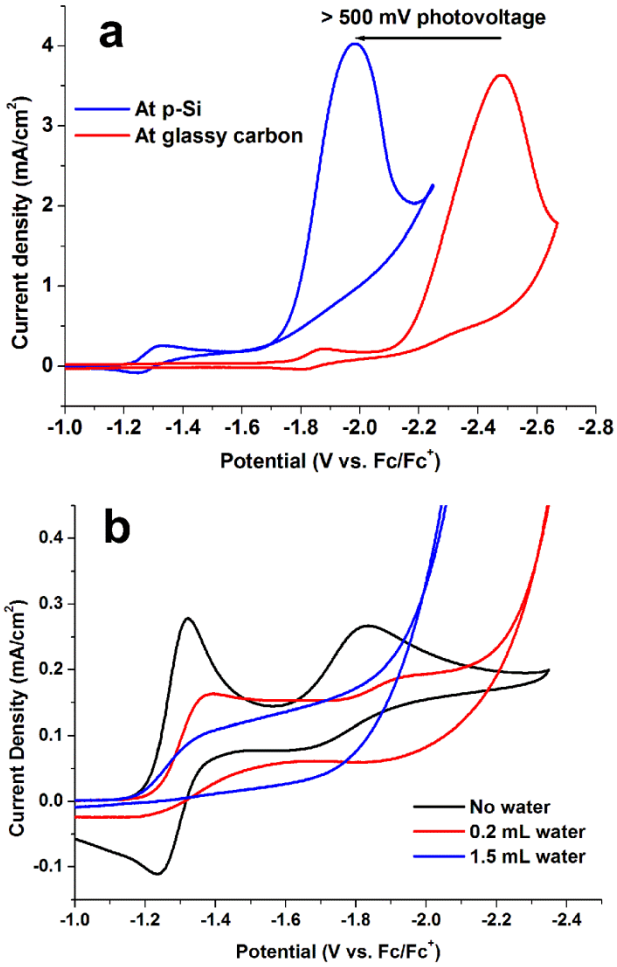

Figure 5-1. (a) Re(bipy-*t*Bu)$(CO)_3$Cl electrochemistry under a CO_2 atmosphere on both glassy carbon and p-Si working electrodes showing more than 500 mV of photovoltage at illuminated p-Si. 0.5 mM catalyst, 0.1 M TBAH electrolyte, Pt counter electrode, 100 mV/s scan rate. (b) Cyclic voltammograms of 1 mM Re(bipy-*t*Bu)$(CO)_3$Cl in 30 mL of acetonitrile on illuminated p-Si photocathode without water addition (black), 0.4 M (0.2 mL) water (red) and 2.6 M (1.5 mL) water (blue).

Bradley et al. reported the photoelectrochemical reduction of tetraazomacrocyclic metal complexes on illuminated p-Si[15] which were later shown to catalyze the photoreduction of CO_2 to CO on p-Si.[16] This system achieved its best results with 18 mM $[(Me_6[14]aneN_4)Ni^{II}]^{2+}$ in a 1:1 acetonitrile-water solution with 0.1 M $LiClO_4$ as the supporting electrolyte. Under those conditions, a H_2/CO ratio of 0.5 and

Faradaic efficiency of 95 ± 5% were obtained. In our work, the ratio of H_2/CO could be increased from 0.4 to 1.2 as water content was increased from 1% to 5% (by volume) with 5 mM Re(bipy-*t*Bu)$(CO)_3$Cl. The Faradaic efficiencies for co-generation in those cases were between 90 ± 5% and 100 ± 5% for co-generation. Further addition of water did not change the H_2 to CO ratio at a catalyst concentration of 5 mM. It should be noted that the concentration of CO_2 in acetonitrile/water mixture is constant up to water concentration of 3 M, but for concentrations of water higher than that the CO_2 solubility in acetonitrile decreases considerably.[17] To fully utilize the activity of Re(bipy-*t*Bu)$(CO)_3$Cl for reduction of CO_2 to CO, therefore, the water concentration must be kept at or below 3 M. In addition, at higher concentrations of water both the tetrabutylammonium hexafluorophosphate (TBAH, electrolyte) and Re(bipy-*t*Bu)$(CO)_3$Cl are not fully soluble.

At a high Re(bipy-*t*Bu)$(CO)_3$Cl concentration, the molecular catalyst is able to compete with the heterogeneous water reduction at illuminated p-Si even at water concentrations (2.5 M) much higher than the CO_2 concentration (0.28 M in acetonitrile at one atmosphere of CO_2).[17] To achieve a H_2/CO ratio of 2:1 (a ratio suitable for liquid fuel formation by the Fischer-Tröpsch process) the Re complex concentration was decreased from 5 mM to 0.5 mM. Figure 5-2a shows the effect of water in an illuminated p-Si/Re(bipy-tBu)$(CO)_3$Cl junction system under an atmosphere of CO_2. Initial addition of a small amount of water lowers the catalytic current density at the 2nd reduction of Re(bipy-*t*Bu)$(CO)_3$Cl. At higher concentrations of water, the decrease in homogeneous CO_2 reduction by Re(bipy-*t*Bu)$(CO)_3$Cl is compensated for by heterogeneous water reduction at illuminated p-Si so that the catalytic current density recovers. Co-generation of H_2 and CO was confirmed by simultaneous detection in a split column gas chromatograph (GC). The H_2 to CO ratio could then be calculated quantitatively from the number of moles of H_2 and CO produced by comparing GC peak areas with calibration curves. Figure 5-2b shows consistent co-generation of H_2 and CO with a ratio near 2:1 during bulk electrolysis experiments run at a potential of -1.90 V vs. Fc/Fc^+.

Control experiments were conducted with glassy carbon as the working electrode under the same conditions as those described above and H_2/CO ratios of only 1:7 (or 0.14) were observed. This experiment

confirms the role of p-Si as the heterogeneous catalyst for H_2 production from water and the role of Re(bipy-*t*Bu)$(CO)_3$Cl as the only CO_2 reduction catalyst.

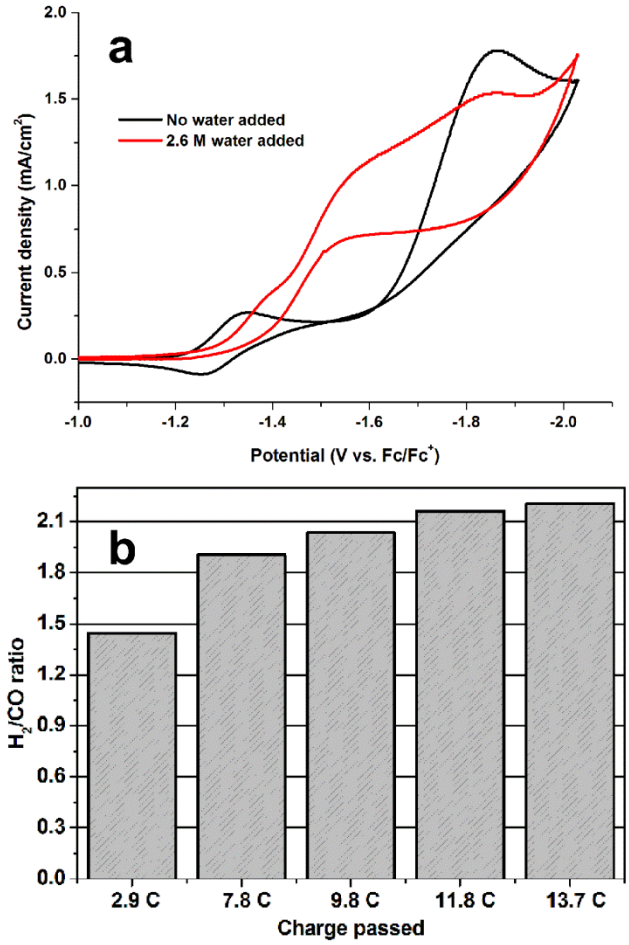

Figure 5-2. (a) Water addition to 0.5 mM Re(bipy-*t*Bu)$(CO)_3$Cl in 40 mL of acetonitrile under CO_2 at illuminated p-Si results in a distortion of the voltammogram's shape and a redistribution of current as a result of heterogeneous water reduction to hydrogen gas; without water (black) and 2.6 M (2 mL) water added (red). Intermediate additions of water are omitted for clarity in this figure, but show a gradual distortion of the CV trace. (b) Chart shows the ratio of H_2 to CO with increase in charge passed during bulk electrolysis. 2:1 H_2/CO is near the ideal ratio for most cobalt-based Fischer-Tropsch systems and provides for the highest possible percentage of liquid fuel molecules.

The gas chromatographs of CO and H_2 are shown in Figure 5-3a and b. As the amount of charge passed during bulk electrolysis is increased from 0 to 13.7 C, the total area of both the CO and H_2 peaks increased linearly. Figure 5-4a shows that the increase in charge passed is linear with time during bulk electrolysis, indicating little to no degradation of the catalysts during the course of the experiment. Dividing

the slope of the curve in Figure 5-4a by the area of the electrode gives a current density for CO and H_2 co-generation of 5.6 mA/cm^2. There is linear relationship between the total number of moles of electrons passed during bulk electrolysis and the total number of moles of gas (H_2+CO) with a slope 1.94 (indicative of both CO_2 and water reduction being two electron processes) as shown in Figure 5-4b. Based on Figure 4b, the Faradaic efficiency for co-generation of H_2 and CO under these conditions is 102 ± 5%.

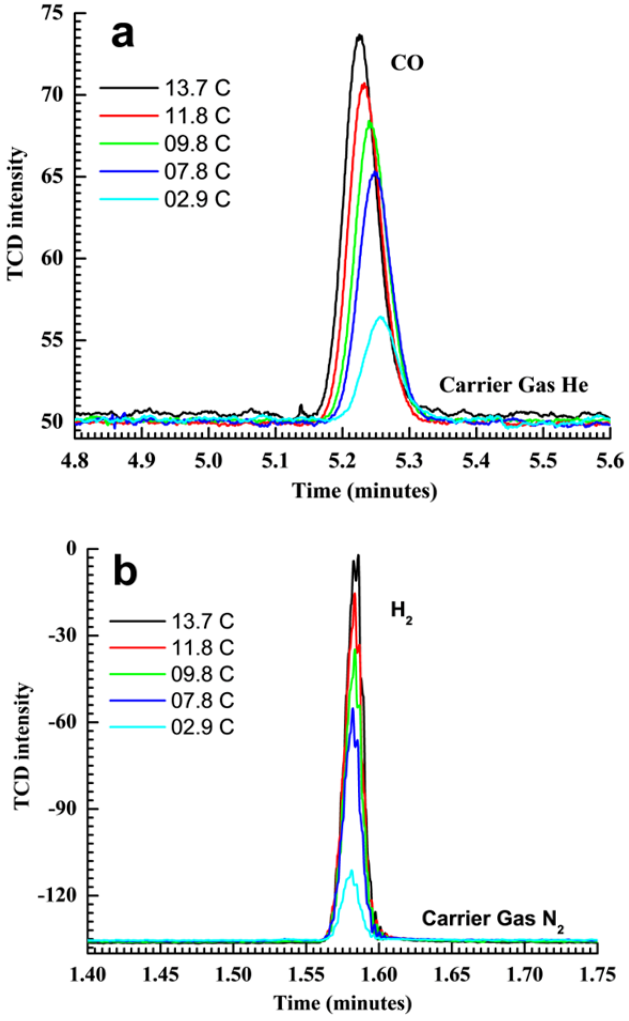

Figure 5-3. Growth of (a) the carbon monoxide peak and (b) the hydrogen peak with increased charge passed over the course of a bulk electrolysis experiment with 0.5 mM Re(bipy-*t*Bu)$(CO)_3$Cl at p-Si under an atmosphere of CO_2 with 2.6 M water.

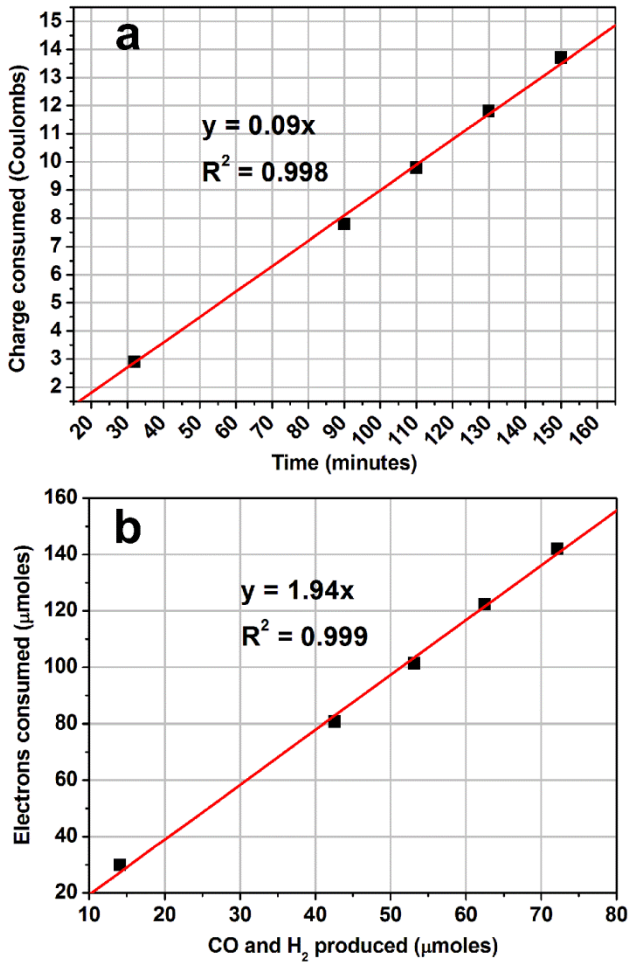

Figure 5-4. (a) Plot of charge consumed over time showing consistency (lack of degradation) over a period of nearly three hours and (b) a plot of electrons consumed versus gasses produced ($CO + H_2$). The slope of nearly two represents the two electron processes for both CO_2 to CO and $2H^+$ to H_2 reductions and a Faradaic efficiency of 102 ± 5% for the overall process.

In the three electrode set-up for the cathodic half reaction only (chapter 1's equation 11) , the total light-to-chemical energy conversion efficiency for CO_2 and water photoreduction is given by [18,19]:

$$\eta = \frac{J_m\left[\sum_i \xi_i\left\{\left(\frac{\Delta H_i}{Z_i}\right) - V_{i,op}\right\}\right] - \{IR\ \text{loss}\}}{I_{h\nu}} \quad (1)$$

where, J_m = catalytic current density, ξ_i = Faradaic efficiency, ΔH_i = heat of combustion, Z_i = number of electrons involved in the reduction, $V_{i,op}$ = overpotential, IR loss = loss associated with non-Faradaic processes, and I_{hv} = incoming light intensity (power density). In the above approach, fuels produced as a

result of CO_2 and water reduction are considered mainly as thermal combustion fuels. The ΔH_i for CO and H_2 are 2.93 eV/coulomb and 2.96 eV/coulomb, respectively, and the overpotential for CO generation is 1.25 V with a Faradaic efficiency of 32%. In the case of water reduction, the thermodynamic potential of proton reduction to hydrogen in acetonitrile with water as the proton source is not available in the literature. Therefore, the thermodynamic potential (-1.46 V vs. Fc/Fc^+) of proton reduction with acetic acid (weak acid) as the proton source in acetonitrile was used in the conversion efficiency calculation as the thermodynamic potential for water reduction.[20] The overpotential for H_2 generation is 0.44 V. The co-generation process has a Faradaic efficiency of nearly 100 %, so IR loss is zero in this case. With a monochromatic light (661 nm) illumination intensity of 95 mW/cm^2 on the photocathode surface and catalytic current density of 5.6 mA/cm^2, the total light to chemical energy conversion efficiency for the cathodic half-cell reaction calculated by equation 1 is 4.6 %.

5.3 Conclusions

It has been successfully shown that in the p-Si/Re(bipy-*t*Bu)$(CO)_3$Cl molecular catalyst junction system, both homogeneous and heterogeneous photocatalytic reaction can occurs simultaneously (Figure 5-5). Here we have shown the efficient co-generation of CO and H_2 from CO_2 and H_2O in a mixed homogeneous/heterogeneous system that allows for tunability in product distribution. We are able to tune the H_2/CO ratio from 0 to 2:1 by addition of water and variation of Re(bipy-*t*Bu)$(CO)_3$Cl concentration. To our knowledge this is the first example of co-generation of this type and may provide for opportunities to co-generate H_2 and CO in the future at lower overpotential and higher overall light-to-chemical energy conversion efficiency. Further improvement in the performance of this system can be achieved by decorating p-Si surface with moderate proton reduction catalyst (like Au) and by lowering the overpotential of molecular catalyst for CO_2 reduction to CO. It is essentially a combination of the heterogeneous and the homogeneous photoelectrochemical reduction systems. The heterogeneous photoelectrochemical reduction system is consists of metal particles on semiconductor surface as catalyst as described in chapter 1 section 1.4. The homogeneous photoelectrochemical reduction system is consists of molecular in solution as catalyst as described in chapter 2.

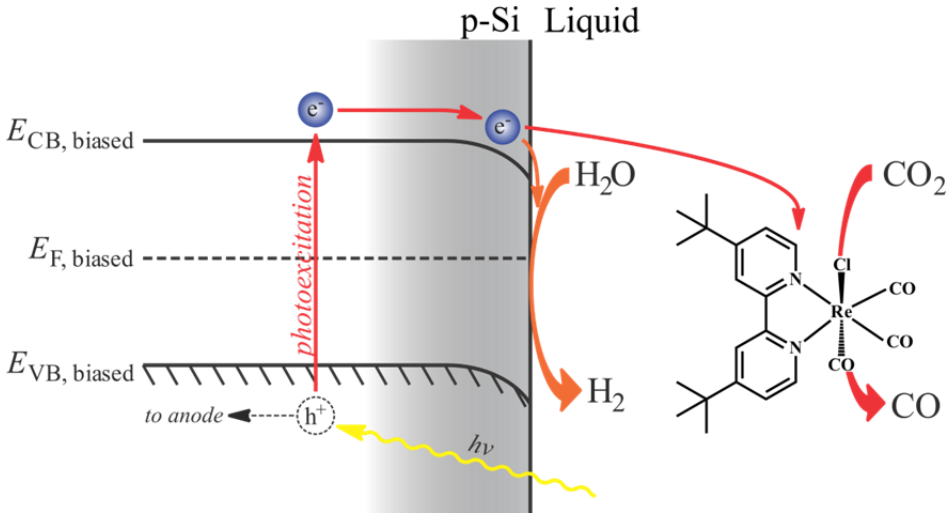

Figure 5-5. Schematic representation for light-driven co-generation of H_2 and CO at biased illuminated p-Si by heterogeneous H_2O reduction (depicted by orange arrows) at the p-Si surface and homogeneous reduction of CO_2 by Re(bipy-*t*Bu)$(CO)_3$Cl (where bipy-*t*Bu = 4,4'-di-*tert*-butyl-2,2'-bipyridine) (depicted by red arrows), respectively.

Note: Much of the material in this chapter comes directly from a manuscript entitled "Tunable, light-assisted co-generation of CO and H_2 from CO_2 and H_2O by Re(bipy-tbu)$(CO)_3$Cl and p-Si in non-aqueous medium" by Bhupendra Kumar, Jonathan M. Smieja, Alissa F. Sasayama and Clifford P. Kubiak, which has been published in *Chem. Commun.*, **2012**, 48, 272-274.

5.4 References

(1) Rostrup-Nielsen, J. R. *Catal. Today* **2000**, *63*, 159.

(2) Rostrup-Nielsen, J. R. *Catal. Today* **2002**, *71*, 243.

(3) Underwood, A. J. V. *Ind. Eng. Chem.* **1940**, *32*, 449.

(4) Benson, E. E.; Kubiak, C. P.; Sathrum, A. J.; Smieja, J. M. *Chem. Soc. Rev.* **2009**, *38*, 89.

(5) Morris, A. J.; Meyer, G. J.; Fujita, E. *Acc. Chem. Res.* **2009**, *42*, 1983.

(6) Roy, S. C.; Varghese, O. K.; Paulose, M.; Grimes, C. A. *ACS Nano* **2010**, *4*, 1259.

(7) Gloaguen, F.; Rauchfuss, T. B. *Chem. Soc. Rev.* **2009**, *38*, 100.

(8) Rakowski Dubois, M.; Dubois, D. L. *Acc. Chem. Res.* **2009**, *42*, 1974.

(9) Tard, C. d.; Pickett, C. J. *Chem. Rev.* **2009**, *109*, 2245.

(10) Delacourt, C.; Ridgway, P. L.; Kerr, J. B.; Newman, J. *J. Electrochem. Soc.* **2008**, *155*, B42.

(11) Stamatiou, A.; Loutzenhiser, P. G.; Steinfeld, A. *Chem. Mater.* **2009**, *22*, 851.

(12) Stamatiou, A.; Loutzenhiser, P. G.; Steinfeld, A. *Energy & Fuels* **2010**, *24*, 2716.

(13) Smieja, J. M.; Kubiak, C. P. *Inorg. Chem.* **2010**, *49*, 9283.

(14) Kumar, B.; Smieja, J. M.; Kubiak, C. P. *J. Phys. Chem. C* **2010**, *114*, 14220.

(15) Bradley, M. G.; Tysak, T. *J. Electroanal. Chem.* **1982**, *135*, 153.

(16) Bradley, M. G.; Tysak, T.; Graves, D. J.; Viachiopoulos, N. A. *J. Chem. Soc., Chem. Commun.* **1983**, 349.

(17) Tomita, Y.; Teruya, S.; Koga, O.; Hori, Y. *J. Electrochem. Soc.* **2000**, *147*, 4164.

(18) Zafrir, M.; Ulman, M.; Zuckerman, Y.; Halmann, M. *J. Electroanal. Chem.* **1983**, *159*, 373.

(19) Barton, E. E.; Rampulla, D. M.; Bocarsly, A. B. *J. Am. Chem. Soc.* **2008**, *130*, 6342.

(20) Felton, G. A. N.; Glass, R. S.; Lichtenberger, D. L.; Evans, D. H. *Inorg. Chem.* **2006**, *45*, 9181.

6 Chapter 6

Photoelectrochemical Hydrogen Generation by an [FeFe] Hydrogenase Active Site Mimic at a p-type Silicon/Molecular Electro-Catalyst Junction

6.1 General introduction

Solar fuels are imperative to our future energy needs and provide a proven method to store sustainable and environmentally benign solar energy.[1-4] Solar hydrogen plays a particular role in this context as it is the only carbon-free, high energy content fuel. Also, mother nature uses hydrogen as an energy carrier and has evolved a class of metalloenzymes known as hydrogenases (H_2ases) that catalyze proton reduction and hydrogen oxidation at high turnover numbers and low overpotentials albeit not in a photo-reaction.[5] Over the last decade, many attempts have been made to mimic the active site of H_2ases and to develop molecular catalyst for proton reduction.[6-9] Among them, dithiolate bridged [FeFe] complexes that are inspired by the [FeFe] H_2ase active site have been shown to be one of the more promising classes of molecular electrocatalysts for proton reduction in the presence of acids in non-aqueous media.[6-8,10-16] Because of these qualities, the [FeFe] complex was selected for this study.

Few schemes for the photoreduction[17-25] or photoelectrochemical reduction[26] of protons to hydrogen by tethered or free hydrogenases or their artificial active site mimics have been reported. Previous studies have usually employed semiconductor nanoparticles[21,24] and dyes[18-20,22] as light absorbers, sacrificial electron donors and in some cases, an electron relay (TiO_2 nanoparticles[19,20]) in addition to the catalytic unit. This type of multiple component photoreduction system is inherently plagued with limited operational lifetime, photo degradation of both electrocatalyst and dye, segregation of semiconductor nanoparticles, and a high total cost of the system from using non-renewable sacrificial reductant. Utilizing photoelectrochemical reduction methods eliminates the requirement for sacrificial donors completely. Nann et al.[26] reported the photoelectrochemical reduction of protons to hydrogen by a dithiolate bridged [FeFe] complex tethered to InP nanoparticles, The system however suffered from low faradaic efficiency (60 %)

and extremely low current density (375 $nAcm^{-2}$). In addition, no photoelectrochemical reduction of the molecular catalyst tethered to InP nanoparticles was reported.

In this chapter, an inexpensive and robust photoelectrochemical reduction system for the homogenous catalytic reduction of protons to hydrogen is discussed, which consists of an illuminated and biased p-type Silicon (Si) photocathode, an [FeFe] electrocatalyst, and a proton source ($HClO_4$). [Fe_2(μ-bdt)$(CO)_6$] (bdt = benzene-1,2-dithiolate) ([FeFe] complex) has reversible reductive electrochemistry and maintains its structural integrity to a large extent even in reduced and protonated state.[13-15] The [FeFe] complex can be reduced reversibly by a single two electron process at -1.32 V vs Fc^+/Fc[015,27], exhibits a high rate constant for proton reduction at approximately 500 $M^{-1}s^{-1}$ in the presence of strong acid[14] and was thus selected for this study.

As depicted in Figure 6-1 and discussed earlier in chapter 2 for the semiconductor/molecular catalyst junction for CO_2 reduction, three distinct processes are involved in the complete photoelectrochemical reduction of protons to hydrogen by a p-type semiconductor/molecular catalyst junction. First, an electron-hole pair is created by photon absorption followed by charge separation. In the second step, heterogeneous charge transfer from the semiconductor to the molecular electrocatalyst results in the reduction of the catalyst. Once the first two steps have been repeated, the reduced [FeFe] complex is able to reduce protons to hydrogen in the final step of the sequence.

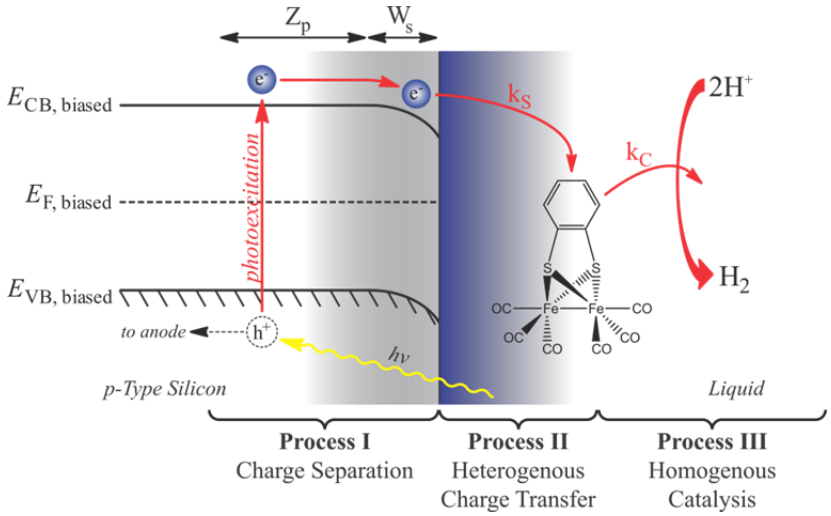

Figure 6-1. Schematic representation of [FeFe] complex assisted photoelectrochemcial reduction of proton to hydrogen on p-type Si, where Z_p is diffusion length of electrons in p-type Si, W_s is depletion width in p-type Si, $E_{VB,biased}$ is valence band of p-type Si, $E_{F,\ biased}$ is Fermi level of p-type Si, $E_{CB,\ biased}$ is conduction band of p-type Si, k_S is the rate constant for heterogeneous charge transfer and k_C is the catalytic rate constant for homogeneous catalysis.

6.2 Experimental section

[FeFe] complex was synthesized in accordance to the literature procedure.[27] Prime (111) p-type silicon with a resistivity of 1-30 ohm.cm was purchased from the Ultrasil Corporation. A 100 mm diameter p-type silicon wafer was first cut into 1 cm^2 pieces and all silicon shreds were cleaned in freshly prepared 3:1 H_2SO_4:H_2O_2 (caution: potentially explosive) for 30 minutes and then rinsed with deionized (DI) water and dried under an N_2 stream immediately before preparing photo-electrodes. In-Ga eutectic was then applied to the back side of freshly scratched samples. Ag paste was then used to affix a coil of tinned Cu wire to the back of the sample. The back contact was then covered with Hysol 1C epoxy (Loctite, Rocky Hill, CT) and subsequently the sample active front area was also defined by Hysol 1C epoxy (3 to 1 mm diameter). The sample with a Cu wire was sealed into glass tubing of 3 mm diameter to make side facing photo-electrodes, using same epoxy as shown in Figure 6-1(a). Then, the sample dried for 30 minutes in open air followed by curing in oven for 30 to 120 minutes at 60 °C. The samples were etched for 1 minute in 6:1 buffered oxide etch (BOE), then rinsed with DI water and followed by etching in concentrated HCl for 5 minutes. Freshly etch samples were then etched again etched for 1 minute in 6:1 buffered oxide etch (BOE), then rinsed with DI water and dried under a stream of N_2 immediately before transferring to a glove box and introducing onto an in-house designed air tight PTFE photoelectrochemical (PEC) cell. The in-

house designed PEC cell contains one glassy carbon electrode, two reference electrodes (one each for glassy carbon and p-type Si photoelectrode) and a common Pt counter electrode with 1 cm diameter quartz windows for illumination as shown in Figure 6-1(b). All electrochemical measurements were performed with a BASi EC Epsilon instrument using a three electrode configuration containing a Ag/AgCl pseudo reference or Pt wire reference, a Pt as counter electrode, and either a glassy carbon disc working electrode with a diameter of 0.3 cm or a p-type Si working electrode with an exposed diameter of 0.1 cm to 0.3 cm. The Fc^{+}/Fc^{0} was used as internal reference and all electrochemical potentials were reported with respect to Fc^{+}/Fc^{0} couple. The electrolyte in all experiments was 0.5 M tetrabutyl ammonium hexafluorophosphate (TBAH) and experiments were carried out in dry acetonitrile. Solvents were dried by a custom dry solvent system and were purged with argon before use. TBAH was recrystallized from methanol and dried under vacuum at 80 ºC. 70 % $HClO_4$ (caution: potentially highly explosive) was purchased from sigma-aldrich as used as proton source. For low concentrations (μM) $HClO_4$ was diluted with dry acetonitrile and then added to the PEC, whereas, for the high concentrations (more than 10 mM) it was directly added to the PEC. A 661 nm laser diode (ML101J27) was used as a monochromatic light source. The laser diode was controlled by LDC240C laser driver purchased from Thorlabs. The laser power was calibrated using an OPHIR PD300-3W-V1 photodetector and OPHIR NOVA II power monitor/meter. Gaseous products were identified and quantified by Agilent technologies 7890A gas chromatograph with a mol sieve column and TCD detector using N_2 as the carrier gas.

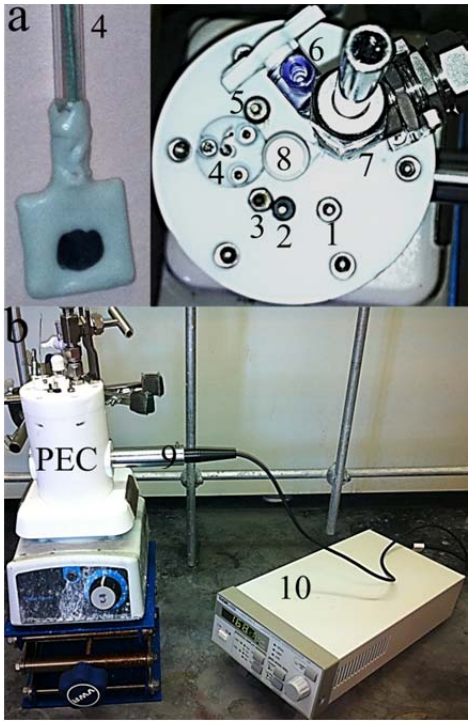

Figure 6-2. (a) Micrograph of photoelectrochemical (PEC) cell cap with lollipop electrode[(4)], common counter electrode(1), dark glassy carbon electrode(2), reference electrodes for drak electrode(3) and photoelectrode(5), p-Silicon photoelectrode (lollipop electrode)(4), gas outlet(6), gas inlet(7), and septum sealing(8) for gaseous product collection. (b) Complete photoelectrochemical experimental set-up with PEC cell, collimated tunable laser diode (9) and laser diode power supply.

6.3 Results and Discussions

Previously, Bookbinder et al. used N,N'-dimethyl-4,4' bipyridine as an electron relay to transfer photogenerated electrons from illuminated p-type Si to a noble metal particle catalyst for hydrogen generation.[28] Photoelectrochemical reduction of a homogenous, molecular electrocatalyst using illuminated semiconductors for proton reduction, however, is not known to the best of our knowledge. The two-electron reduction potential of the [FeFe] complex[16] is approximately 100 mV above the conduction band edge of p-type Si in acetonitrile[29] (chapter 2 Figure 2-5(a)). Assuming ideal semiconductor/liquid junction behaviour, photoelectrochemical reduction of the [FeFe] complex should thus not be feasible on illuminated p-type Si. It has, however, been shown that the photoelectrochemical reduction of species with redox potentials above the conduction band edge of p-type Si can nevertheless be achieved.[29-31] This phenomenon is typically explained based on Fermi level pinning[31] and/or an unpinned band edge.[29] In this

case, the semiconductor/liquid junction behaves more like a semiconductor/metal/liquid junction and also produces a useful photovoltage.

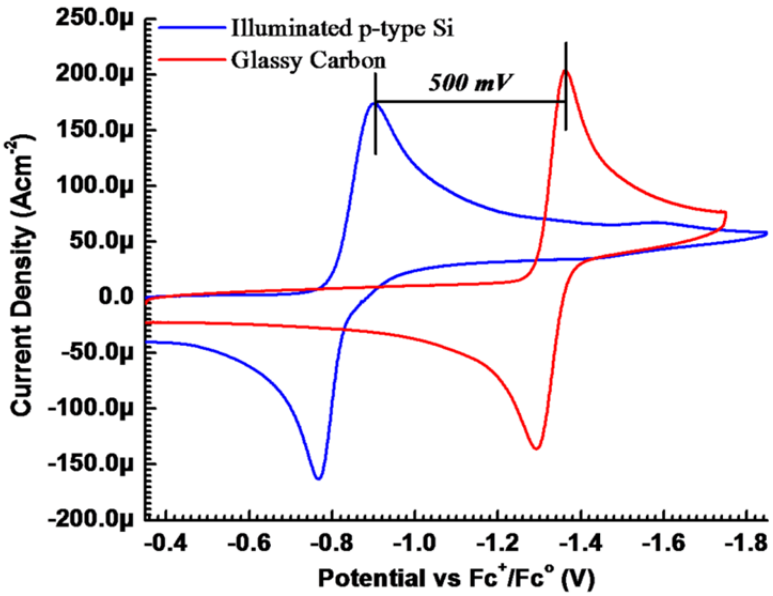

Figure 6-3. Cyclic voltammograms of 0.3 mM of $[Fe_2(\mu\text{-bdt})(CO)_6]$ (bdt = benzene-1,2-dithiolate) in 0.5 M TBAH/acetonitrile on illuminated p-type Si (blue) and glassy carbon (red) at scan rate of 100 mVs^{-1}. The p-type Si photocathode was illuminated using a 661 nm wavelength laser light source.

Under dark conditions, no reduction of the [FeFe] complex could be observed at p-type Si in cyclic voltammetry (CV) experiments. However, under monochromatic illuminated (661 nm) on p-type Si photocathode, a single reversible two electron reduction wave of the [FeFe] complex was observed at approximately 500 mV less negative potential than that observed for the same complex on a glassy carbon electrode under identical conditions as shown in Figure 6-3. The observation of a photovoltage, i.e. the difference between the redox potential of the [FeFe] complex on an illuminated p-type Si photocathode and a glassy carbon electrode, confirms the light-assisted reduction of the [FeFe] complex on the illuminated p-type Si photocathode. A plot of the reductive peak current density for the [FeFe] complex vs. the square root of scan rate shows a linear dependence as shown in Figure 6-4 implying that there is no adsorption of the [FeFe] complex on p-type Si, i.e. that the catalyst is freely diffusing in solution.

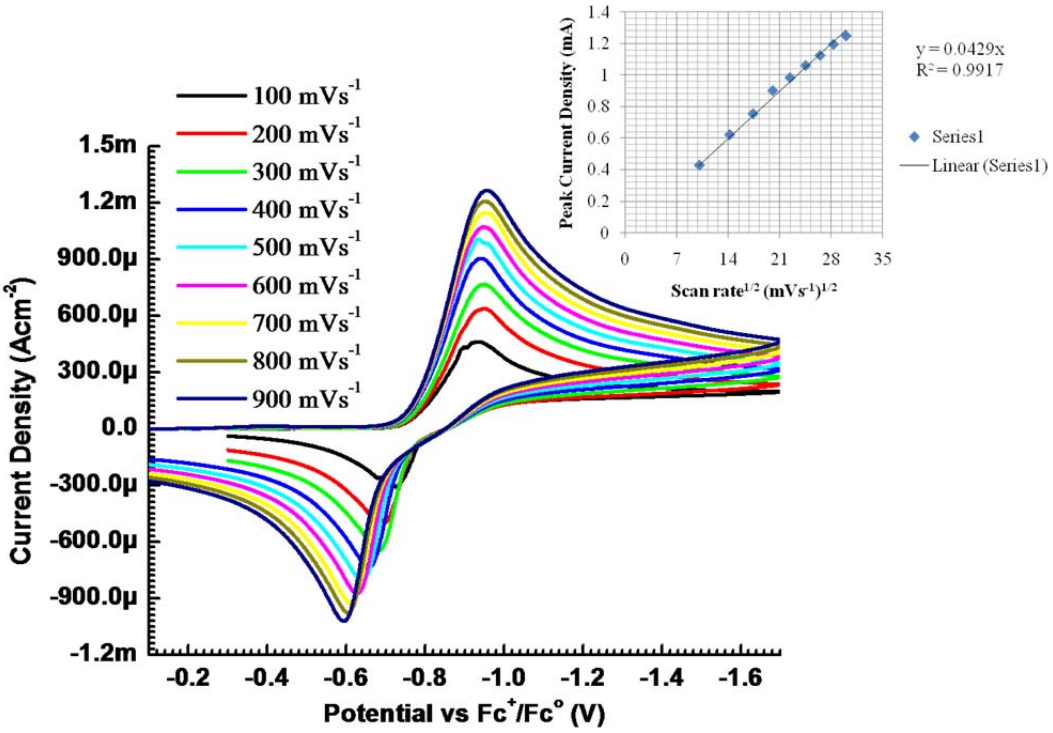

Figure 6-4. Cyclic voltammograms of 1mM $[Fe_2(\mu\text{-bdt})(CO)_6]$ (bdt = benzene -1,2-dithiolate) in 0.5 M of TBAH/acetonitrile at different scan rates on illuminated p-type Si photocathode. Insert: plot of the reductive peak current density versus the square root of scan rate.

In the presence of a weak acid such as acetic acid (pK_a = 22.3 in CH_3CN[32]), the [FeFe] complex reduces protons at a potential 700 mV more negative than its first two-electron reduction wave.[15] In the presence of stronger acids, *p*-toluenesulfonic acid (pK_a = 8.7 in CH_3CN[32]) and $HClO_4$ (pK_a = 2.1 in CH_3CN[32]), the [FeFe] complex reduces protons at the potential of the two-electron reduction.[13,14] For this work, the latter acid was chosen because the epoxy that was used for photo-electrode fabrication is not stable in organic acids. Figure 6-5 shows the CVs of the [FeFe] complex on illuminated p-type Si and glassy carbon in the presence of increasing amounts of $HClO_4$. In both the cases, the current density increases with increasing acid concentration, a behaviour that is indicative for catalytic proton reduction. Moreover, photogenerated hydrogen was identified and quantified by gas chromatography (vide infra). The illuminated p-type Si/[FeFe] complex junction is able to realize a photovoltage of 600 mV for proton reduction (Figure 6-6(a)) with 0.2 mM [FeFe] complex and 3.375 mM $HClO_4$. The photovoltage was measured as the difference between $Ep_{1/2}$ on p-type Si and glassy carbon because two electrodes have

different catalytic current density.[32] In the absence of the [FeFe] complex, negligible proton reduction was detected on the illuminated p-type Si at a potential less negative than -1.2 V vs. Fc^{+}/Fc^{0} (Figure 6-6(b)).

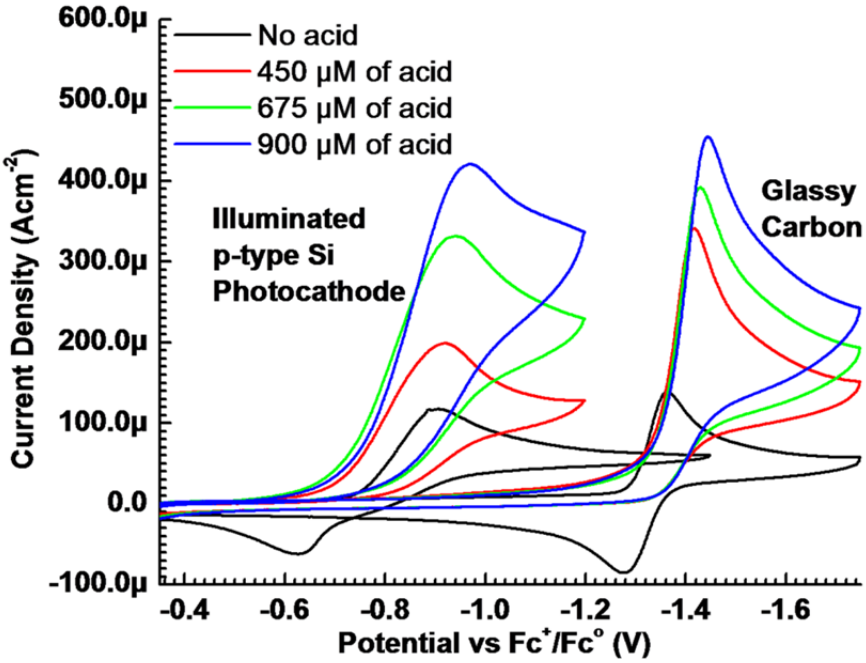

Figure 6-5. Cyclic voltammograms of 0.2 mM $[Fe_2(\mu\text{-bdt})(CO)_6]$ (bdt = benzene-1,2-dithiolate) in 0.5 M TBAH/acetonitrile with varying $HClO_4$ concentrations [0 µM (black), 450 µM (red), 675 µM (green), 900 µM (blue)] on illuminated p-type Si (left side) and glassy carbon (right side) at scan rate of 100 mVs^{-1}. The p-type Si photocathode was illuminated using a 661 nm wavelength monochromatic laser light source.

Bulk electrolysis experiments of the [FeFe] complex on illuminated p-type Si were performed with 10 mM (low) and 110 mM (high) $HClO_4$ concentrations under 661 nm wavelength monochromatic illumination for 5 hours at -900 mV vs. Fc^{+}/Fc^{0}. A current efficiency (Faradaic efficiency) of 105 ± 5 % for hydrogen generation was observed for both $HClO_4$ concentrations. There was a linear relationship between the charge passed through the cell and the amounts of hydrogen generated with a slope of approximately two (actual slope = 1.9), consistent with the fact that proton reduction is a two electron process (Figure 6-7). For longer electrolysis times, both current density and Faradaic efficiency decrease, presumably due to catalyst degradation.

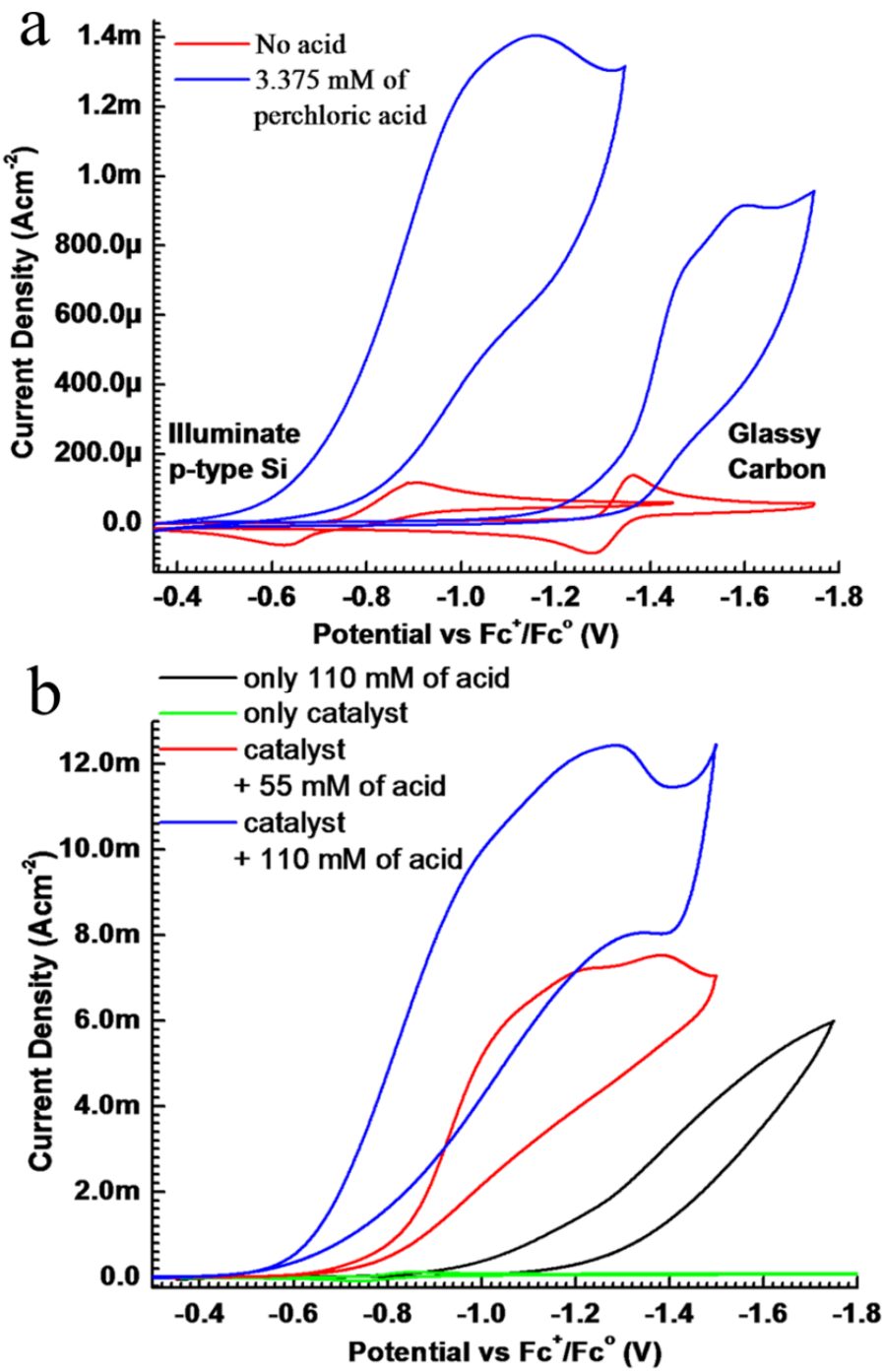

Figure 6-6. (a) Cyclic voltammograms of 0.2 mM $[Fe_2(\mu\text{-bdt})(CO)_6]$ (bdt = benzene -1,2-dithiolate) in 0.5 M TBAH/ acetonitrile on illuminated p-type Si (red) and glassy carbon (red) with no acid and on illuminated p-type Si (blue) and glassy carbon (blue) with 3.375 mM of perchloric acid, respectively. (b) Cyclic voltammograms of 0.3 mM [FeFe] complex on illuminated p-Si (green), with 55mM $HClO_4$ (red), with 110 mM $HClO_4$ (blue) and 110 mM $HClO_4$ without catalyst (black). All measurements were made at a scan rate of 100 mVs^{-1}.

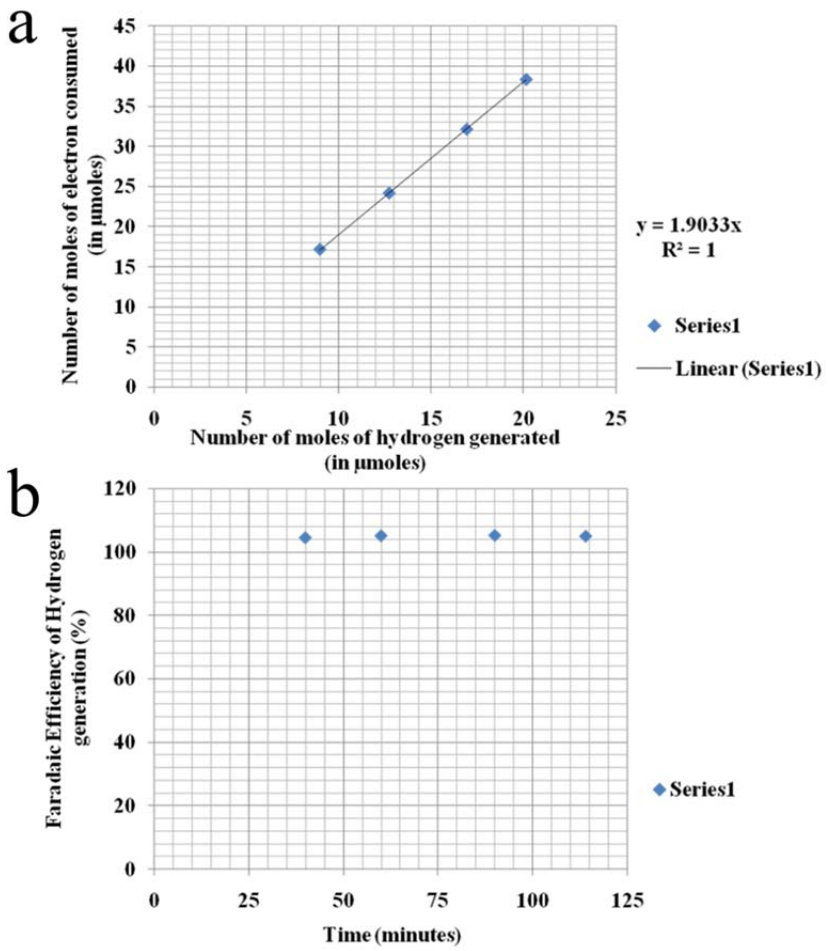

Figure 6-7. (a) Relationship between the numbers of moles of electrons consumed to the moles of H_2 produced (quantified by GC) as a result of bulk electrolysis of 0.5 mM [FeFe] complex on illuminated p-type Si in presence of 110 mM $HClO_4$. (Faradaic efficiency curve) (b) Variation of Faradaic efficiency of H_2 generation with time (in minutes).

The simplest form of photocurrent density for a p-type semiconductor/liquid junction is given by

$$J_{photo} = eQ\left[1 - \frac{e^{(-\alpha W_S)}}{1 + \alpha Z_p}\right] \qquad (1)$$

where, Q is the photon flux, α is the absorption coefficient, W_S is the depletion width, and Z_p is the electron diffusion length in the p-type semiconductor.[33,34] The above expression for photocurrent density is based on the assumptions that there is no recombination of photo-generated charge carriers in the depletion region of the semiconductor and that there is very fast heterogeneous charge transfer from the semiconductor to the redox species through the semiconductor/liquid junction. The actual photocurrent density has linear

dependence on the photon flux in addition to semiconductor properties. Figure 6-8(a) shows linear sweep voltammograms of 1 mM [FeFe] complex on illuminated p-type Si in the presence of 150 mM $HClO_4$. Similar to a standard semiconductor/liquid junction photoelectrochemical device, the photocurrent density is also scale with photon flux in the semiconductor/molecular catalyst junction under catalytic conditions. Under these conditions, the catalytic current density is clearly modulated by incoming light intensity and shows a linear dependence on illumination intensity (Figure 6-8(b)) similar to the photocurrent density in case of the standard semiconductor/liquid junction photoelectrochemical devices. In the p-Si/Re(bipy-tBu)$(CO)_3Cl$ molecular catalyst system, the relationship between homogeneous catalytic current density and light intensity has the form of Y=mX+C. Since C is non zero, the line does not pass through the origin. This is beacuse Re-catalyst has two single electron reduction; at lower illumination intensity and high catalyst concentration all the photogenerated carrier are used up for first single electrode reduction of Re-catalyst (no catalysis). The [Fe-Fe] complex has two simultaneous single electron reduction (single reversible two electrons reduction). This means that even at low intensity and high catalyst concentartion, the photogenerated carrier will be used for the homogeneous catalytic reduction of protons. Therefore, the relationship between homogeneous catalytic current density and light intensity has the form of Y=mX for p-Si/[Fe-Fe] complex as shown in Figure 6-8(b) for proton reduction. From the above discussion and 100 % faradaic efficiency, it is clear that the differences in current densities are caused by the incident light, and are not due to trivial catalyst photo-degradation. The short circuit quantum efficiency under these conditions is still low (39±1 %) over the whole range of photon fluxes. For good light to chemical energy conversion, the homogeneous catalytic current density should match the theoritical photocurrent density given by equation 1. The short circuit current efficiency is a measure of how well the homogeneous catalytic current density matches the theoretical photocurrent density. The homogeneous catalytic current density depends on catalytic concentration and substrate concentration. By increasing the acid concentration to 300 mM, the short circuit quantum efficiency improved to 73±1 % over the whole range of photon fluxes (Figure 6-9). Similar light intensity dependences are observed irrespective of whether the measurements are done with decreasing (Figure 6-9(a)) or increasing light intensity (Figure 6-9(b)). Figure 6-10 shows the relationship between homogeneous catalytic current density with illumination intensity,

where slope of the curve is 0.39 and 0.21 for perchloric acid concentration 300 mM and 150 mM, respectively. This shows the substrate concentration and illumination intensity dependence of homogeneous catalytic current and supports the hypothesis that theoretical photocurrent density should be match with homogeneous catalytic current density to optimize the performance of the semiconductor/molecular catalyst type system.

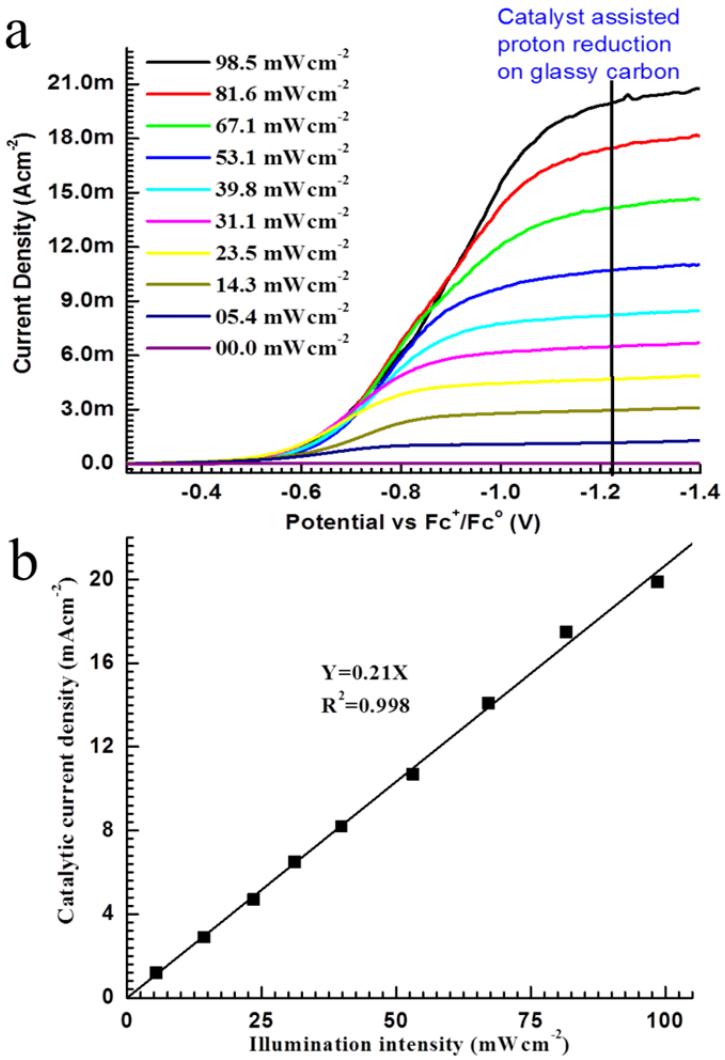

Figure 6-8. (a)Current density-voltage characteristics of the p-type Si/[FeFe] complex (1mM) junction in presence of 150 mM $HClO_4$ under 661 nm wavelength monochromatic light illumination. Measurements were performed at a scan rate of 10 mVs^{-1} and the solution was stirred. Black vertical line indicates the proton reduction on glassy carbon with the assistance of the [FeFe] complex. (b) Relationship between homgeneous catalytic current density and illumination intensity for the p-type Si//[FeFe] complex (1mM) junction in presence of 150 mM $HClO_4$ under 661 nm wavelength monochromatic light illumination.

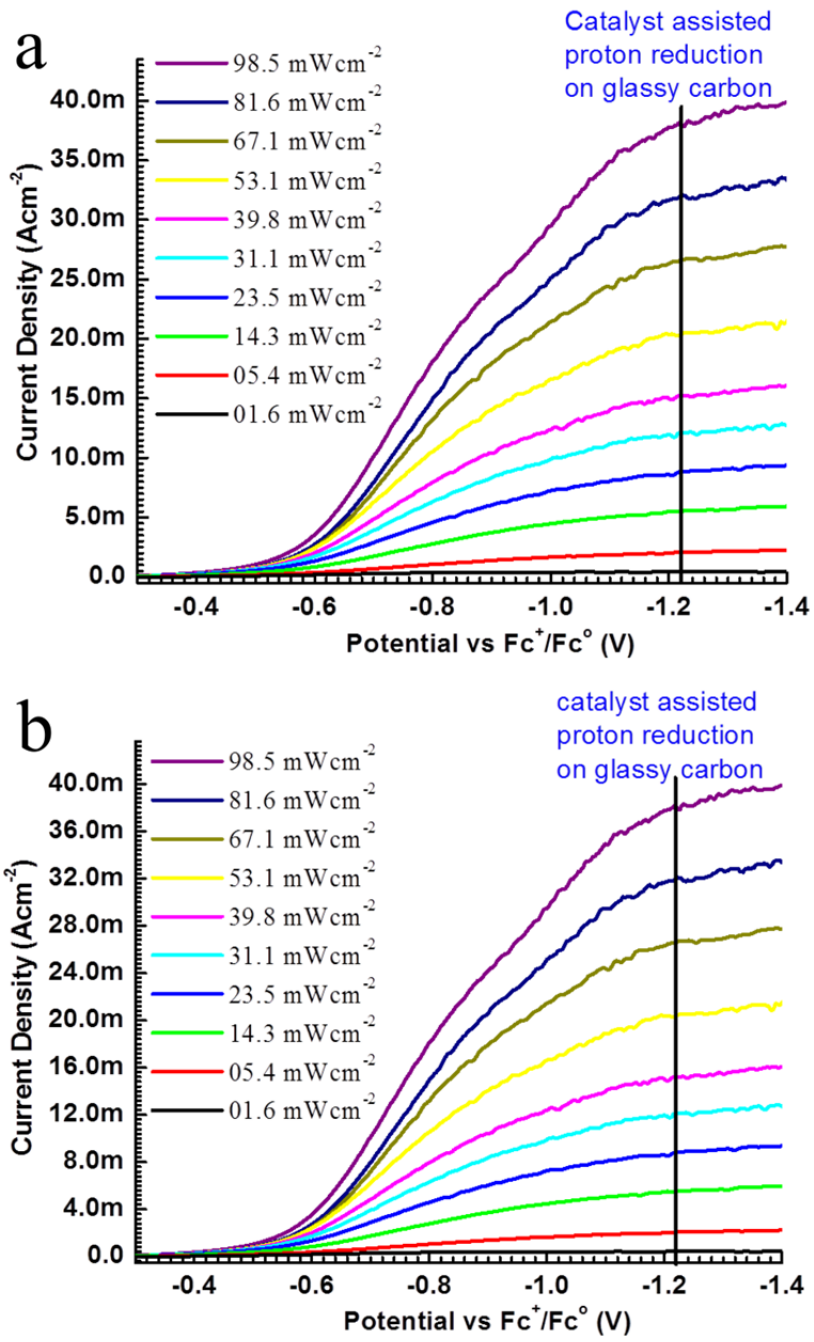

Figure 6-9. Current density-voltage characteristics of the p-type Si/[FeFe] complex junction in presence of 300 mM $HClO_4$ under a 661 nm wavelength monochromatic light illumination where (a) was measured with decreasing light intensity and (b) was measured with decreasing light intensity. Measurements were performed at a 10 mVs^{-1} scan rate and solution was stirred. Black vertical line indicates the proton reduction on glassy carbon with the assistance of the [FeFe] complex.

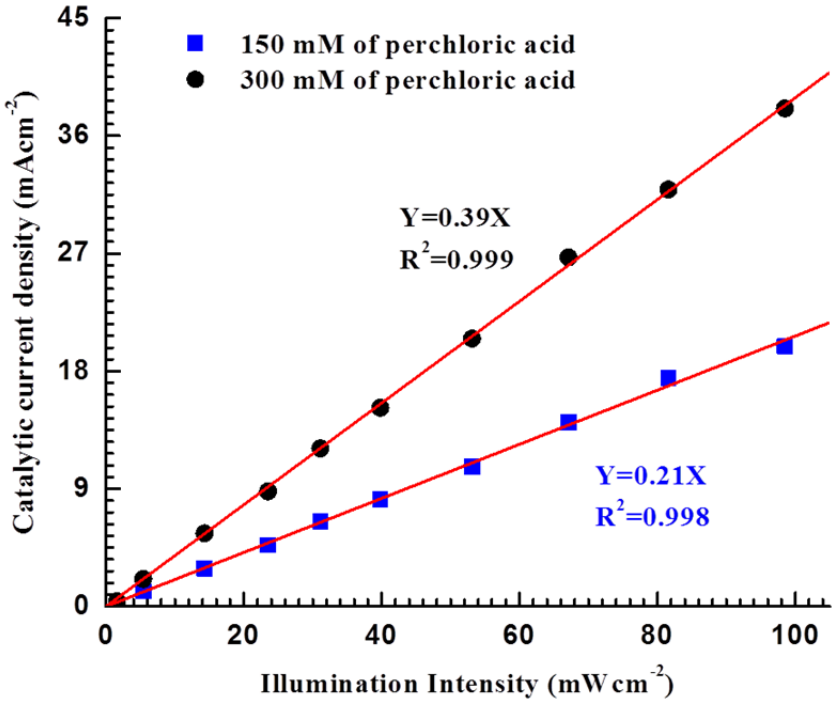

Figure 6-10. Variation of homogeneous catalyst current density of proton reduction through p-type H-Si/[Fe-Fe] complex molecular catalyst junction with illumination intensity.

The main characteristics of a photo-electrode are open circuit voltage (V_{oc}), short circuit current density (J_{sc}), fill factor (*ff*) and efficiency (η) and can be calculated from the current density vs. voltage plots.[35-37] Efficiency and fill factor are given as

$$P_{PA} = J_{mp} V_{mp}; \quad ff = \frac{J_{mp} V_{mp}}{J_{sc} V_{oc}}; \quad \eta = \frac{J_{mp} V_{mp}}{P_{in}} \tag{2}$$

where, J_{mp} and V_{mp} are current density and voltage at maximum power point and P_{in} is the optical power supplied. For our calculation, the zero potential is taken as the potential at which a glassy carbon electrode reduces proton to hydrogen via the [FeFe] complex. For this system with a p-type Si/[FeFe] complex junction and 150 mM acid, V_{oc} was 600 mV, J_{sc} was 20 mAcm^{-2}, *ff* was 30 %, and η was 3.5 %. For the p-type Si/[FeFe] complex junction with 300 mM of acid, V_{oc} was 640 mV, J_{sc} was 38 mAcm^{-2}, *ff* was 33%, and η was 8 %. The thermodynamic reduction potential for protons in acetonitrile with $HClO_4$ as the proton source is -0.26 V vs. Fc^{+}/Fc^{0}.[32] Therefore, the efficiency of the photo-electrode in the above case represents the portion of the light energy utilized in the catalytic process and not the light to chemical energy conversion efficiency.

6.4 Conclusions

In conclusion, photoreduction of the [FeFe] complex was achieved at illuminated p-type Si at a reduction potential 500 mV less negative than that at a glassy carbon electrode. Homogeneous photocatalytic reduction of protons was achieved with 100 % Faradaic efficiency, a high current density of 38 $mAcm^{-2}$, and 640 mV of open circuit voltage under 661 nm wavelength monochromatic illumination with a light conversion efficiency of 8 %. It can be concluded from the above observations that the [FeFe] complex is fast enough to keep pace with incoming light intensity up to 100 $mWcm^{-2}$ (one sun). This work has established the p-type Si/[FeFe] complex junction as a robust and inexpensive system for photoelectrochemical proton reduction that is commendable for applications with homogenous catalysts that feature lower dark overpotentials. With a proton reduction molecular catalyst which has lower over potential, the direct conversion of the solar energy to hydrogen can be achieved by a p-type semiconductor/molecular catalyst junction.

Note: Much of the material in this chapter comes directly from a manuscript entitled "Photoelectrochemical hydrogen generation by a [FeFe] hydrogenase active site mimic at a p-type Silicon/molecular electrocatalyst junction" by Bhupendra Kumar, Maryline Beyler, Clifford P. Kubiak and Sascha Ott, which has been published in *Chem. Eur. J.*, **2012**, 18, 1295-1298.

6.5 References

(1) Lewis, N. S.; Nocera, D. G. *Proc. Natl. Acad. Sci. USA* **2006**, *103*, 15729.

(2) Armaroli, N.; Balzani, V. *Angew. Chem. Int. Ed.* **2007**, *46*, 52.

(3) Gust, D.; Moore, T. A.; Moore, A. L. *Acc. Chem. Res.* **2009**, *42*, 1890.

(4) Magnuson, A.; Anderlund, M.; Johansson, O.; Lindblad, P.; Lomoth, R.; Polivka, T.; Ott, S.; Stensjö, K.; Styring, S.; Sundström, V.; Hammarström, L. *Acc. Chem. Res.* **2009**, *42*, 1899.

(5) Frey, M. *ChemBioChem* **2002**, *3*, 153.

(6) Gloaguen, F.; Rauchfuss, T. B. *Chem. Soc. Rev.* **2009**, *38*, 100.

(7) Tard, C. d.; Pickett, C. J. *Chem. Rev.* **2009**, *109*, 2245.

(8) Lomoth, R.; Ott, S. *Dalton Transactions* **2009**, 9952.

(9) Felton, G. A. N.; Mebi, C. A.; Petro, B. J.; Vannucci, A. K.; Evans, D. H.; Glass, R. S.; Lichtenberger, D. L. *J. Organomet. Chem.* **2009**, *694*, 2681.

(10) Gloaguen, F.; Lawrence, J. D.; Rauchfuss, T. B. *J. Am. Chem. Soc.* **2001**, *123*, 9476.

(11) Ott, S.; Kritikos, M.; Åkermark, B.; Sun, L.; Lomoth, R. *Angew. Chem. Int. Ed.* **2004**, *43*, 1006.

(12) Borg, S. J.; Behrsing, T.; Best, S. P.; Razavet, M.; Liu, X.; Pickett, C. J. *J. Am. Chem. Soc.* **2004**, *126*, 16988.

(13) Capon, J.-F.; Gloaguen, F.; Schollhammer, P.; Talarmin, J. *J. Electroanal. Chem.* **2004**, *566*, 241.

(14) Capon, J.-F.; Gloaguen, F.; Schollhammer, P.; Talarmin, J. *J. Electroanal. Chem.* **2006**, *595*, 47.

(15) Felton, G. A. N.; Vannucci, A. K.; Chen, J.; Lockett, L. T.; Okumura, N.; Petro, B. J.; Zakai, U. I.; Evans, D. H.; Glass, R. S.; Lichtenberger, D. L. *J. Am. Chem. Soc.* **2007**, *129*, 12521.

(16) Schwartz, L.; Singh, P. S.; Eriksson, L.; Lomoth, R.; Ott, S. *Comptes Rendus Chimie* **2008**, *11*, 875.

(17) Krassen, H.; Ott, S.; Heberle, J. *PCCP* **2011**, *13*, 47.

(18) Gärtner, F.; Sundararaju, B.; Surkus, A.-E.; Boddien, A.; Loges, B.; Junge, H.; Dixneuf, P. H.; Beller, M. *Angew. Chem. Int. Ed.* **2009**, *48*, 9962.

(19) Reisner, E.; Fontecilla-Camps, J. C.; Armstrong, F. A. *Chem. Commun.* **2009**, 550.

(20) Reisner, E.; Powell, D. J.; Cavazza, C.; Fontecilla-Camps, J. C.; Armstrong, F. A. *J. Am. Chem. Soc.* **2009**, *131*, 18457.

(21) Brown, K. A.; Dayal, S.; Ai, X.; Rumbles, G.; King, P. W. *J. Am. Chem. Soc.* **2010**, *132*, 9672.

(22) Streich, D.; Astuti, Y.; Orlandi, M.; Schwartz, L.; Lomoth, R.; Hammarström, L.; Ott, S. *Chemistry – A European Journal* **2010**, *16*, 60.

(23) Zhang, P.; Wang, M.; Na, Y.; Li, X.; Jiang, Y.; Sun, L. *Dalton Transactions* **2010**, *39*, 1204.

(24) Wang, F.; Wang, W.-G.; Wang, X.-J.; Wang, H.-Y.; Tung, C.-H.; Wu, L.-Z. *Angew. Chem.* **2011**, *123*, 3251.

(25) Krassen, H.; Schwarze, A.; Friedrich, B. r.; Ataka, K.; Lenz, O.; Heberle, J. *ACS Nano* **2009**, *3*, 4055.

(26) Nann, T.; Ibrahim, S. K.; Woi, P.-M.; Xu, S.; Ziegler, J.; Pickett, C. J. *Angew. Chem. Int. Ed.* **2010**, *49*, 1574.

(27) Schwartz, L.; Singh, P. S.; Eriksson, L.; Lomoth, R.; Ott, S. *C. R. Chimie* **2008**, *11*, 875.

(28) Bookbinder, D. C.; Lewis, N. S.; Bradley, M. G.; Bocarsly, A. B.; Wrighton, M. S. *J. Am. Chem. Soc.* **1979**, *101*, 7721.

(29) Turner, J. A.; Manassen, J.; Nozik, A. J. *Appl. Phys. Lett.* **1980**, *37*, 488.

(30) Bard, A. J.; Bocarsly, A. B.; Fan, F. R. F.; Walton, E. G.; Wrighton, M. S. *J. Am. Chem. Soc.* **1980**, *102*, 3671.

(31) Bocarsly, A. B.; Bookbinder, D. C.; Dominey, R. N.; Lewis, N. S.; Wrighton, M. S. *J. Am. Chem. Soc.* **1980**, *102*, 3683.

(32) Felton, G. A. N.; Glass, R. S.; Lichtenberger, D. L.; Evans, D. H. *Inorg. Chem.* **2006**, *45*, 9181.

(33) Butler, M. A. *J. Appl. Phys.* **1977**, *48*, 1914.

(34) Soedergren, S.; Hagfeldt, A.; Olsson, J.; Lindquist, S.-E. *J. Phys. Chem.* **1994**, *98*, 5552.

(35) Lewis, N. S. *Annu. Rev. Mater. Sci.* **1984**, *14*, 95.

(36) Lewis, N. S. *Acc. Chem. Res.* **1990**, *23*, 176.

(37) Walter, M. G.; Warren, E. L.; McKone, J. R.; Boettcher, S. W.; Mi, Q.; Santori, E. A.; Lewis, N. S. *Chem. Rev.* **2010**, *110*, 6446.

7 Chapter 7

Photocatalytic reduction through a p-type semiconductor/molecular catalyst interface: Uniqueness of the light intensity dependence of the homogeneous photocatalytic current density

7.1 Introduction

As discussed in chapter 1 and experimentally proven in subsequent chapters that a photocatalytic semiconductor/molecular electrocatalyst junction systems have three critical sequential steps in complete photo assisted homogeneous catalysis process, namely, (1) first step; light absorption and charge carrier generation and separation in the semiconductor, (2) second step; heterogeneous charge transfer from illuminated semiconductor to molecular electrocatalyst, and (3) third step; homogeneous catalytic reduction. In addition, it is also shown in earlier chapters that the homogeneous photocatalytic current densities for CO_2 as well as proton reduction via p-type semiconductor/molecular electrocatalyst interface vary linearly with incoming light intensity. This behavior is similar to the photocurrent density relationship with incoming light intensity for a conventional semiconductor/liquid junction photovoltaic device. For homogeneous electrocatalysis, the electrocatalysts freely diffuses in the solution which also has substrate in same phase. Most of the homogeneous catalysis used in this work, come in the category where substrate concentration is very large compared to electrocatalyst concentration. Under these conditions, the shape of cyclic voltammetric response is S-shaped curve independent to the scan rate as the scan rate decreases in quiescent solution.[1,2] Based on the assumptions, the homogeneous limiting catalytic current density (plateau current density) for a EC' type mechanism is given by

$$J_{cat} = n_{cat} F[catalyst]\left(D_{catalyst} k[sub]^{x}\right)^{1/2} \quad (1)$$

where n_{cat} = number of electrons involved in the homogeneous catalysis, F = Faraday's Constant, [catalyst] = catalyst concentration, $D_{catalyst}$ = the diffusion coefficient of the catalyst, k = pseudo first order rate constant of the catalysis, [sub] = substrate concentration, x = order of the homogeneous catalysis reaction.[3,4] One of the interesting aspects of this expression is that it contains the diffusion coefficient of the molecular catalyst. Equation (1) does not contain any scan rate term, but it contains the diffusion coefficient of the molecular catalyst. This means that the homogeneous limiting catalytic current density is

independent of the bulk mass transport and the molecular catalyst has to diffuse to the electrode surface after being regenerated during catalysis within the diffusion layer. However, most of the experimental condition employed in the current work involved moderate stirring of the solution to maximize the photocatalytic current density at a given catalyst concentration. The diffusion layer of any given system becomes thinner with increase in the stirring rate and the diffusion layer (δ) is related to the stirring rate (U) by following equation

$$\delta = \frac{B}{U^{\alpha}} \tag{2}$$

In the equation, B and α are constants for a given system.[5] Therefore, it is reasonable to employ the equation (1) for the case where stirring is used as long as stirring does not disturb the catalytic cycle of the molecular catalyst. Under stirring condition, the homogeneous limiting catalytic current density will be higher. This will lead to over estimation of the rate constant for the homogeneous catalysis. When there are multiple electrochemical and chemical steps involved for the homogeneous catalysis, a vigorous stirring might disturb the catalytic cycle by removing some of the intermediates out of the diffusion layer before the completion of the catalysis. Figure 7.1(a) shows the effect stirring on the linear scan voltammograms of Lehn catalyst [Re(bipy)CO_3Cl][6] under CO_2 on an illuminated p-Si photocathode. It is clear from the Figure 7.1(a) that the on-set potential for CO_2 reduction is moved to more negative potential at higher scan rate. At higher stirring rate, catalytic cycle which consists of ECEC' (electrochemical-chemical-electrochemical-catalytic) steps[7] as shown in Figure 7.1(b) are disturbed by stirring (take out singly reduced catalyst from diffusion layer before it gets a chance to diffuse back to electrode because of thinner diffusion layer). This means that it is reasonable to use the equation (1) to establish the limiting homogeneous catalytic current density with stirring for a given molecular catalyst concentration and substrate concentration. The proposed mechanistic model for semiconductor/molecular electrocatalyst junction suggests that the light intensity dependence of the limiting homogeneous photocatalytic current density should be independent of both catalyst as well as substrate concentration. This means that the slope of the homogeneous photocatalytic current density vs. the light intensity curve (linear curve as shown in chapter 2 and 6) must be same irrespective of the catalyst and substrate concentration. However, different slopes are observed for the different catalyst concentration (in case of Re-based CO_2 reduction molecular catalyst) and substrate

concentration (in case of [Fe-Fe] proton reduction catalyst). This unique property of semiconductor/molecular catalyst junction is discussed in detail in section 7.2 results and discussion.

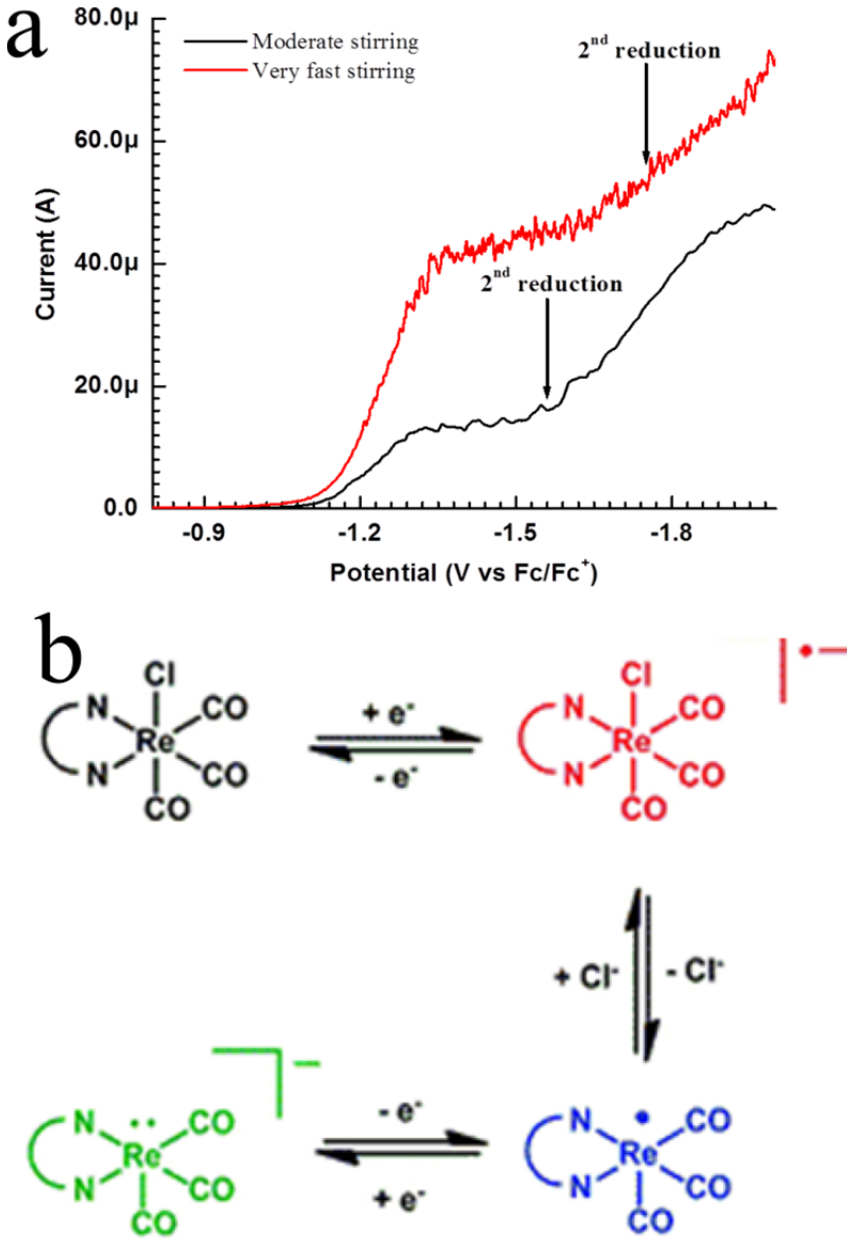

Figure 7-1. (a) Linear scan voltammograms of Re(bipyridine)$(CO)_3Cl$ [molecular catalyst] on an illuminated p-Si photocathode. (b) Mechanistic cycle of the two single electron reductions of Re(bipyridine)$(CO)_3Cl$ which involves a chemical step between two electrochemical step and doubly reduced specie is active form of the catalyst for homogeneous CO_2 reduction.

7.2 Results and discussions

The photo assisted electrochemical reduction of Re(bipy-tBu)$(CO)_3Cl$ on illuminated p-Si photocathode is shown in the Figure 7-2 (a). The separation of peak potentials of a completely reverse single electron redox couple is 59 mV.[5] The separation of peak potentials for the 1st reduction of Re(bipy-tBu)$(CO)_3Cl$ on illuminated p-Si is only 70 mV. This shows that there is excellent heterogeneous charge transfer from p-Si to Re(bipy-tBu)$(CO)_3Cl$ molecular catalyst. The peak photocurrent and photovoltage for both the reduction of Re(bipy-tBu)$(CO)_3Cl$ on illuminated p-Si decrease with decrease in the illumination intensity. Increase in the photovoltage is consistent with the quasi Fermi lever splitting.[8,9] The intensity dependence of the peak photocurrent density of Re(bipy-tBu)$(CO)_3Cl$ under Ar is unexpected. Since, the number of photo generated carrier is very large compared to Re(bipy-tBu)$(CO)_3Cl$ concentration and there is no change in the scan rate. So ideally, there should not be any change in the peak photo current density with the illumination intensity. This behavior is more pronounced at the lower illumination intensity and catalytic condition (limiting catalytic photocurrent density). A similar phenomenon was observed in the theoretical models and electrochemical studies of p-Si/Me_2-$CoCp_2PF_6$ under illumination.[10,11] In the theoretical model, a semiconductor/liquid junction is replaced by a metal/liquid junction in series with a photo diode. These models are unable to provide accurate fit to cyclic voltammetry curves at low light intensity. It is likely that at low light intensity when a limited flux of minority carrier is generated by an illumination source. The intensity dependent charge transfer rate is predicated by second order rate law for the photogenerated minority carrier by redox acceptor in the solution phase.[10,12] This particular characteristic of a semiconductor/liquid junction is not included in the above proposed model.[10,11] Similar intensity dependence of the peak photocurrent density of Re(bipy-tBu)$(CO)_3Cl$ under non catalytic condition is observed on both nanostructured p-Si and surface modified p-Si photocathode (not shown here). The intensity dependence of the peak photocurrent density of the molecular catalyst on a semiconductor photoelectrode under non catalytic condition is the source of intensity dependence of the limiting catalytic photocurrent density under catalytic condition.

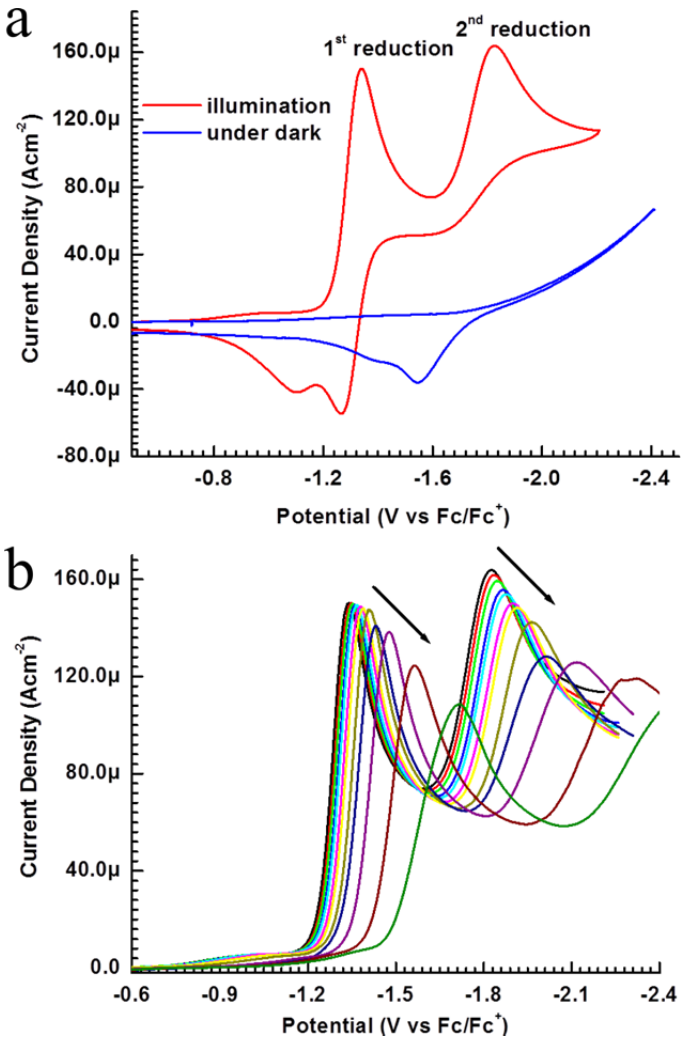

Figure 7-2. (a) Cyclic voltammograms of Re(bipy-tBu)$(CO)_3$Cl at p-Si under polychromatic illumination (88 mWcm-2 intensity, blue trace) and without illumination (red trace). (b) Cyclic voltammograms of Re(bipy-tBu)$(CO)_3$Cl at p-Si under varying polychromatic light intensities. p-Si working photocathode, Pt counter, Ag/AgCl reference, scan rate 100 mVs-1, 0.2 mM catalyst with 0.5 M TBAH supporting electrolyte in acetonitrile under argon.

Under catalytic condition, the limiting catalytic current density is a function of the catalyst concentration given by equation (1). The limiting catalytic photocurrent density of CO_2 reduction to CO through p-Si/Re(bipy-tBu)$(CO)_3$Cl is shown in the Figure 7.3(a) for the molecular catalyst concentration of 2.0 mM and 6.0 mM under polychromatic light intensity of 66 mWcm^{-2}. The integrated maximum photocurrent under Air Mass 1.5 illumination (100 mW cm^{-2}) using the conventional Shockley-Quiesser limit for solar energy conversion for p-Si (1.12 eV) is 44.0 mA cm^{-2}.[13] The limiting catalytic photocurrent densities (at 66 mWcm^{-2} polychromatic illumination) are 15.8 and 5.7 mAcm^{-2}, respectively, for 6 mM and 2mM Re(bipy-tBu)$(CO)_3$Cl concentration. Although, the catalytic photocurrent density (15.8 mAcm^{-2}) at 6

mM molecular catalyst is consistent with the maximum photocurrent density for a p-Si/liquid junction under polychromatic illumination considering reflection from flat p-Si surface which around 20%. The conversion efficiencies for the homogeneous photocatalytic reduction of CO_2 to CO for 2.0 mM and 6.0 mM are 10% and 2.2%, respectively, at the same polychromatic illumination. The illumination intensity dependence of the homogeneous photocatalytic current density is shown in the Figure 7.3(b). For both catalyst concentrations, the homogeneous photocatalytic current density is directly proposition to the illumination intensity with different slopes. The photo-generated electrons transfer from p-Si to Re(bipy-tBu)$(CO)_3$Cl molecular catalyst is thermodynamically downhill process. Therefore, it would be reasonable to assume that the heterogeneous charge transfer does not vary with the change the molecular catalyst concentration. The change in the catalyst concentration does change the number occupied site on the semiconductor electrode surface by the molecular catalyst. Same theory was also proposed for the better conversion efficiency for the homogeneous photocatalytic reduction of CO_2 to CO through p-type semiconductor/Ni$(cyclam)^{2+}$ molecular catalyst junction.[14] In addition, the different slopes also indicate that the number of occupied sites on semiconductor electrode does not change under catalytic condition i.e. during turning over process of the molecular catalyst.

Another critical parameter of molecular catalyst is turn over frequency which is defined as catalyst turn overs per unit time. The turn over frequency of a molecular catalyst is function of the rate of catalysis and the substrate concentration.[1] At higher turnover frequency, there will be greater concentration gradient within the diffusion layer which will lead to higher limiting catalytic current density. The catalyst turnover frequency can be charged by changing the substrate concentration. The homogeneous catalytic photoreduction of protons is achieved by p-Si/[Fe-Fe] complex molecular catalyst junction.[15] Figure 7.4 shows the catalytic current density depends on the illumination intensity for proton reduction by p-Si/[Fe-Fe] complex molecular catalyst junction for 300 mM and 150 mM of perchloric acid. The linear relationship between the catalytic current density and the illumination intensity is indicative of light driven homogeneous reduction of protons to hydrogen. At higher proton source (perchloric acid in this case), the [Fe-Fe] catalyst turnover faster, this leads to larger concentration gradient within diffusion layer. The direct consequence of this is a larger limiting catalytic photocurrent density. This can be also seen from the

different slopes of the catalytic current density vs illumination intensity curve for 300 mM and 150 mM of perchloric acid. This result also consistent with the assumption that number of occupied sites on semiconductor is fixed by the initial catalyst concentration and the heterogeneous charge transfer is fast.

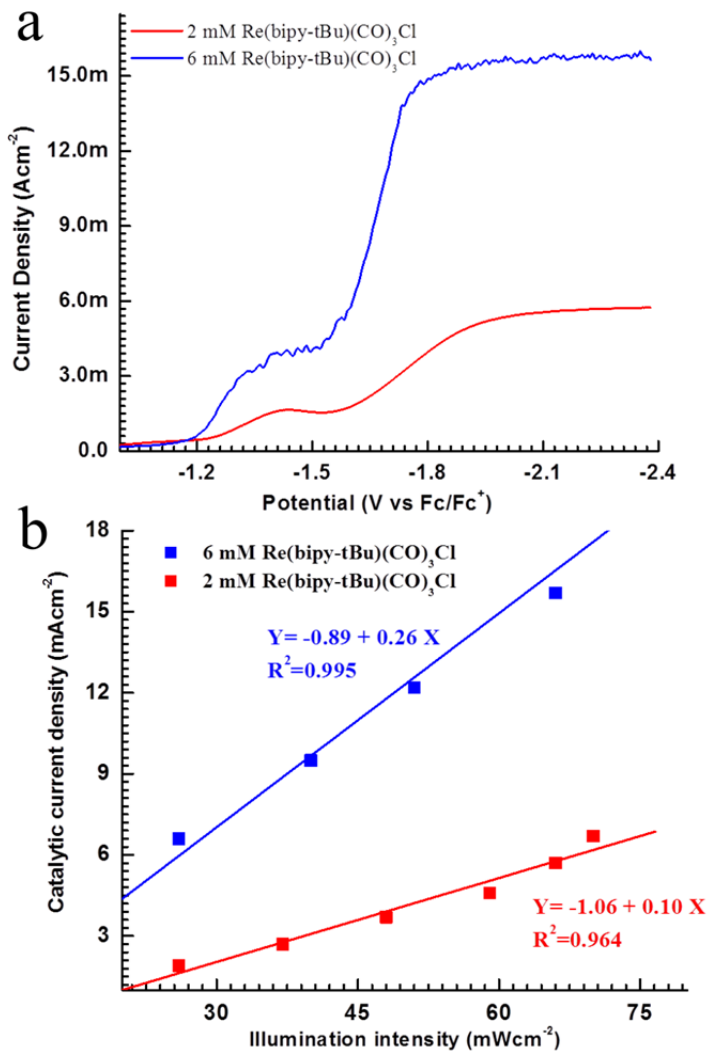

Figure 7-3. (a) Current density-voltage characteristics of p-Si/Re(bipy-tBu)$(CO)_3$Cl molecular catalyst junction under 1 atmosphere of CO_2 with 2 mM (red) and 6 mM (blue) Re(bipy-tBu)$(CO)_3$Cl. (b) The variation of the homogeneous photocatalytic current density of p-Si/Re(bipy-tBu)$(CO)_3$Cl molecular catalyst junction with the polychromatic illumination intensity where blue and red solid square represent 6 mM and 2 mM Re(bipy-tBu)$(CO)_3$Cl. Here solvent is acetonitrile, electrolyte is 0.1 M of TBAH, counter electrode is Pt, Ag/AgCl as reference electrode.

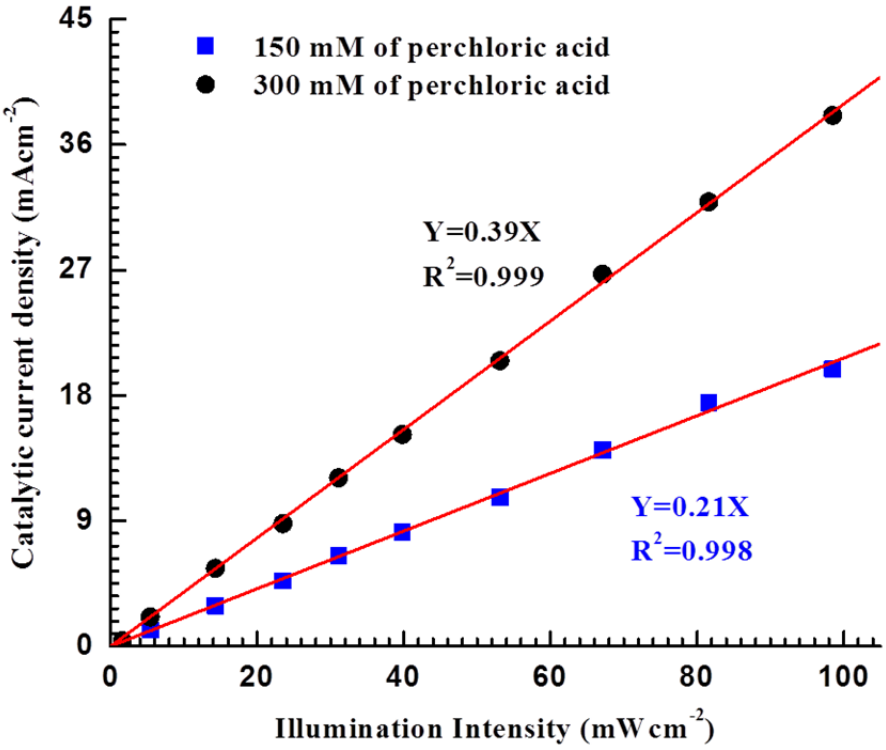

Figure 7-4. Variation of homogeneous catalyst current density of proton reduction through p-Si/[Fe-Fe] complex molecular catalyst junction with illumination intensity.

7.3 Conclusions

In the homogeneous photocatalytic reduction by a p-type semiconductor/molecular catalyst junction, the initial catalyst concentration dictates the number of occupied sites by the catalyst on the semiconductor electrodes. For a molecular catalyst with a given rate of homogeneous catalysis, the limiting catalytic current density depends upon both the catalyst concentration (the number of occupied sites on the semiconducting electrode) and the substrate concentration (control the concentration gradient of catalyst in the diffusion layer under catalytic condition). As stated in earlier chapters, for optimal conversion efficiency, the catalyst and substrate concentration should be such that the short circuit quantum efficiency is close to 100%. This understanding of the homogeneous photocatalytic reduction by a p-type semiconductor/molecular catalyst junction is particularly important for "heterogenizing" the molecular catalyst on a semiconducting photoelectrode. The number of occupied sites (number of hereogenized molecular catalyst), rate of catalysis for a heterogenized catalyst, substrate concentration must be considered to judge whether a "heterogenized" catalyst is better than it homogeneous form.

7.4 References

(1) Savéant, J.-M. *Chem. Rev.* **2008**, *108*, 2348.

(2) Bard, A. J.; Faulkner, L. R. *Electrochemical Methodes: Fundamentals and Applications*; 2 ed.; John Wiley & Sons, Inc., 2001.

(3) DuBois, D. L.; Miedaner, A.; Haltiwanger, R. C. *J. Am. Chem. Soc.* **1991**, *113*, 8753.

(4) Savéant, J. M.; Vianello, E. *Electrochim. Acta* **1962**, *8*, 905.

(5) Wang, J. *Analytical Electrochemistry*; 3 ed.; Wiley-VCH, A John Wiley & Sons, Inc., 2006.

(6) Hawecker, J.; Lehn, J.-M.; Ziessel, R. *J. Chem. Soc., Chem. Commun.* **1984**, 3.

(7) Smieja, J. M.; Kubiak, C. P. *Inorg. Chem.* **2010**, *49*, 9283.

(8) Kenyon, C. N.; Tan, M. X.; Krüger, O.; Lewis, N. S. *J. Phys. Chem. B* **1997**, *101*, 2850.

(9) Tan, M. X.; Kenyon, C. N.; Krüger, O.; Lewis, N. S. *J. Phys. Chem. B* **1997**, *101*, 2830.

(10) Santangelo, P. G.; Lieberman, M.; Lewis, N. S. *J. Phys. Chem. B* **1998**, *102*, 4731.

(11) Santangelo, P. G.; Miskelly, G. M.; Lewis, N. S. *J. Phys. Chem.* **1989**, *93*, 6128.

(12) Lewis, N. S. *Annu. Rev. Phys. Chem.* **1991**, *42*, 543.

(13) Walter, M. G.; Warren, E. L.; McKone, J. R.; Boettcher, S. W.; Mi, Q.; Santori, E. A.; Lewis, N. S. *Chem. Rev.* **2010**, *110*, 6446.

(14) Petit, J.-P.; Chartier, P.; Beley, M.; Deville, J.-P. *J. Electroanal. Chem.* **1989**, *269*, 267.

(15) Kumar, B.; Beyler, M.; Kubiak, C. P.; Ott, S. *Chemistry – A European Journal* **2012**, *18*, 1295.

8 Chapter 8

Lessons learned and future work

8.1 Effect of internal reference (Fc/Fc^+) on stability of p-Si/molecular catalyst junction system

One of the common practices in the electrochemistry is to add an internal reference to verify the redox potential of the species of interest. It is well known that semiconducting photoelectrodes are extremely sensitive to impurities in the solution. With the goal of reducing the cell resistance, a Pt reference electrode is used with a mixture of ferrocene/ferrocinium added to the solution of Re(bipy-*t*Bu)$(CO)_3Cl$ (Re-catalyst) in acetonitrile with 0.1 M TBAH as a supporting electrolyte and a p-Si photoelectrode as the working photoelectrode. Consecutive cyclic voltammetric scans of this system are shown in Figure 8.1(a). The first cyclic voltammogram shows a reversible 1st reduction and a well-defined 2nd reduction of the Re-catalyst at illuminated p-Si. With each scan, the 1st reduction of the catalyst moves towards a more negative potential and the 2nd reduction becomes less defined. In addition, re-oxidation of the 1st reduction of the catalyst also disappears with each consecutive scan. All the attempts (changing the cell design, changing the cell material from Teflon to glass, changing the electrode preparation techniques, and chemicals (catalyst, solvent, electrolyte) purification) to restore the stability of the p-Si photoelectrode for the Re-catalyst photoreduction failed as long as ferrocene was directly added to the solution. The reduction of the Re-catalyst on a glassy carbon dark electrode in the same solution remained stable (not shown here). The above observations indicated that there was some sort of degradation going on in this system which only affected the semiconductor photoelectrode and not the glassy carbon dark electrode. The Re-catalyst, solvent (acetonitrile), electrolyte, and epoxy used to make the photoelectrodes are stable under the experimental condition. The Fc/Fc^+ couple is completely reversible and a well behaved redox species. Under the strong reducing conditions (-1.8 V vs Fc/Fc^+) employed in these measurements, the degradation of ferrocene leads to the deposition of a yet unidentified product (most likely Iron (Fe)) on the p-Si photoelectrode. This hypothesis is consistent with the fact that a stable reduction the Re-catalyst can occur on the glassy carbon electrode with added ferrocene (only a few metal particles of Fe will not affect the performance of a glassy carbon electrode). As shown in Figure 8.1(b), the continuous multiple cyclic voltammetric scans of the Re-catalyst is completely stable at an illuminated p-Si photoelectrode without the

addition of ferrocene in the electrochemical solution. When Platinum (Pt) is used as a reference electrode, it is not stable, but it does affect the redox behavior of the Re-catalyst or any other redox species. A three compartment cell where both reference and counter are separated from the working photoelectrode compartment is the best way to test or examine photoelectrochemistry of semiconducting electrodes.

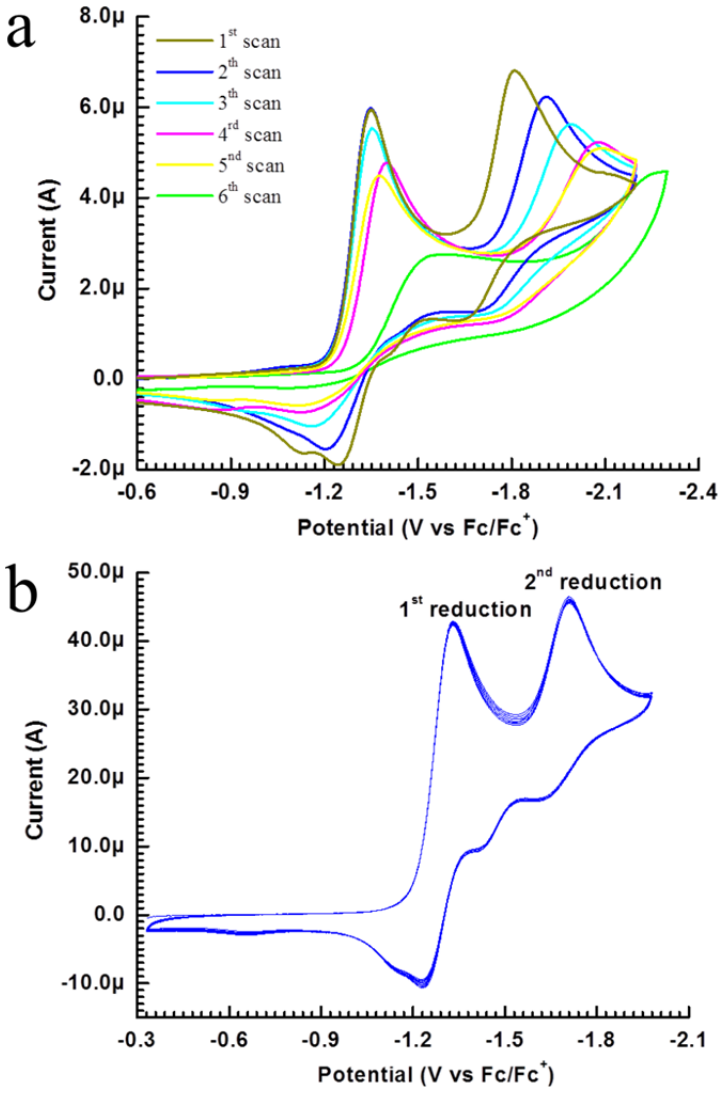

Figure 8-1. Cyclic voltammograms of Re(bipy-*t*Bu)$(CO)_3$Cl at a p-Si photocathode under the polychromatic illumination (a) with Fc/Fc^+ as internal reference and (b) without Fc/Fc^+ as an internal reference. The solution consist of 0.1 M TBAH (supporting electrolyte) in acetonitrile with two Pt wires were used as both as the counter electrode and reference electrode. The reduction peaks of the catalyst at p-Si are referenced to the reduction peaks of the catalyst on glassy carbon.

8.2 Covalent attachment of the molecular catalysts from Re(bipyridyl)$(CO)_3Cl$ family to a p-Si photocathode

A two-step scheme is used to covalently attach the molecular catalyst from Re(bipyridyl)$(CO)_3Cl$ to a p-Si photoelectrode. The first step is the covalent attachment of 4-methyl-4'-allyl-2,2'-bipyridine (ligand synthesis is reported in Jonathan M. Smieja's dissertation) to hydrogen terminated p-Si using the Lewis acid method described in chapter 3. The second step is the addition of rhenium to the ligand by refluxing the ligand modified p-Si with $Re(CO)_5Cl$ in toluene under an atmosphere of argon at 110 ^oC overnight (samples are prepared in the glove box for flux and flux is done outside under argon environment). After reflux samples were rinsed with hot toluene followed by THF, acetonitrile, and finally water. The modified samples appeared hydrophobic at the end of both first and second steps. No carbonyl peaks were observed in the FT-IR for the catalyst covalently attached to planar p-Si. The three characteristic carbonyl peaks were, however, observed for the Re-catalyst covalently attached to nanowire p-Si (nanowire fabrication and it's surface modification is reported chapter 4 of this dissertation) as shown in Figure 8.2. For all the samples both nanowire and planar, no redox behavior or catalysis of the covalently attached catalyst was observed.

There could be several reasons for the lack of catalytic activity of the catalyst when covalently attached to p-Si photocathode. The linker to the surface had only three carbon chain. This short chair may restrict the structural changes required for electrochemical reduction of the catalyst. Reduction of the catalyst labilizes the chloride ligand in the axial position. That open coordination site is the only available sites for CO_2 binding. (There are six sites at Rhenium metal center (octahedral structure) of the catalyst, out of six sites only one site is available for CO_2 binding (labile ligand "Chloride" site).) The lack of catalytic activity, therefore, might be due to the fact that the available sites are not accessible when the catalyst is covalently attached to p-Si photocathode with a short linker or in a monolayer. Unconjugated long linker will provide freedom for structural changes, but will adversely affect the heterogeneous charge transfer from the Si photoelectrode to the covalently attached Re-catalyst.[1,2]

A new scheme for anchoring the catalyst to p-Si was designed where the bipyridine ligand for the catalyst has a twelve carbon linker and phenyl ethyl group are attached to the p-Si as a spacer between the

catalysts and charge transfer assistant as shown in Figure 8.3. An excellent homogeneous catalytic activity is reported (chapter 3) at a phenyl ethyl modified p-Si photoelectrode and the Re-catalyst due to favorable π-π bond interactions between the bipyridine ligand of the Re-catalyst and the phenyl group on the surface of the photoelectrode. With the above mentioned scheme a similar π-π bond interactions can be achieved between covalently bound the catalyst with the phenyl groups on the surface of photocathode. X-ray photoelectron spectroscopy (XPS) analysis done on ligand modified p-Si electrodes with the phenyl ethyl group as spacers before and after metalation showed the presence of Nitrogen and Re metal in addition to nitrogen, respectively. Conclusive detection of aromatic rings on surface is not feasible due to contamination of samples. The nitrogen signal in XPS spectra confirmed the presence of bipyridine ligands on the surface. The Re metal and nitrogen signals together confirmed the successful metalation and covalent attachment of the catalyst to p-Si. p-Si surfaces remained very hydrophobic before and after the metalation. Electrochemistry was not done on these samples because the epoxy method used for sample preparation was not compatible with the surface modified samples. A new process (using epoxy) has been developed that is compatible with surface modified samples and techniques have been transferred to new members (Jerry and Alissa) in the group. The key to the success of this project will depend on the ability to make the lollipop electrodes without damaging the modified surface. Another important requirement for this project is that all electrochemistry must be done in a three compartment cell where both the counter and the reference electrodes are separated from main chamber by Vycor glass frits.

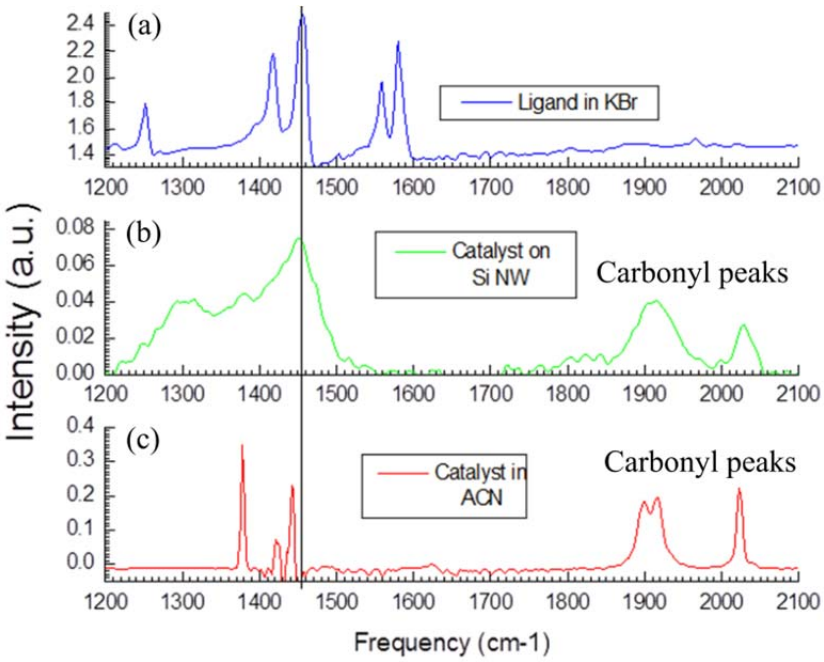

Figure 8-2. FTIR absorption spectra of (a) 2,2'-bipyridine ligand in a KBr pellet, (b) p-Si nanowires surface modified with the catalyst and (c) the catalyst in acetonitrile solution. The three characteristics carbonyl peaks of the catalyst are observed for the covalently attached catalyst to p-Si nanowires. This confirms the successful heterogenization of the catalyst on the p-Si photocathode.

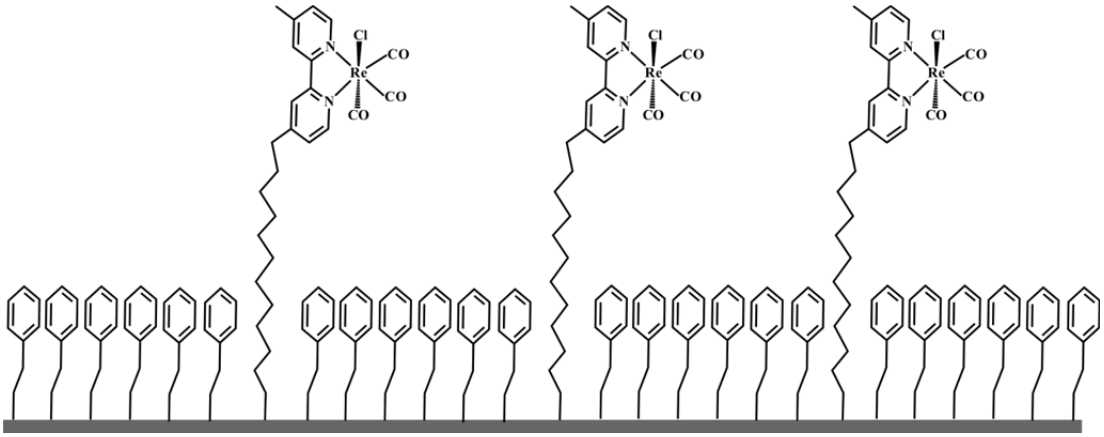

Figure 8-3. Schematic representation of the new scheme for covalent attachment of the catalyst on p-Si with phenyl ethyl groups as spacer s and charge transfer mediators.

8.3 Extension of the p-Si/molecular catalyst junction system to other members of the Re(bipyridyl)$(CO)_3Cl$ molecular catalyst family

Among all the variants of the 2.2'-bipyridine ligand for the Re(bipyridyl)$(CO)_3Cl$ molecular catalyst system, bipy-*t*Bu = 4,4'-di-*tert*-butyl-2,2'-bipyridine ligand has shown the best catalytic activity towards CO_2 reduction.[3] Therefore, Re(bipy-tBu)$(CO)_3Cl$ was selected for the photoelectrochemical reduction of CO_2 to CO by p-Si/ molecular catalyst junction. This system is discussed in detailed in Chapters 2 to 5. The three other members of this catalytic system that have also shown catalytic activity towards CO_2 are Re(bipy)$(CO)_3Cl$, Re(dmb)$(CO)_3Cl$ and Re(dnb)$(CO)_3Cl$ (bipy = 2,2'-bipyridine, dmb = 4,4'-di-*methyl* -2,2'-bipyridine and dnb = 4,4'-di-n-*nonyl* -2,2'-bipyridine). At low concentration (1 mM or less) of molecular catalyst, all three molecular catalysts have two reduction peaks under argon on illuminated p-Si at approximately 500 to 530 mV more positive potential compared to a glassy carbon electrode (Figure 8.4). Under an atmosphere of CO_2, there is an increase in current at the 2^{nd} reduction peak for all three p-Si/Re(bipyridyl)$(CO)_3Cl$ junctions (Figure 8.4). At catalyst concentration around 5 mM (a necessity for good solar conversion efficiency), the cyclic voltammograms of all three molecular catalysts on both illuminated p-Si and glassy carbon have three reduction peaks as shown in Figure 8.5(a) and (b) for Re(bipy)$(CO)_3Cl$ and Re(dmb)$(CO)_3Cl$, respectively(cyclic voltammograms of Re(dnb)$(CO)_3Cl$ is not clean at 5 mM concentration and not shown here). No such feature was observed for Re(bipy-*t*Bu)$(CO)_3Cl$ on both illuminated p-Si photoelectrode and glassy carbon dark electrode.[4] This behavior is possibly due to the higher degree of dimerization in these molecular catalysts at high concentration of the catalyst. Under an atmosphere of CO_2, there is an increase in the current around 2^{nd} and 3^{rd} peaks for both Re(bipy)$(CO)_3Cl$ and Re(dmb)$(CO)_3Cl$ molecular catalyst as shown in Figure 8.5(c) and (d), respectively. The homogeneous catalytic current densities increased with the catalyst concentration for all the three catalysts. This observation is consistent with theory proposed in chapter 7 about the sites occupancy of the molecular catalysts on semiconducting photoelectrodes in this type of systems.

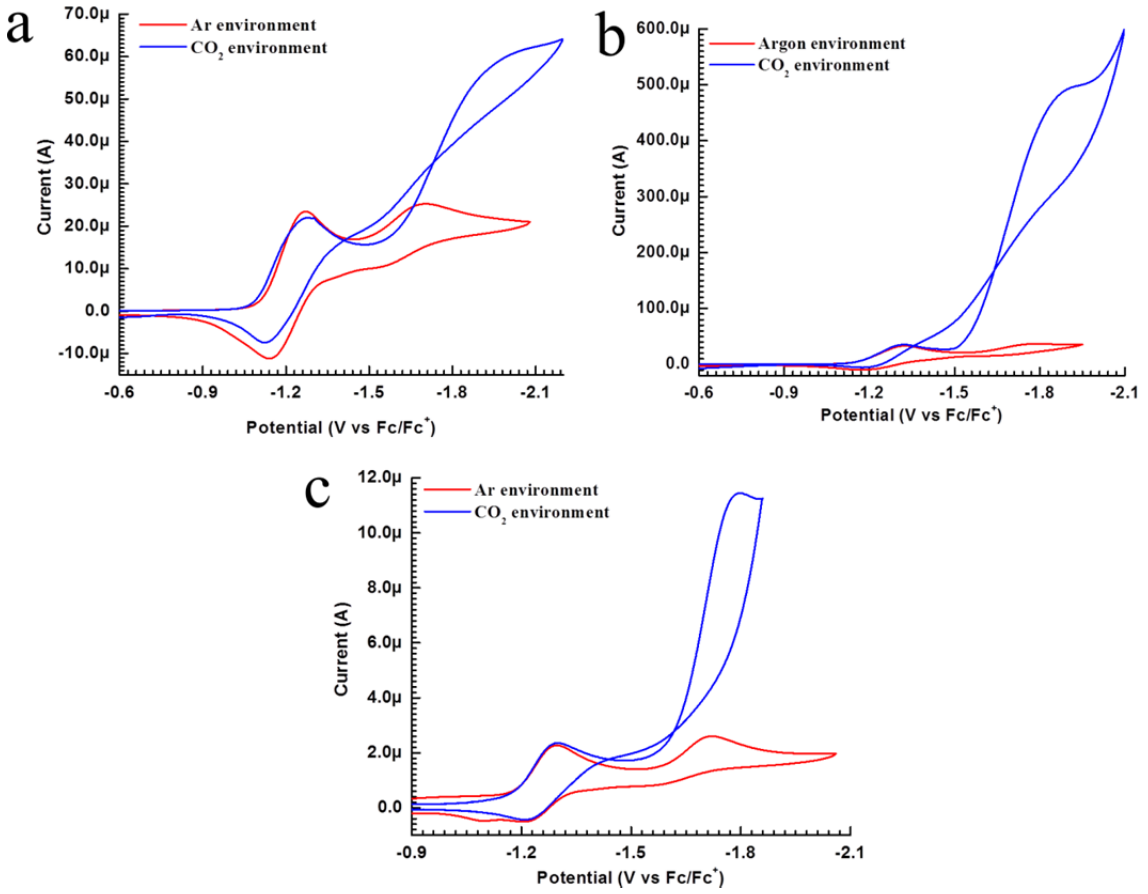

Figure 8-4. Cyclic voltammograms of (a) $Re(bipy)(CO)_3Cl$ (0.5 mM), (b) $Re(dmb)(CO)_3Cl$ (1mM) and (d) $Re(dnb)(CO)_3Cl$ (0.3 mM) in Ar environment (red line) and CO_2 environment (blue line) on p-Si photocathode under 95 $mWcm^{-2}$ monochromatic illumination (661 nm) . 0.1 M TBAH in acetonitrile as supporting electrolyte and Pt wires are used as the reference and the counter electrodes. Electrode areas are (a) 0.15 cm^{-2}, (b) 0.15 cm^{-2} and (c) 0.02 cm^{-2}.

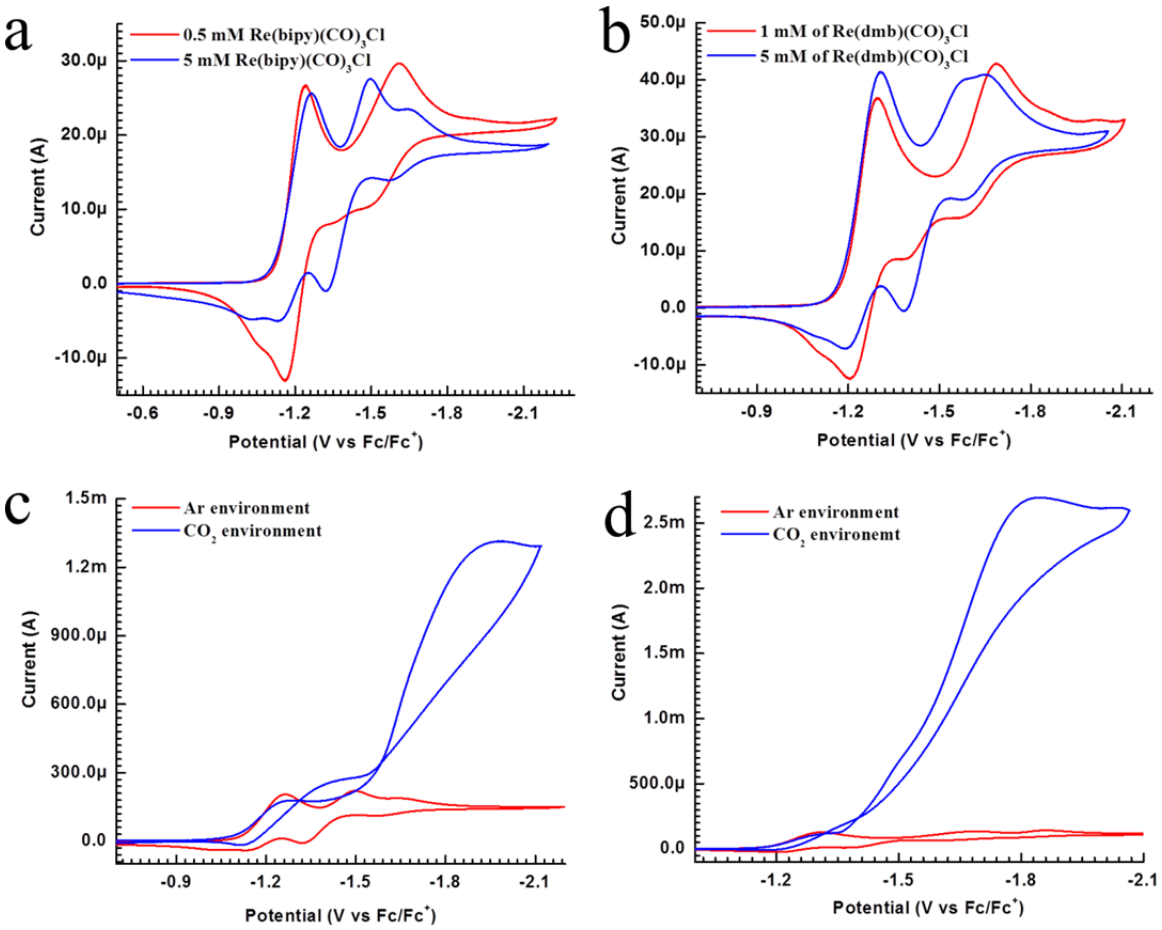

Figure 8-5. Effect of the catalyst concentration on the cyclic voltammograms of (a) $Re(bipy)(CO)_3Cl$ with concentration 0.5 mM (red line) and 5 mM (blue line) (current is scaled down by a factor of 7) and (b) $Re(dmb)(CO)_3Cl$ with concentration 1mM (red line) and 5 mM (blue line) (current is scaled down by a factor of 3) on a p-Si photocathode under monochromatic illumination. Cyclic voltammograms of (c) $Re(bipy)(CO)_3Cl$ (5 mM) and (d) $Re(dmb)(CO)_3Cl$ (5mM) in Ar environment (red line) and CO_2 environment (blue line) on p-Si photocathode under 95 $mWcm^{-2}$ of monochromatic illumination (661 nm). 0.1 M TBAH in acetonitrile as supporting electrolyte and Pt wires are used as the reference and the counter electrodes. Electrode area is 0.15 cm^{-2}.

8.4 Photoelectrochemical reduction of Cobalt difluororyl-diglyoximate complex (a proton reduction molecular catalyst)

The disadvantages of [Fe-Fe] complex reported in Chapter 6 for the proton reduction are its high over potential and the lack of stability under visible irradiation. A series of cobalt macrocyclic glyoxime complexes have low overpotentials for proton reduction in non-aqueous media (acetonitrile) and are stable under visible irradiation.[5,6] Among them, Cobalt difluororyl-diglyoximate (Co-catalyst) has the Co (II/I)

couple at -0.55 V vs SCE (Fc/Fc^+ is 0.38 V vs SCE in acetonitrile[7]) and it's structure is shown in Figure 8.6(a). The thermodynamic potential for the proton reduction in acetonitrile solution with HCl as a proton is -0.29 V vs SCE.[5] Therefore, the overpotential of the proton reduction with Co-catalyst and HCl as the proton source in acetonitrile is only 0.26 V. With p-Si as a photocathode, a photovoltages greater than 0.5 V are achieved for p-Si/Re(bipyridyl)$(CO)_3Cl$ molecular catalyst junction for CO_2 reduction and p-Si/[Fe-Fe] complex molecular catalyst junction for the proton reduction. So theoretically, it is feasible to produce hydrogen at it's thermodynamic potential on an illuminated p-Si (has around 1 V overpotential for the proton reduction without any catalyst) by the p-Si/Co-catalyst junction.

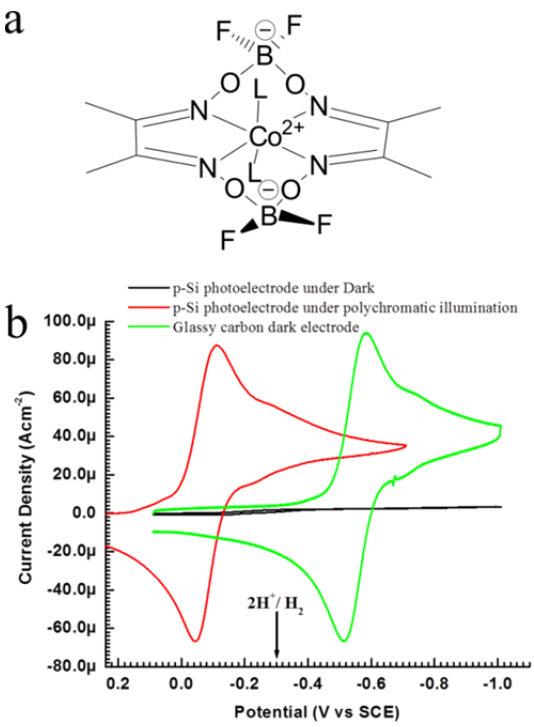

Figure 8-6. (a) Cobalt difluoroboryl-diglyoximate complex (Co-catalyst); where L is acetonitrile. (b) Cyclic voltammograms of 0.4 mM Co-catalyst on p-Si (red line under 100 $mWcm^{-2}$ polychromatic illumination and black line under dark condition) and on glassy carbon (green line) in acetonitrile with 0.5 M TBAH as a supporting electrolyte, Ag/AgCl as the reference and Pt as a counter electrode.

The electrochemical reduction of Co-catalyst on a glassy carbon and an illuminated p-Si is shown in Figure 8.6(b). Co(II/I) couple of the Co-catalyst on illuminated p-Si photocathode was 0.47 V more positive potential compared to the glassy carbon electrode. This implies that the homogeneous catalytic reduction of proton can be achieved at its thermodynamic potential via p-Si/Co-catalyst junction. This

system is suitable to directly convert solar energy into chemical energy. This is similar to the heterogeneous proton reduction with assistance of light using a platinum nanoparticles decorated p-Si photocathode. Figure 8.7(a) shows the cyclic voltammograms of the Co-catalyst on an illuminated p-Si photoelectrode at different scan rates. The scan rate dependence of the peak current density of the Co(II/I) couple and it's re-oxidation are shown in Figure 8.7(b). The peak current density for the reduction and re-oxidation of the Co(II/I) couple are directly proportional to the square root of the scan rate. This indicates that thete is no adsorption of Co-catalyst on p-Si photoelectrode and the Co-catalyst is free diffusing in solution.

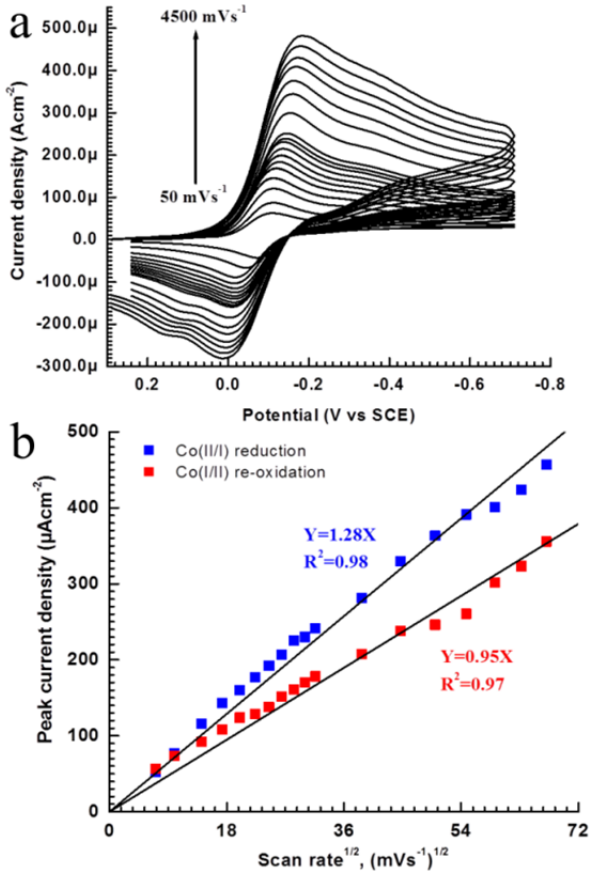

Figure 8-7. (a) Cyclic voltammograms of Cobalt-catalyst on an illuminated p-Si photocathode with varying scan rate. (b) The variation of the peak current densities of Co-catalyst with the square root of scan rate on an illuminated p-Si photocathode in acetonitrile with 0.5 M TBAH as a supporting electrolyte, Ag/AgCl as the reference and Pt as a counter electrode. Blue dots and red dots represent the reduction and the re-oxidation of Co(II/I) couple, respectively .

8.5 Transferring pyridine/pyridinium chemistry of CO_2 reduction to p-Si photocathode

Direct electrochemical reduction of CO_2 to methanol has been achieved with 100 % current efficiency on an illuminated p-GaP photoelectrode at underpotential[8] and with 30% current efficiency on hydrogenated Pd and Pt electrode at 200 mV overpotential[9]. It have been proposed that the electrochemical reduction CO_2 to methanol catalyzed by pyridinium is a homogeneous catalytic reaction (single electron shuttle for multielectrons reduction of CO_2 to methanol).[9,10] 4, 4'-bipyridine catalyzed CO_2 electrochemical reduction to methanol and propan-2-ol is also achieved on illuminated p-GaP, p-$GaInP_2$, and p-Si with varying faradaic efficiencies and extremely low quantum efficiencies.[11] On p-Si photocathode, the quantum efficiency of 4, 4' bipyridine catalyzed CO_2 reduction was 0.27 % for 530 nm wavelength light illumination. However, there is no report of photoreduction of pyridinium on illuminated p-Si. Figure 8.8 shows photoelectrochemical reduction of pyridinium on an illuminated p-Si in an aqueous medium containing 10 mM pyridine with 0.5 M KCl as a supporting electrolyte at pH 5.2 (buffer solution) in argon environment. A photovoltage of 460 mV was observed for pyridinium reduction, but no catalytic activity was observed for both buffered and non-buffered CO_2 saturated aqueous solution containing 10 mM pyridine on freshly etched p-Si photocathode. This is a surprising result if consider that the "pyridine/pyridinium" system of CO_2 reduction is supposedly a homogeneous system.

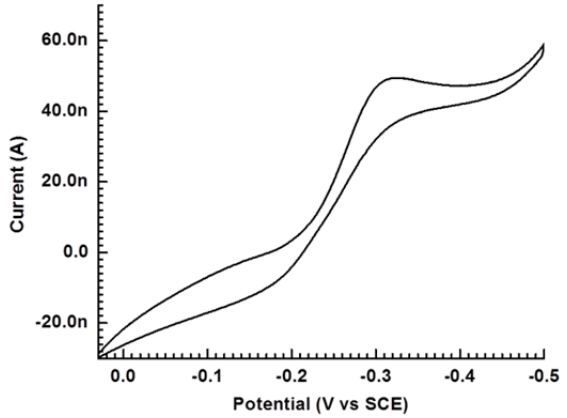

Figure 8-8. Cyclic voltammograms of pyridinium on an illuminated p-Si photocathode in 10 mM pyridine aqueous solution with 0.5 KCl as supporting electrolyte at 5 mVs^{-1} scan rate with Ag/AgCl as reference and Pt as a counter electrode. The light source used is a monochromatic laser diode with 661 nm wavelength.

It is a well-known fact that the water reduction can be achieved on platinum particles modified p-Si[12-14] at underpotential upon illumination. A photovoltage as high as 600 mV was observed on Pt/n+-p-Si

microwire arrays for hydrogen generation.[15] Pyridine/pyridinium system is active only on few electrodes including Pt. Planar p-Si electrodes (lollipop electrode) were coated with 1.5 nm Pt film by e-beam evaporation. The method to fabricate a planar p-Si electrode by using the epoxy method is described in detail in Chapter 6's experiment section. For Pt-p-Si electrode, there was not much current both under dark and under polychromatic illumination (around 90 $mWcm^{-2}$) in absence of CO_2 and water reduction onset potential was higher than -0.70 V vs SCE (actual reference is Ag/AgCl in Vycor tipped glass tube) as shown in Figure 8.9(a). Significant increase in the photocurrent density was observed in CO_2 saturated solution as shown in Figure 8.9(a). The shape of cyclic voltammogram of pyridine/pyridinium system on illuminated Pt-p-Si photoelectrode in CO_2 saturated solution at 10 mVs^{-1} is shown in Figure 8.9(a) as insert is very similar to the reported cyclic voltammograms for pyridine/pyridinium system on Pt dark electrode[9,10] under similar condition. The scan rate dependence of the peak catalytic current in CO_2 saturated solution shows that the peak catalytic current density is proportional to the square root of scan rate as shown in Figure 8.9(b). But, this does not confirm the proposed homogeneous nature this catalytic system. It means that the catalytic reduction of CO_2 in this system is scan rate dependent at scan rate higher than 100 mVs^{-1} and is mass transport limited in this scan rate ranges.

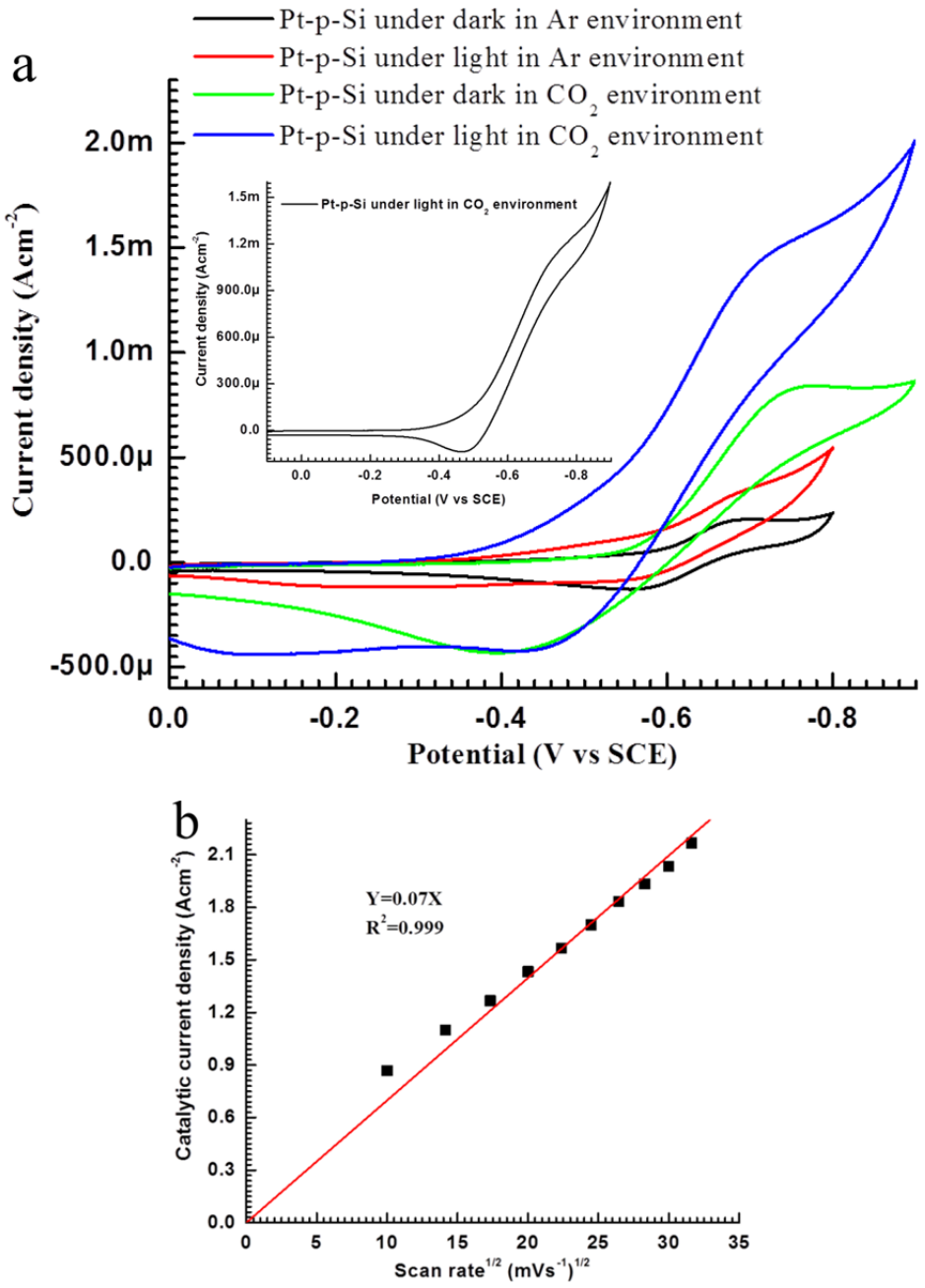

Figure 8-9. (a) Cyclic voltammograms of pyridinium in Ar (black and red lines) and CO_2 (green and blue line) saturated aqueous solution of 10 mM pyridine with 0.5 M KCl as supporting electrolyte at 100 mVs^{-1} scan rate on illuminated Pt-p-Si photocathode. Insert is the cyclic voltammogram of pyridinium on illuminated Pt-p-Si photocathode in CO_2 saturated aqueous solution of 5 mM pyridine with 0.5 M KCl as supporting electrolyte at 10 mVs^{-1} scan rate. (b) The scan rate dependence of the peak photocatalytic current density of CO_2 reduction in aqueous solution of 5 mM pyridine with 0.5 M KCl as supporting electrolyte on illuminated Pt-p-Si photocathode. Illumination source is a polychromatic light source with illumination intensity of 90 $mWcm^{-2}$, Ag/AgCl in glass tube with Vycor glass frit is used as a reference, 1 mm diameter glassy carbon electrode in glass tube with Vycor glass frit is used as counter electrode.

The illumination intensity dependence of the photocurrent density-voltage characteristics of Pt-p-Si photoelectrode under catalytic condition is shown in Figure 8.10(a). A significant amount of current under dark with onset potential around 0.58 V vs SCE was observed. It is most likely due to the CO_2 reduction on Pt nanoparticles at Pt-p-Si photoelectrode under dark condition. The cyclic voltammetry behavior of Pt-p-Si photoelectrodes under dark in Ar saturated and CO_2 saturated aqueous solution of 10 mM of pyridine with 0.5 M KCl as supporting electrolyte is shown in Figure 8.10(b). A comparison between Pt-p-Si photocathode in dark and Pt dark electrode reported in literature[9,10] for pyridine/pyridinium system showed identical behavior. These evidences validate that the Pt nanoparticles are active even on p-Si surface and there is a non-rectifying contact between Pt nanoparticles and p-Si. When polychromatic illumination intensity increases from 0 to 90 $mWcm^{-2}$; the onset potential of CO_2 reduction moves towards positive potential and the catalytic current density also increases. Similar behavior is observed when illumination intensity decreases from 90 to 0 $mWcm^{-2}$. The onset potential movement towards positive potential is consistent with the lowering of the onset potential due to the photovoltage generated by semiconductor/liquid junction. The increase in the catalytic current density with the illumination intensity suggests that the bare p-Si surface is also playing a role in the catalysis together with Pt nanoparticles on the illuminated Pt-p-Si photoelectrode surface. This confirms that the "pyridine/pyridinium" chemistry for CO_2 reduction is successfully transferred to the p-Si decorated with Pt nanoparticles. This is also consistent with the conditions proposed for the effective transfer of the catalytic activity of a catalyst to semiconductor photoelectrode in recently published review for the heterogeneous photocatalytic reduction of CO_2 on a metal decorated p-type semiconductor.[16] The maximum photovoltage achieved for this system is only 260 mV. The reason behind the low photovoltage is the high density of Pt nanoparticles on p-Si surface as shown in SEM micrograph of Pt-p-Si (Figure 8.10(c)). A photovoltage around 460 mV should be achievable at a lower density of Pt nanoparticles on p-Si surface and this can be obtained by lowering the thickness of Pt films during e-beam evaporation.

The formation of methanol after bulk electrolysis experiment of CO_2 saturated aqueous solution of 10 mM pyridine with 0.5 M KCl as supporting electrolyte on illuminated Pt-p-Si under short circuit condition (i.e. 0.58 V vs SCE) was confirmed by water suppression NMR and gas chromatography (GC) of

liquid sample (with capillary column and flame ionization detector). Faradaic efficiency for methanol formation is varied from 5 % (with Pt counter electrode without fritted) to 100 % (with Pt and glassy carbon counter in separate chamber with Vycor glass frit). In addition to methanol, there are some unknown species were also observed in both water suppression NMR and gas chromatography. The maximum current density obtained in the bulk electrolysis experiment was 2 $mAcm^{-2}$ (Figure 8.11(a)). Gas chromatography of the head space during the bulk electrolysis experiment confirmed the formation of hydrogen as a byproduct. The methanol quantification done at Caltech was not consistent, but overall, the concentration of methanol increased with the increase in the amount of charge passed. The formation of hydrogen stopped after some time even though the amount of charge passed through the cell continued at the same rate as shown in Figure 8.11(b). Hydrogen generation as a byproduct in this process is possibly due to the heterogeneous reduction of water on Pt surface. This indicates that Pt surface was no longer exposed to water. But, the methanol production is continued with the time and with the increasing amount of charge passed. This is an important observation about this system because this suggests that "pyridine/pyridinium" can work without Pt. More work is needed to be done to figure out a way to mark this system work without expensive metal like Pt. Solid state NMR experiment to determine the nature of surface deposition during bulk electrolysis is important for the better understanding of the system.

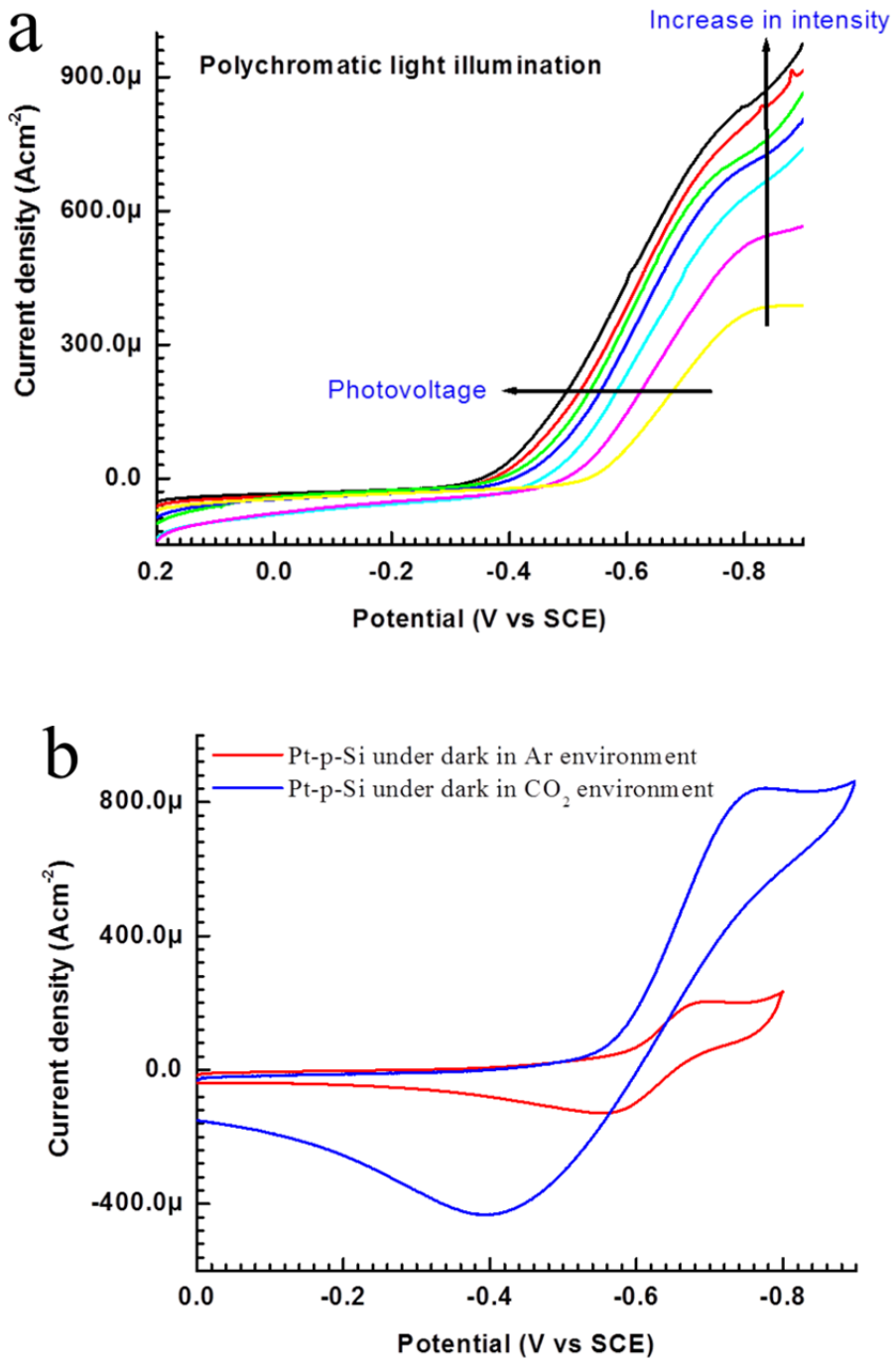

Figure 8-10. (a) Illumination intensity dependence of current density-voltage characteristic of the Pt-p-Si photocathode in CO_2 saturated aqueous solution of 10 mM pyridine with 0.5 M KCl as supporting electrolyte at scan rate of 10 mVs^{-1} without stirring. Polychromatic illumination intensity varied from 0 to 90 $mWcm^{-2}$. (b) Cyclic voltammograms of pyridinium on Pt-p-Si photocathode under dark with (blue line) and without (red line) CO_2 in aqueous solution of 10 mM pyridine with 0.5 M KCl as electrolyte at scan rate of 100 mVs^{-1}. Ag/AgCl in glass tube with vycor glass frit as reference, 1 mm diameter glassy carbon electrode in glass tube with vycor glass frit as counter electrode. (c) SEM micrograph of Pt-p-Si photocathode showing discontinuous Pt film on p-Si surface.

C

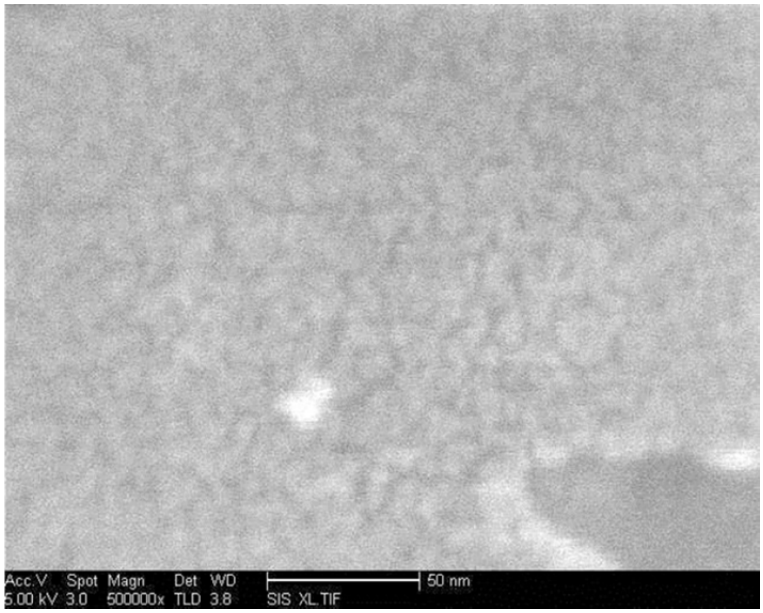

Figure 8-10. continued

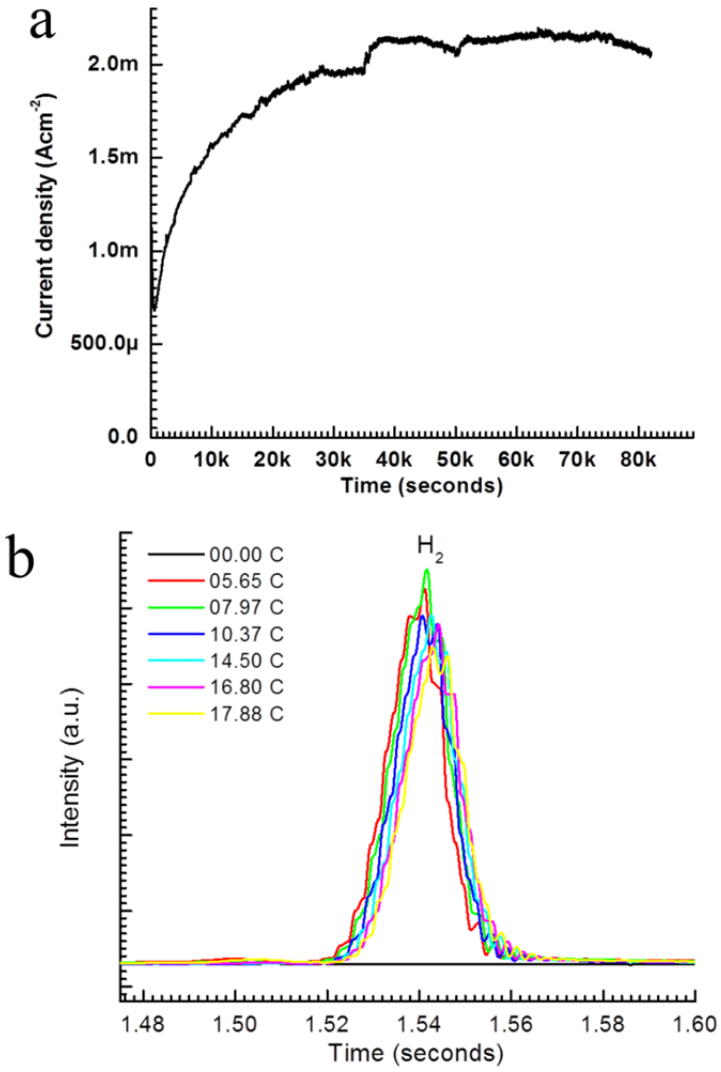

Figure 8-11. (a) Current density vs time curve for constant potential electrolysis (bulk electrolysis) under short circuit condition i.e. -0.52 V vs SCE with stirring for Pt-p-Si photocathode in a CO_2 saturated solution of 10 mM of pyridine with 0.5 M KCl as a supporting electrolyte. (b) Growth of hydrogen peak in GC with increased amount of charge passed over the course of bulk electrolysis in a CO_2 saturated solution of 5mM of pyridine with 0.5 M KCl as supporting electrolyte on illuminated Pt-p-Si photocathode at short circuit condition. Ag/AgCl in glass tube with Vycor glass frit is used as a reference electrode and 1 mm diameter glassy carbon electrode in glass tube with Vycor glass frit is used as a counter electrode.

Contrary to popular believe about this system, my observation is that platinum is acting as a proton donor and not as CO_2 binding sites. This observation is also supported by the fact that this system works on GaP, $GaInP_2$ and FeS_2 without Pt or hydrogenated Pd. All of these electrodes are good proton reduction heterogeneous catalytic surfaces. In addition, the head space GC analysis during bulk electrolysis experiment; no CO was detected as byproduct. And the system continued to work even when Pt surface

was covered during bulk electrolysis. Some of the key control experiments needed to be done to develop a better understanding of the system are as follow

(a) Electrochemistry of Pt-p-Si photoelectrode without removing the native oxide to confirm the involvement of the p-Si in catalysis under illumination.

(b) Careful head space GC of the bulk electrolysis experiment under short circuit condition on illuminated Pt-p-Si in CO_2 saturated aqueous solution of pyridine. And also at lower potential to find the potential where H_2 generation completely stopped with reasonable catalytic current density.

(c) Bulk electrolysis at 0.58 V vs SCE under CO_2 saturated aqueous solution without pyridine and head space measurement. The goal of this measurement to determine if hydrogen production stops after some time without the presence of pyridine. The pH of the solution should be kept at 5.2 by using buffer. This will provide some idea if CO_2 binding to Pt or not under above condition.

(d) Surface modification of p-Si with amine or pyridine or any other proton donor group and study the pyridine/pyridinium chemistry on surface modified p-Si photocathode.

(e) Study this system with InP photocathode.

(f) Study the effect Pt nanowire size and it separation on catalysis.

8.6 Prospective

Multi-junction photoelectrolysis cells are currently used to overcome the high potential that is associated with water splitting. Four types of these cells are currently used: (1) p/n junction photoelectrolysis cells, (2) photoanode-PV cells, (3) photocathode-PV cells, and (4) PV photoelectrolysis cells [17-20]. An excellent analysis of these cells is presented by Walter et al. in their review on solar water splitting [21]. Similar efforts for CO_2 photoreduction are lacking.

Of note, the PV photoelectrolysis cell has a photovoltage that is independent of pH, which is important for pH-sensitive catalyst mediated CO_2 reduction. This cell can also be easily modified with CO_2 reduction catalysts selective for specific products. In addition, this type of cell utilizes a majority of the

solar spectra and has a high photovoltage, unlike wide band gap semiconductor photoelectrodes. The total thermodynamic potential to reduce CO_2 to products like CH_3OH or CH_4 and oxidize water to oxygen is only around 1.2 V. In practice, however, the applied potential required for simultaneous reduction of CO_2 and oxidation of water is at least 2.0 V. Water oxidation using PV electrodes has been explored by Yamane et al. [20]. Photovoltages of 2.2 V and 1.7 V were reported with "n-Si/p-CuI/ITO/n-i-p a-Si/n-p GaP/ITO/RuO_2" and "n-i-p a-Si/n-p GaP/ITO/RuO_2", respectively, with 0.1 M Na_2SO_4 (pH = 6.3) as the supporting electrolyte.

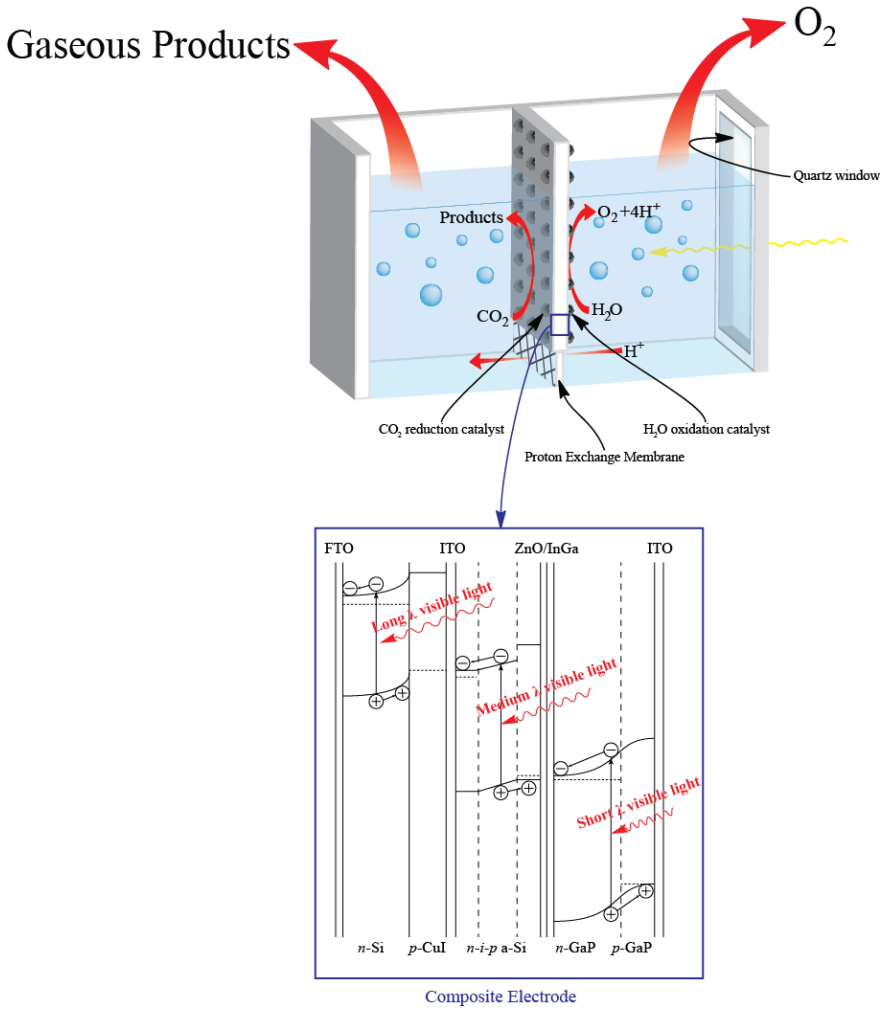

Figure 8-12. Schematic of proposed photochemical cell with a multijunction tandem photoelectrode for solar fuel application. The electrode structure is adapted from Yamane et al.[20] and FTO is fluorine-doped tin oxide and ITO indium tin oxide.

It is possible for this technology to be used as a wireless monolithic two compartment PV-type photoelectrolysis cell with a single dual face photoelectrode. A proposed cell which is using a CO_2 reduction catalysts/FTO/n-Si/p-CuI/ITO/n-i-p a-Si/n-p GaP/ITO/water oxidation catalysts electrode configuration is shown in Figure 8.12. The fabrication cost of the electrode may be high; however, the simple structure of the cell, the ease of product separation, and the robustness of the electrode could lead to a long operation time, and an environmentally friendly process.

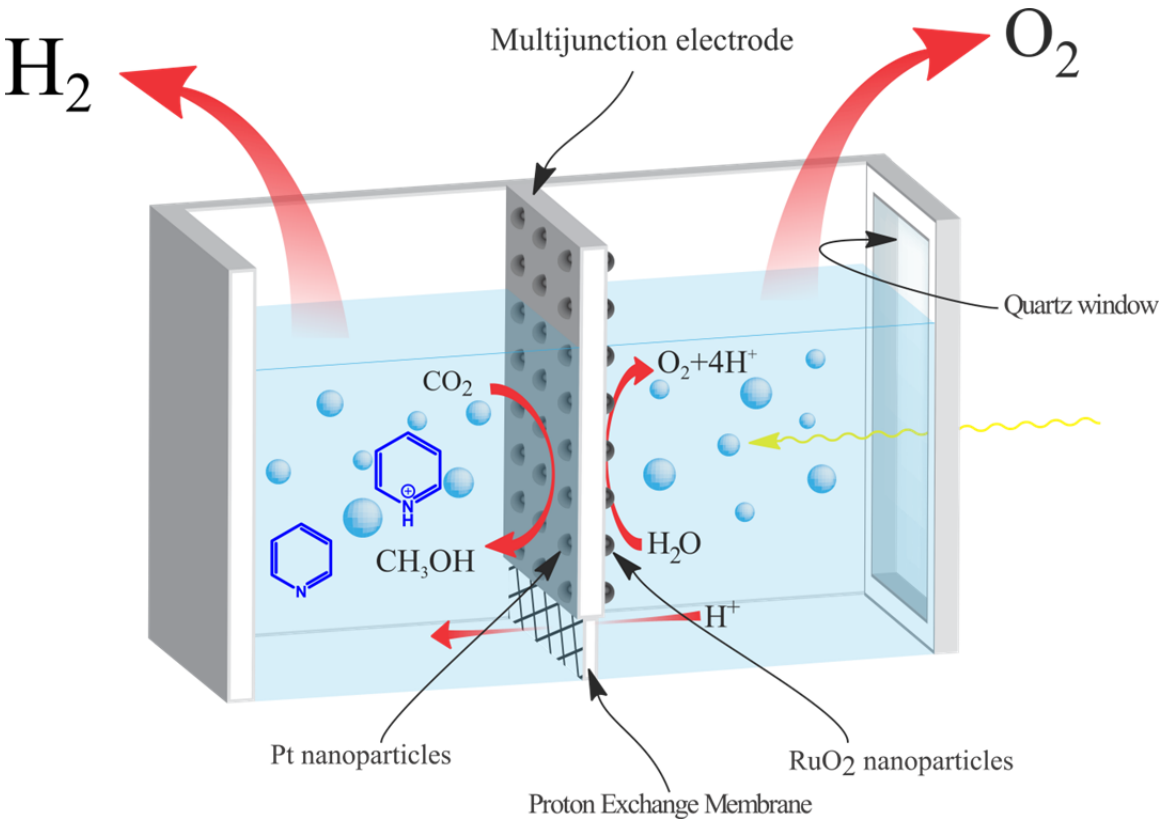

Figure 8-13. Schematic of a photochemical electrolyzer for methanol formation from CO_2 and water.

The overpotential of water oxidation in acidic medium is 200 mV for RuO_2 catalyst [22] and overpotential for CO_2 reduction to CH_3OH is 200 mV and 100 mV on Pd and Pt with pyridine/pyridinium catalyst [9], respectively. So, minimum total overall potential required to reduce CO_2 to CH_3OH and oxidize water to oxygen simultaneously with the assistance of these catalysts is 1.6 V. Based on these observations, it is possible to make a fully functioning photoelectrochemical cell consist of a composite electrode which can generate a photovoltage of 1.6 V and with above described catalytic system for oxidation and reduction

as shown in Figure 8.13. There are two major challenges for these types of cells: (1) identifying catalysts based on earth abundant materials which have low overpotentials for CO_2 reduction and water oxidation, and (2) finding a reliable and robust proton exchange membrane. It is clear that the advantages of this type of system will outweigh the cost. Therefore, it is imperative to explore and adopt water splitting/hydrogen generation technology for solar splitting of CO_2 for liquid fuel applications as well as broaden the search for new robust, selective, and efficient catalytic systems.

Note: Some of the material in this chapter comes directly from a manuscript entitled, "Photochemical and photoelectrochemical reduction of CO_2," by Bhupendra Kumar, Mark Llorente, Jesse Froehlich, Tram Dang, Aaron Sathrum and Clifford P. Kubiak, which has been published in *Ann. Rev. Phys. Chem.* **2012**, *63,* 24.1-24.29.

8.7 References

(1) Yu, H.-Z.; Boukherroub, R.; Morin, S.; Wayner, D. D. M. *Electrochem. Commun.* **2000**, *2*, 562.

(2) Fabre, B.; Hauquier, F.; Allongue, P. *J. Electroanal. Chem.* **2009**, *629*, 63.

(3) Smieja, J. M.; Kubiak, C. P. *Inorg. Chem.* **2010**, *49*, 9283.

(4) Kumar, B.; Smieja, J. M.; Kubiak, C. P. *J. Phys. Chem. C* **2010**, *114*, 14220.

(5) Dempsey, J. L.; Brunschwig, B. S.; Winkler, J. R.; Gray, H. B. *Acc. Chem. Res.* **2009**, *42*, 1995.

(6) Hu, X.; Brunschwig, B. S.; Peters, J. C. *J. Am. Chem. Soc.* **2007**, *129*, 8988.

(7) Pavlishchuk, V. V.; Addison, A. W. *Inorg. Chim. Acta* **2000**, *298*, 97.

(8) Barton, E. E.; Rampulla, D. M.; Bocarsly, A. B. *J. Am. Chem. Soc.* **2008**, *130*, 6342.

(9) Barton Cole, E.; Lakkaraju, P. S.; Rampulla, D. M.; Morris, A. J.; Abelev, E.; Bocarsly, A. B. *J. Am. Chem. Soc.* **2010**, *132*, 11539.

(10) Morris, A. J.; McGibbon, R. T.; Bocarsly, A. B. *ChemSusChem* **2011**, *4*, 191.

(11) Barton Cole, E., Thesis, Princeton University, 2009.

(12) Nakato, Y.; Ueda, K.; Yano, H.; Tsubomura, H. *J. Phys. Chem.* **1988**, *92*, 2316.

(13) Nakato, Y.; Tsubomura, H. *Electrochim. Acta* **1992**, *37*, 897.

(14) Nakato, Y.; Yano, H.; Nishiura, S.; Ueda, T.; Tsubomura, H. *J. Electroanal. Chem. Interfacial. Electrochem.* **1987**, *228*, 97.

(15) Boettcher, S. W.; Warren, E. L.; Putnam, M. C.; Santori, E. A.; Turner-Evans, D.; Kelzenberg, M. D.; Walter, M. G.; McKone, J. R.; Brunschwig, B. S.; Atwater, H. A.; Lewis, N. S. *J. Am. Chem. Soc.* **2011**, *133*, 1216.

(16) Kumar, B.; Llorente, M.; Froehlich, J.; Dang, T.; Sathrum, A.; Kubiak, C. P. *Annu. Rev. Phys. Chem.* **2012**, *63*, 24.1.

(17) Licht, S.; Wang, B.; Mukerji, S.; Soga, T.; Umeno, M.; Tributsch, H. *J. Phys. Chem. B* **2000**, *104*, 8920.

(18) Khaselev, O.; Bansal, A.; Turner, J. A. *Int. J. Hydrogen Energy* **2001**, *26*, 127.

(19) Yamada, Y.; Matsuki, N.; Ohmori, T.; Mametsuka, H.; Kondo, M.; Matsuda, A.; Suzuki, E. *Int. J. Hydrogen Energy* **2003**, *28*, 1167.

(20) Yamane, S.; Kato, N.; Kojima, S.; Imanishi, A.; Ogawa, S.; Yoshida, N.; Nonomura, S.; Nakato, Y. *J. Phys. Chem. C* **2009**, *113*, 14575.

(21) Walter, M. G.; Warren, E. L.; McKone, J. R.; Boettcher, S. W.; Mi, Q.; Santori, E. A.; Lewis, N. S. *Chem. Rev.* **2010**, *110*, 6446.

(22) Trasatti, S.; Buzzanca, G. *J. Electroanal. Chem. Interfacial. Electrochem.* **1971**, *19*, A1.